University of Alberta

Quantifying Methane Emission from Surface Sources using the Backward Lagrangian Stochastic Method

by

Tarana Mahzbain

A thesis submitted to the Faculty of Graduate Studies and Research in partial fulfillment of the requirements for the degree of **Master of Science**.

Department of Earth and Atmospheric Sciences

Spring 2012
Edmonton, Alberta

Abstract

The subject of this thesis is the micrometeorological estimation of the rate of transfer ("flux") of gases from surface area sources to the atmosphere. More specifically, it is an investigation of a particular implementation of the "inverse dispersion" method (ID), whereby rather than measuring the wanted flux directly, one instead measures the *gas concentration rise* attributable to the source, and deduces the flux necessary to explain that measurement under the prevailing meteorological conditions. The ID method used here is called "bLS" for "backward Lagrangian stochastic", a name which alludes to the type of meteorological model used to relate the flux (Q) to the concentration rise (ΔC). The thesis will demonstrate the practicalities involved in implementing bLS to quantify methane emission both from well defined, homogeneous sources and also from inhomogeneous, scattered, and poorly delineated source areas on complex topography.

Acknowledgements

I am grateful for the guidance of my supervisor Dr. John D. Wilson, for providing continuous monitoring and supervision. It would not have been possible to complete this dissertation without his support.

I also wish to express my gratitude to Dr. Thomas Flesch (Dept. of Earth & Atmospheric Science, UofA) whose valuable suggestions and help reflect a long experience with the type of measurement that is central to my thesis, and to Professor Gerhard Reuter (also of Earth & Atmospheric Science) for his kind support in diverse ways during my program. Thanks are due also to Dr. Ray Desjardins (Agriculture and Agri-Food Canada.) for the loan of instrumentation needed for this project, to Drs. Christian Felske and Kathleen Londry for access to the research site, and to Dr. Zaher Hashisho for serving as my external examiner.

Finally I thank my respected parents, whose trust and affection has inspired me, and underlies my confidence to have embarked on these studies.

Table of Contents

List of Tables

List of Figures

Chapter 1

Introduction

1.1 Background Information

The focus of this thesis is to demonstrate the application of a relatively novel micrometeorological technique to quantify the rate of emission of methane from small surface area sources. To place that aim in context, some background on the significance of methane will be given. Methane is a colorless, odourless gas with a wide distribution in nature. It is the most abundant organic trace gas in the atmosphere, with a residence time (defined as atmospheric methane mass divided by the magnitude of the surface-atmosphere exchange rate) that is cited as (only) 10 years. The three main sources of methane to the atmosphere are (1) biological production of natural origin; (2) abiotic production from lithospheric sources (this being a factor only on geological time scales); and (3) anthropogenic methane from industry and agriculture. As such, methane is present in natural gas (75%), swamp gas, sewer gas and is one of the main components of landfill gas (40-60%) (Reinhart & Townsend, 1998). Methane is a radiatively active, effective greenhouse gas. Like carbon dioxide, it traps infrared radiation that would otherwise escape into space. Indeed, molecule for molecule, it traps 25 times as much long wave radiation of the atmosphere as does carbon dioxide. Moreover global mean methane release rate is suspected to be temperature dependent e.g. melting of permafrost may permit peat bogs to release methane (Heikkinen *et al.*, 2002), while gas hydrates may also liberate methane (Friborg *et al.*, 2003). It is likely, then, that methane production may increase with atmospheric warming in mid to high northern latitudes. Finally, methane strongly reacts with the atmospheric hydroxyl radical (OH) and can be involved in the produc-

tion of tropospheric carbon monoxide and ozone (O_3) (Wuebbles & Hayhoe, 2002). These chemical transformations constitute the principal sink for methane deposited to the atmosphere.

Methane is also produced by specialized anaerobic bacteria that couple the oxidation of reduced compounds (principally hydrogen and acetate) to the reduction of carbon dioxide to methane. These bacteria are found in anaerobic environments within natural wetland ecosystems and rice paddies, in the anoxic rumen of cattle, and in the gut of termites and other wood-consuming insects (Ito *et al.*, 2000).

Although methane is normally present at very low atmospheric concentrations (less than 2 ppm by volume, or ppm v/v), increases in atmospheric methane concentrations are linked (as noted above) to climate change/global warming. The concentration of methane in the atmosphere has increased by 150% between the years 1750 and 1998, from a global mean concentration of 700 ppb to 1745 ppb (IPCC, 2001). Carbon dioxide is expected to account for 55% of future GHG driven temperature increase, while methane should account for 15% .

To a large extent this trend is probably caused by increasing agricultural and industrial activities linked to the growth of population. Rice paddy fields, cattle, production of oil and gas and waste decomposition associated with the growth of urban areas (Ehhalt & Schmidt, 1978; Khalil & Rasmussen, 1983) are the main anthropogenic sources . Since the 1700s, accelerating human activities, particularly in the areas of agriculture, fossil fuel use, waste disposal, including enteric fermentation, animal and human wastes, biomass burning, and landfills have more than doubled methane emissions. There are vast, deep coalbeds in Alberta, which are unmineable but contain trapped methane. The Alberta Research Council (ARC) is leading a group of provincial, national and international organizations to exploit the coalbed methane. Natural gas processing is a major industry in Alberta and a significant source of fugitive emissions of methane. For five gas plants surveyed in Alberta, Differential Absorption Lidar (DIAL) measured methane emissions ranged from 100 to 146 kghr^{-1}, which equates to about 3% of the national total of greenhouse gas emissions (CGGI-2003). Also methane emitted from the livestock sector accounts for 38% of all agricultural greenhouse gas (GHG) emissions in Canada (Environment Canada 2002). The average methane emissions from a commercial feedlot in central

Alberta were estimated $0.32\,\mathrm{kgCH_4\,animal^{-1}\,d^{-1}}$ (Haarlem *et al.*, 2008).

The Alberta Ambient Air Data Management System (AAADMS), also known as the CASA Data Warehouse, is a central repository for ambient air quality data collected in Alberta. At several locations in Alberta the atmospheric concentrations of various hydrocarbons are monitored continuously by means of a hydrogen flame ionization detector, and the CASA web site archives continuous hourly station data for several air pollutants. Evidently the concentration of methane changes both on hourly and the seasonal time scales. One-hour average concentration of methane ranged from 1.5 to 3 ppm for July, and from 1.5 to 3.5 ppm for December. While daily variation is seen, no particular pattern is shown.

The above generalities should make it clear why it is of interest to be able to measure the rate of methane emission from both natural and anthropogenic sources. The interest here is to demonstrate a method to measure methane emission rate "Q" (typical units, $\mathrm{kg\,m^{-2}\,s^{-1}}$) from localised surface area sources (typical horizontal scale of the order of 10 - 100 m) with high temporal resolution (say, order of 30 minutes). Methods capable of achieving that level of temporal and spatial resolution are almost exclusively micrometeorological[1], i.e. they focus on determining the rate of gain *by* the atmosphere *from* the source. A later chapter briefly categorizes the available methods, but suffice to say that this thesis focuses on what is called an "inverse dispersion method," whereby instead of directly measuring Q one measures instead the *rise* ΔC *in methane concentration attributable to the source*, and infers the value of Q that satisfactorily explains that methane loading, under the prevailing atmospheric conditions. The thesis couples gas concentration measurements, associated atmospheric measurements (wind speed, direction, and more – details to follow), and the interpretation of the gas concentration measurements using a micrometeorological model. The model is called a "backward Lagrangian stochastic" model, and in essence it computes the paths of hypothetical gas particles *backward* in time from the concentration detector to the methane source or sources. Loosely speaking the function of the model can be said to be that it provides the needed $\Delta C - Q$ relationship

[1]An excepion might be a hypothetical industrial source, wherein knowledge of reactants and processes might permit to compute the rate of loss to the atmosphere from a stack without need of any measurements within the atmosphere itself.

that permits known ΔC to be translated to inferred Q.

1.2 Objectives of the Research

The opening objective of this thesis project was to assess whether there might be a recognizable *pattern* to the daily variability in methane concentration in the atmospheric boundary layer (ABL) at a site (or sites) in Central Alberta, to document any such pattern, and to interpret its cause. Explanation of cause would necessitate reference to the depth of the ABL and the strength of atmospheric mixing, as well as the probable spatial and temporal distribution of the most imporatnt methane sources in the region. This objective was addressed experimentally, and (as will be made evident below) the outcome is negative in the sense that no "easy" pattern has been elucidated. It is perhaps useful here to mention that to comprehend systematically the *cause* of methane concentration variation on a regional scale is a challenge that is being actively addressed by several research groups at present, groups with access to high resolution data bases of emission rates and to interpretive meteorological models that are "driven" by weather model outputs providing analysed fields of wind throughout the troposphere. The present effort could hardly match that scale and type of science, but served to familiarize the author with the methane sensors to be used in the subsequent and main objective of the research, namely to apply an inverse dispersion method to demonstrate the quantification of methane sources at a waste management centre.

1.3 Main Scientific Question

The experimental side of this research project entailed methane "monitoring" observations during summer 2010, and an intensive campaign of field work in spring 2011. The main scientific questions to be addressed in this thesis are as follows:

1. Atmospheric concentration of methane at Edmonton

    (a) Is there a *regular* (tightly-patterned) daily cycle of methane concentration observed in Edmonton?

    (b) Does methane concentration correlate with atmospheric conditions?

2. Application of bLS inverse dispersion method for well-delineated methane sources (waste lagoons)

   (a) How best to quantify emissions from multiple sources?

   (b) What is the impact of assumptions in regard to the prevailing *background* concentration on calculated source strength?

3. Application of bLS inverse method for poorly-delineated methane sources (LFG seepage from landfill)

   (a) Can a plausible figure be given for the strength of LFG seepage sources?

   (b) How sensitive is such an estimate to the range of plausible assumptions as to the spatial distribution of emissions?

Analysis of the methane measurements to estimate source strength hinged on the use of the freely available software "WindTrax."

1.4 Thesis Outline

The first chapter has provided an introduction to the topic of the thesis, and relayed current knowledge of methane related research in and around Canada. Chapter 2 will summarize the meteorology of the Atmospheric Boundary Layer, discuss atmospheric transport and dispersion in general, give some theoretical background on the Lagrangian Stochastic model, and provide some basic information regarding the particular Lagrangian model WindTrax. Chapter 3 conveys an analysis of the observed variation of atmospheric methane concentration in Edmonton, placed in context with the known daily, seasonal and annual cycle of methane concentration around the world. Chapters 4 and 5 will contain the analysis of the field campaign of 2011. Chapter 4 focuses on application of the bLS model to deduce the emission rate from a waste lagoon. Chapter 5 explores differing assumptions as to the spatial distribution of LFG seepage from a landfill, giving the associated estimates of emission rate. Finally Chapter 6 is a discussion and conclusion of the thesis.

Chapter 2

Relevant Meteorological Theory for Inverse Dispersion on the Micrometeorological Scale

As constituting the environment for all terrestrial living beings and the vegetation that sustains them, the atmospheric boundary layer is worthy of study. Within this turbulent lower kilometer (or so) of the atmosphere occurs a constant exchange and redistribution of mass and energy between the surface (ecosphere or biosphere) and the atmosphere. This chapter briefly covers the theoretical basis for the existing scientific comprehension of processes in the atmospheric boundary layer, focusing on the "governing equations" (which stem from the conservation principles for mass, momentum and energy) and models (conceptual and numerical) that are derived from them.

2.1 Atmospheric Boundary Layer

The lowest layer of the atmosphere, whose depth ranges roughly from a minimum of about 100 m to a maximum of about 3000 m, is "stirred" by turbulent eddies such that, as a generalization, rather complete mixing occurs on a time scale of the order of hours. This layer is called the atmospheric boundary layer (ABL), Fig. 2.1 [Arya,1982 (p2)]. The balance of the troposphere is named the *free atmosphere*, for the effects of surface friction (and other surface-atmosphere exchanges) are felt (so far as the hourly-daily timescale is concerned) only within the ABL (also known as the planetary boundary layer, or friction layer) and the flow in the free troposphere is

approximately geostrophic. The ABL, a sort of short term reservoir with which the solid and liquid earth communicate, is conditioned by the surface exchange processes — exchange of momentum (frictional drag), of heat, of water vapour, and of all manner of minor constituents, natural or artificial.

The crucial characteristic of the boundary layer necessitating that it be treated differently from the rest of the atmosphere is turbulence. Because its properties fluctuate rapidly in time and space, any practical theory of processes in the ABL must be framed in terms of *statistics*, e.g. 30-min average wind direction, temperature, humidity, etc. Turbulence – its causation, its nature – is a whole field of study in and of itself, but here we shall be interested in that minimum of knowledge that will suffice in the context of the thesis.

For convenience, wherever the land surface is reasonably level and uniform, it is commonly assumed that the ABL is "horizontally homogeneous," the technical meaning of which is that statistical properties *are constant on horizontal planes*. In that case, by definition, statistical properties vary only with height, and time. So far as horizontal transport is concerned, it is a common approximation to neglect the turbulent fluctuations in horizontal velocity components such that transport occurs only due to the (height-varying) *mean wind*, whereas (the mean vertical velocity in a horizontally-homogeneous ABL being nominally zero) vertical transport is entirely due to the eddies, ie. fluctuating vertical velocity field. The decomposition of the ABL motion field (and other fields) into its average and the departure from average is almost a universal practise. Let us suppose local Cartesian coordinate axes oriented such that x points in the direction of the average wind near ground, y points across the mean wind and z is vertical. Then if the corresponding velocity components are (u, v, w) the decomposition into average and fluctuation is symbolized thus:

$$u(\mathbf{x}, t) = U(\mathbf{x}, t) + u'(\mathbf{x}, t) \tag{2.1}$$

where $\mathbf{x}$ is position, U is the mean velocity, and u' the velocity fluctuation. Although the notation above allows for the possibility that the mean velocity U depends on all four independent variables, the exuberance of its variation is very much suppressed, by virtue of its being an average. And if the symmetries of "horizontal homogeneity" and "stationarity" apply, then indeed $U = U(z)$. In the balance of the thesis averages will

often be denoted by using an overbar, e.g. the mean wind in the x direction could be denoted either as U (capitalization) as as $\overline{u}$. For some species the overbar notation is the only option, for example $\overline{w'T'}$ is the *covariance* of the vertical velocity fluctuation and the temperature fluctuation. At one level this is a mere statistic. It may seem an arcane quantity. But it is in fact the mean kinematic heat flux density. It need only be multiplied by the product ρc_p of mean air density and the specific heat capacity of air and we have

$$Q_H = \rho \, c_p \, \overline{w'T'} \, , \tag{2.2}$$

which is rigorously the rate of flow of sensible heat along the vertical — a key property both practically and scientifically, that will figure much in the theory (briefly) espoused below.

Now returning to the decomposition of the x-wise velocity into mean and fluctuation, the fluctuation u', which is the instantaneous departure from average, expresses or "carries" essentially all the spatial and temporal variability of the ABL. It is possible to introduce the notion of eddy size and timescale both qualitatively and quantitatively. Qualitatively, eddy size spans from the scale of millimeters (or smaller) out to roughly the depth of the ABL itself. The latter varies in time (seasonally and diurnally). Responding essentially to mixing, which in turn is a consequence of windiness and the injection of heat at ground, the ABL grows in depth from a morning minimum (elusive in its magnitude, but nominally in the order of hundreds of metres) to an afternoon maximum (again, elusive because it is hard to measure) that may exceed two kilometers. The diurnal evolution of the ABL and the turbulent motion within it are influenced by the diurnal cycle in the components of the surface energy budget (Munn, 1966), viz.

$$Q^* = Q_H + Q_E + Q_G \tag{2.3}$$

where Q^* is the net radiation, positive if directed towards the surface; Q_H the sensible heat flux (defined above); Q_E is the latent heat flux (both Q_H and Q_E are defined to be positive if directed from the surface towards the atmosphere); and Q_G is the heat flux to the substrate below the reference plane, positive if directed from the surface into ground/lake/ocean. The latent heat flux is related to the vertical flux of

water vapour E by the relationship $Q_E = L_v E$, where L_v [$\mathrm{J\,kg^{-1}}$] is the latent heat of vapourization. All fluxes have the unit: [$\mathrm{W\ m^{-2}}$].

Early on in the study of micrometeorology (e.g. Sutton, 1953) it became conventional — because it is useful — to treat the ABL as consisting of two sub-layers: the *Outer Layer* and the *Inner Layer (Surface Layer)*, also known as the "constant flux layer." This separation is particularly meaningful if the ABL *is* horizontally homogeneous.

- **Outer Layer**: The region above the lowest $50 - 100$ m from the surface is known as outer layer. In this layer the shearing stress (along with most other properties) varies with height, and the influence of earth's rotation cannot be neglected. In contrast to the surface layer, no existing simplification of the governing equations or semi-empirical similarity theory gives a paradigm for the outer layer that is at once *realistic* and *simple*.

- **Inner Layer**: The lowest $50 - 100$ m of the ABL is named the "inner layer" or, more commonly, the "surface layer." Early researchers, perhaps especially A.M. Obukhov in the Soviet Union, realized that in this "ground layer" (as the Russian was translated, or perhaps mis-translated) the vertical flux of horizontal momentum (the turbulent shearing stress) is effectively height independent, as too are the concomitant fluxes of heat and water vapour. Thus this surface layer is a sort of valve through which pass the exchange fluxes (heat, water, momentum, methane...) between the surface and the outer ABL. Accordingly the surface layer is also called the "constant flux layer." It is characterized by height independent fluxes, and strongly height-dependent (i.e. sheared) profiles of mean velocity, temperature, humidity, etc.

As the main goal of this chapter (and indeed this thesis) is to study the lowest layer of the ABL that is in contact with the surface, and the atmospheric transport/diffusion processes of pollutants within it, further discussion will be restricted to the *surface layer*.

2.2 Atmospheric Surface Layer

The paradigm of the height-constancy of the fluxes across the surface layer is based on an approximation. A pragmatic definition of the surface layer is that it is that layer across which the fluxes of momentum and heat and vapour vary by less than about 10% of their magnitudes at the surface (Stull, 1950). Of course, it is entirely possible for the surface layer to be *disturbed* (e.g. by topography or surface obstacles or variations in land use) such that its statistical properties vary not only with height, but also along the horizontal coordinates. Here we exclude such cases from consideration, and address the *horizontally-homogeneous surface layer*.

A semi-empirical, quantitative description of the mean flow and turbulence statistics within the thermally-stratified atmospheric surface layer was provided by Monin and Obukhov (Obukhov, 1971), the Monin-Obukhov Similarity Theory (MOST). MOST does not solve the governing equations, but instead is based on the principle of dimensional analysis. The state of the surface layer is assumed to be controlled by a small number of salient statistical properties.

2.3 Monin-Obukhov Similarity Theory

According to Monin-Obukhov Similarity Theory (MOST), for any height z in the layer $z_0 \ll z \ll \delta$ (where δ is the boundary layer depth and z_0 is the surface roughness length) (Stull, 1950), the properties that control the state of the surface layer are the kinematic momentum flux (u_*^2), the kinematic heat flux ($\overline{w'T'} = Q_H/\rho c_p$), and a buoyancy parameter g/T_0 where T_0 is the layer mean temperature and g is the gravitational acceleration. Here the kinematic momentum flux has been expressed in terms of a friction velocity that is defined by

$$u_* = \sqrt[4]{(\overline{u'w'})^2 + (\overline{v'w'})^2}\,, \tag{2.4}$$

where $\overline{u'w'}$and $\overline{v'w'}$, evidently velocity covariances, are the kinematic momentum fluxes. The quantity

$$\tau \equiv \rho u_*^2 \tag{2.5}$$

(where ρ is the air density) is the turbulent shear stress [$\mathrm{N\,m^{-2}}$], giving the mean force of the wind on the ground.

A scale for turbulent temperature fluctuations is formed as

$$T_* = -\frac{\overline{w'T'}}{u_*}\,, \tag{2.6}$$

and (most importantly) the "Obukhov length" can be formed from the governing scales as the combination

$$L = -\frac{u_*^3}{k_v(g/T_0)(\overline{w'T'})}\,. \tag{2.7}$$

Here the von Karman constant k_v is included by convention (as is usual, we assume $k_v = 0.4$). The Obukhov length L, or rather the ratio z/L, functions in MOST as the "stability parameter". When L is positive ($L > 0$), stratification is stable. When L is negative ($L < 0$) stratification is unstable, and if L is infinite ($|L| \approx \infty$) the surface layer is neutrally stratified.

By a straightforward dimensional analysis based on the above set of governing scales, one may show that the mean wind shear and mean temperature gradient within the surface-layer are

$$\frac{k_v z}{u_*}\frac{\partial U}{\partial z} \;=\; \varphi_m\left(\frac{z}{L}\right) \tag{2.8}$$

and

$$\frac{k_{vh} z}{T_*}\frac{\partial \overline{T}}{\partial z} \;=\; \varphi_h\left(\frac{z}{L}\right) \tag{2.9}$$

where k_v and k_{vh} are the (potentially distinct) von Karman constants for momentum and heat, and φ_m and φ_h are universal empirical dimensionless functions of the ratio z/L. Integrating Eqs. (2.8 & 2.9), (Paulson, 1970), it is found that,

$$U(z) \;=\; \frac{u_*}{k_v}\left[\ln\frac{z}{z_0} - \Psi_m\left(\frac{z}{L}\right) + \Psi_m\left(\frac{z_0}{L}\right)\right] \tag{2.10}$$

$$\overline{T}(z) - \overline{T}(z_{0T}) \;=\; \frac{T_*}{k_v}\left[\ln\frac{z}{z_{0T}} - \Psi_h\left(\frac{z}{L}\right) + \Psi_h\left(\frac{z_{0T}}{L}\right)\right] \tag{2.11}$$

where the "psi" are functions of the MO universal functions, viz.

$$\Psi_m \;=\; 2\ln\left(\frac{1+\varphi_m^{-1}}{2}\right) + \ln\left(\frac{1+\varphi_m^{-2}}{2}\right) + 2\,\mathrm{atan}\left(\varphi_m^{-1}\right) + \frac{\pi}{2} \tag{2.12}$$

$$\Psi_h \;=\; 2\ln\left[\frac{1}{2}\left(1+\varphi_h^{-1}\right)\right]\,. \tag{2.13}$$

In the above equations z_{0T} is the "roughness length for temperature," the level at which $\overline{T} = \overline{T}_0$ (often one sets z_{0T} equal to z_0).

According to the International Turbulence Comparison Experiment (Dyer, 1982) (ITCE), under unstable stratification the similarity functions for wind speed and temperature are:

$$\varphi_m = \left(1 - 28\frac{z}{L}\right)^{-\frac{1}{4}} , \tag{2.14}$$

$$\varphi_h = \left(1 - 14\frac{z}{L}\right)^{-\frac{1}{2}} . \tag{2.15}$$

Along with other equations of this section, these specifications permit to compute the variation with height of the mean wind speed and temperature.

The significance of the Monin-Obukhov theory to the work of this thesis is as follows. In order to relate a measured methane concentration rise to the strength Q of the methane source(s) responsible, it is necessary to compute an ensemble of particle paths from each concentration detector to the source(s). Those paths must be computed in a manner that is realistic, i.e. they must reflect the true statistics of the wind in the layer they traverse. MOST gives us theoretical profiles of mean wind speed, and all other needed properties of the flow. In particular, the vertical motion is accomplished by fluctuations in vertical velocity, whose variance, again according to MOST, behaves as

$$\frac{\overline{w'^2}}{u_*^2} = \phi_{ww}\left(\frac{z}{L}\right) \tag{2.16}$$

where the ϕ_{ww} function is known (i.e. has been determined empirically). It follows that all needed statistics of the transporting wind field can be computed, provided only that one knows this set of key variables: the friction velocity u_*, the kinematic heat flux $\overline{w'T'}$, the mean wind direction and the roughness lengthz_0. These properties are easily determined by running a single fast-response anemometer such as an ultrasonic anemometer. Thus all methane measurements of the campaign at the waste management center were accompanied by simultaneous measurements with a sonic anemometer.

Monin-Obukhov similarity theory is applicable when $|L|$ is not "too small," a circumstance that loosely equates to the wind not being excessively calm (obviously if the wind is calm, the theory falls apart – the controlling variables must be zero). Experience suggests that the state of the surface layer is usefully described by MOST provided $u_* > 0.1\,\mathrm{m\,s^{-1}}$ and $|L| \geq 2$ m. (Stull, 1950) has discussed some typical

orders of magnitude of the relevant scales based on the surface fluxes, as given below:

.

Monin-Obukhov length, (L)	Order (1 m to 200m)
Roughness length, (z_0)	Order (1 mm to 1m)
Friction velocity, (u_*)	Order (0.05 to 0.5 m/s)
Surface layer Temperature scale, ($\|T_*\|$)	Order (0.1 to 2.0^{o}C)
Surface layer humidity, (q_*)	Order (0.1 to $5 g_{\text{water}}/k g_{\text{air}}$)

2.4 Atmospheric Dispersion

The rapid mixing of fluid in the vertical and horizontal directions is generically known as "atmospheric dispersion." In the following outline of the theory of turbulent dispersion, we focus on a non-buoyant and non-reactive species whose instantaneous concentration (amount of the property per unit volume of the fluid) is $c(x, y, z, t)$, with mean value $C(x, y, z, t)$. If the volumetric source strength for "c" is denoted as S then conservation of mass can be expressed by the equation

$$\frac{\partial c}{\partial t} + \vec{u} \,.\nabla c = \kappa \nabla^2 c + S \tag{2.17}$$

where κ is the molecular diffusivity [m^{2}s^{-1}] of the property and of course the velocity vector $\vec{u} = u\,\hat{i} + v\,\hat{j} + w\,\hat{k}$.

However molecular diffusion is immeasurably slow relative to turbulent transport, so we shall set $\kappa = 0$. We shall also assume that c is neither created nor destroyed in situ in the atmosphere, so that $S = 0$. This would permit us to express the above equation as

$$\frac{dc}{dt} = 0 \tag{2.18}$$

where d/dt is the rate of changing following a fluid parcel, the so-called "Lagrangian time derivative." We shall return to this point later, to explain the role of the Lagrangian stochastic model in this thesis work. However for now, we shall pursue what is known as the "Eulerian" description of dispersion.

As earlier indicated, only a statistical description of turbulent transport is feasible, and so we carry out the "Reynolds decomposition" for the property labelled "c", viz.

$$c = C + c' \tag{2.19}$$

where $C(x, y, z, t)$ is the mean concentration (in some contexts one might call it the "resolved concentration") and c' is the concentration fluctuation. Substituting that decomposition and averaging the resulting equation we obtain

$$\frac{\partial C}{\partial t} = -\frac{\partial}{\partial x_i}\left(U_i C + \overline{\acute{u}_i \acute{c}}\right) \tag{2.20}$$

where we have switched to Cartesian tensor notation, and summation is implied over repeated subscripts. The term $\partial \overline{\acute{u}_i \acute{c}}/\partial x_i$ is the divergence of the flux of c carried by the turbulent motion. We now have an *unclosed theory* of dispersion. For even if we regard wind statistics as known (i.e. provided), this is a single equation involving multiple unknowns. In addition to the fundamental unknown, the mean concentration C, we now have a theory that involves the eddy fluxes $\overline{u'c'}$ (etc.), whose role, moreover, is central to the problem. This is "the closure problem" of turbulence. It can be circumvented only by the introduction of supplementary empirical hypotheses.

The simplest of these is the "eddy diffusion model," or "K-theory," which by analogy with molecular diffusion models the eddy flux(es) as

$$\overline{\acute{u}_j \acute{c}} = -K_{ij}\,\frac{\partial C}{\partial x_i} \tag{2.21}$$

where K_{ij} is the "eddy diffusivity tensor." It has the same units as the molecular diffusivity κ, viz. $[\mathrm{m^2 s^{-1}}]$, but it is immeasurably larger. Most often the eddy diffusivity is assumed to be diagonal, i.e. the K-theory model is reduced to

$$\overline{\acute{u}\acute{c}} = -K_x \frac{\partial C}{\partial x}\,, \tag{2.22}$$

$$\overline{\acute{v}\acute{c}} = -K_y \frac{\partial C}{\partial y}\,, \tag{2.23}$$

$$\overline{\acute{w}\acute{c}} = -K_z \frac{\partial C}{\partial z}\,. \tag{2.24}$$

This formulation allows different diffusivities along different directions of spread. Adopting this formulation and with the mean velocity $U_i \equiv (U, V, W)$, the mass conservation equation becomes

$$\frac{\partial C}{\partial t} + U\frac{\partial C}{\partial x} + V\frac{\partial C}{\partial y} + W\frac{\partial C}{\partial z} = \frac{\partial}{\partial x}\left(K_x \frac{\partial C}{\partial x}\right) + \frac{\partial}{\partial y}\left(K_y \frac{\partial C}{\partial y}\right) + \frac{\partial}{\partial z}\left(K_z \frac{\partial C}{\partial z}\right) \tag{2.25}$$

or using tensor notation

$$\frac{\partial C}{\partial t} + U_i\,\frac{\partial C}{\partial x_i} = K_{(i)}\frac{\partial^2 C}{\partial {x_{(i)}}^2} \tag{2.26}$$

where (i) indicates "no summation." This equation is the basis of the simplest (and still common) models of atmospheric dispersion, which treat the diffusivities as being independent of position (Gaussian puff and plume models).

2.4.1 Scales of dispersion

Atmospheric dispersion problems or processes are habitually classified as entailing dispersion on the local scale, on short-range or on large-range (of course there are many variations of this vague terminology). When the spatial scale of the problem is less than about 1 km one speaks of local scale dispersion (e.g. accidental releases of gas, toxic spills). The intermediate range from about 1 - 20 km is termed short-range (regulatory applications). And wherever the spatial scale of interest exceeds the above we may consider the problem as one of large-range dispersion (volcanic eruption, wide-spread fires). It is worthwhile to note that one would have to regard the prevailing methane concentration in Edmonton as properly being modelled as a large scale dispersion problem. Sources worldwide affect the concentration in Edmonton (via entraiment into the ABL over Edmonton), although local sources surely modulate the picture. And if (exercising the imagination) there happened to be a large source very nearby, of course one might get by treating the problem as local.

2.4.2 Inverse Dispersion

As noted at the beginning of the thesis, "Inverse Dispersion" is the name given to a strategy for inferring the strength (generically "Q") of (otherwise unknown) sources giving rise to a measured concentration (or rise in concentration) of a gas of interest. As such it is a way of determining a flux by, instead, measuring a concentration.

Now before proceeding, what about methods to measure flux directly? Since our focus is surface-air exchange, we would be interested in measuring a vertical flux. The mean vertical flux of c is the quantity $\overline{wc}$, which, if the terrain is level and the flow horizontally homogeneous, is well approximated by $\overline{w'c'}$. This is a covariance. It can be measured using the eddy covariance technique, wherein fast response vertical velocity and gas concentration sensors are co-located at some small distance h (say, order 2 m) above the surface. The cross product of their signals, upon averaging over

some suitable interval (say 15 to 30 minutes) is the eddy flux. This is very do-able, but several complications may arise:

- fast sensors do not exist for all gases that may be of interest
- the eddy covariance technique is posited on assumptions as to the vanishingly small mean vertical velocity, and it is difficult to correct for imperfections of the site, i.e. presence of obstacles to the flow or irregularities of the topography
- the "footprint" of the upwind surface that the measured eddy flux represents may extend for hundreds of metres upwind. If the actual source of interest is small, the measured flux may be "contaminated" by a flux component off other parts of the surface

For these reasons, inverse dispersion (as expounded in this thesis) has a useful niche. One way to envisage inverse dispersion is as follows. Let Q (as usual) be the source strength and let U_r be a reference wind speed. If C is a concentration rise at some point that is attributable to the source then the ratio $n \equiv U_r C/Q$ is dimensionless. Supposing that we can *compute* a theoretical value n^{theory}, in our case using a Lagrangian Stochastic model (Wilson *et al.*, 1982), then we may deduce the source strength as $Q = U_r C/n^{\text{theory}}$ (where U_r is provided by an anemometer and C from a gas sensor). It is worth stating that the gas sensor need only provide the mean concentration – no need for a rapid sensor.

It turns out that the $C - Q$ relationship may be formulated in terms of the "touchdowns" on the ground surface (at locations x_i, y_i) of trajectories computed backwards in time from the concentration detector (backward Lagrangian stochastic method). If the vertical velocities with which trajectories touch down are denoted w_i and if one has computed a total of N trajectories, the flux-concentration relationship can be written as (Flesch *et al.*, 1995)

$$n \equiv \frac{U_r C}{Q} = \frac{1}{N} \sum_i I\left(x_i, y_i\right) \frac{2\,U_r}{|w_i|}. \tag{2.27}$$

In the above equation $I(x_i, y_i)$ is an indicator function whose value is one if (x_i, y_i) lies within the boundary of the source region, and zero otherwise.

2.5 Lagrangian Stochastic Model

In this thesis Inverse Dispersion (inferring Q from measured C) is accomplished by computing an ensemble of backward-in-time paths from a concentration detector upwind and over the sources, as indicated above. Those paths are computed using a (backward) Lagrangian stochastic model, which generates these random paths that must, by whatever criteria are available, be "realistic." It is appropriate here to give an overview of the formulation of a suitable model for the calculation of turbulent trajectories.

By definition, Lagrangian models track the movement of the fluid particles — whereas Eulerian models express conservation of mass in a stationary frame of reference. The first practical Lagrangian stochastic models emerged in the 1980's in the context of atmospheric problems, and they have subsequently been adopted in oceanography and engineering. They are based in the theory of stochastic processes (Lemons & Langevin, 2002), and have evolved in complexity and rigour such that they are now applicable to complex problems (Boughton *et al.*, 1987).

Let $c(X_i(t), t)$ represent the concentration of a species "c" that is carried by a fluid element whose location at time t is $X_i(t)$. Then the change dc over the time interval dt can be written

$$dc = \left(\frac{\partial c}{\partial t}\right)_{x_i = X_i(t)} dt + \left(\frac{\partial c}{\partial X_i}\right)_t dX_i \tag{2.28}$$

Noting that

$$\left(\frac{\partial c}{\partial X_i}\right)_t = \left(\frac{\partial c}{\partial x_i}\right)_t \tag{2.29}$$

Eq. 2.28 becomes

$$\frac{dc}{dt} = \frac{\partial c}{\partial t} + U_i \frac{\partial c}{\partial x_i} \tag{2.30}$$

$$\frac{dc}{dt} = \frac{\partial c}{\partial t} + \vec{u} \,.\nabla c \tag{2.31}$$

(using alternative notations). The L.H.S expresses the "Lagrangian" time derivative as the sum of the "local tendency" and "advection". Using Eq.(2.31) one may rewrite the advection-diffusion Equation (Eq. 2.17) as

$$\frac{dc}{dt} = \kappa \nabla^2 c + Q \; . \tag{2.32}$$

Now, repeating our earlier simplications, i.e. assuming there are no in-situ sources or sinks ($Q = 0$) and that the Peclet number $P_e = \frac{UL}{\kappa}$ (where U, L are velocity and length scales of the turbulence) is sufficiently large that we may neglect molecular diffusion, we obtain

$$\frac{dc}{dt} = 0 \, . \tag{2.33}$$

This states that the property c is conserved along fluid element paths (trajectories), and is the logical basis for the *Lagrangian approach* to turbulent dispersion.

2.5.1 Formal connection between concentration and trajectories

It may be shown that the ensemble mean concentration can be expressed in the most abstract terms as

$$C(x, y, z, t) = \int_{\mathbf{x}_0} \int_{-\infty}^{t_0=t} p\left(x, y, z, t | x_0, y_0, z_0, t_0\right) \;\; Q\left(x_0, y_0, z_0, t_0\right) \; d\mathbf{x}_0 \; dt_0 \tag{2.34}$$

where $p\left(x, y, z, t | x_0, y_0, z_0, t_0\right)$ is the "transition density" and $Q(x_i, t)$ is the volumetric source distribution. The transition density is defined such that $p(\mathbf{x}, t | \mathbf{x}_0, t_0)\, d\mathbf{x}$ gives the probability that a particle located at $\mathbf{x}_0$ at time $t = t_0$ is later (time t) located in the infinitesimal volume $d\mathbf{x}$ centred on $\mathbf{x}$. It is the role of the trajectory model, i.e. Lagrangian stochastic model, to determine the transition density $p\left(x, y, z, t | x_0, y_0, z_0, t_0\right)$.

2.5.2 Heuristic connection between concentration and forward trajectories

Suppose a Lagrangian model is able to compute the forward-in-time trajectories of particles emanating from a source in a turbulent flow, and suppose N_P paths are computed by the model. Let V be the volume of a detector standing at a certain point P downstream from the source, and let $\bar{t}$ be the average time that particles spend within that volume (i.e. the total residence time accumulated by all N_P particles, divided by N_P). Then we could say that if, in the real world, particles were released at the rate one-per second at the source the mean concentration in the detector would

be

$$C = \frac{\bar{t}}{V} \tag{2.35}$$

and it follows that if the real world source strength were Q units (particles or kilograms) per unit time, then

$$C = Q\,\frac{\bar{t}}{V}\ . \tag{2.36}$$

Thus it is clear that by means of a forward LS model it is possible to calculate the mean concentration field due to a source merely by calculating an ensemble of realistic trajectories. We will now switch attention to the nature of the algorithm for computing paths.

2.5.3 1st Order Lagrangian Stochastic Model

As established earlier, however fluid particles become initially "loaded" with c, once away from the source the concentration is constant along trajectories (Eq. 2.33). Accordingly if at time $t = 0$ a fluid element is "tagged" with the concentration c_0, its concentration will remain constant at $c = c_0$.

A "first order Lagrangian Stochastic model" is a method to compute the evolution of the state of a fluid element, where that state is considered to be its position and velocity, i.e. $(\mathbf{X}, \mathbf{U})$. A trajectory is broken up into finite segments, during each of which the increment in time is dt (where in general dt changes along the trajectory). A suitable model for the increment in velocity over a single time step is the "*generalized Langevin equation*" , i.e.

$$dU_i = a_i\left(\mathbf{X}, \mathbf{U}\right)\ dt + b_{ij}\left(\mathbf{X}, \mathbf{U}\right)\ d\xi_i \tag{2.37}$$

where $a_i\left(\mathbf{X}, \mathbf{U}\right)$ is the *conditional mean acceleration*, $d\xi_i$ is a vector of independent Gaussian random numbers each of whose variances is exactly dt, and b_{ij} is a model coefficient that, along with a_{ij}, needs to be determined. The companion to Equation (2.37) is

$$dX_i = U_i\, dt\ . \tag{2.38}$$

(Thomson, 1987) provided two criteria for the selection of the model coefficients. Kolmogorov similarity theory implies that

$$b_{ij} = \delta_{ij}\sqrt{C_0\,\varepsilon(z)} \tag{2.39}$$

where C_0 is a dimensionless (and supposedly universal) constant and ε is the turbulent kinetic energy dissipation rate (for which MOST can provide a formula, see below). The second criterion can be expressed as follows: if applied to compute the motion of a cloud of particles that were initially well-mixed in position and moving with velocities selected at random from the underlying velocity distribution of the flow, i.e. a cloud of particles in the maximum entropy state, a suitable model must have the property that those particles *remain* well-mixed in position and velocity. This is the "well-mixed condition," and since it was provided (Thomson, 1987) researchers have enjoyed a solid basis for the formulation of Lagrangian models. However only in the case of a model that computes a single component of motion (or several *independent* components) can the well-mixed condition select a unique model.

Suppose one wished to compute only the vertical motion of a particle, according to

$$dW = a_w(Z, W)\,dt + \sqrt{C_0\,\varepsilon}\,d\xi\ . \tag{2.40}$$

On the assumption that the probability density function $g_a(w)$ for the *Eulerian* vertical velocity w is a Gaussian with zero mean and variance σ_w^2

$$g_a(w;z) = \frac{1}{\sqrt{2\pi}\,\sigma_w(z)}\exp\left(-\frac{W^2}{2\sigma_w^2}\right) \tag{2.41}$$

the well-mixed condition provides the unique model defined by

$$a_w = \frac{C_0\varepsilon(z)}{2\sigma_w^2(z)}W\ +\ \frac{1}{2}\frac{\partial\sigma_w^2}{\partial z}\left(\frac{W^2}{\sigma_w^2}+1\right)\ . \tag{2.42}$$

The LS model for the evolution of the vertical velocity is therefore

$$dW = \left[-\frac{C_0\varepsilon(z)}{2\sigma_w^2(z)}\,W\ +\ \frac{1}{2}\frac{\partial\sigma_w^2}{\partial z}\left(\frac{W^2}{\sigma_w^2}+1\right)\right]\,dt\ +\ \sqrt{C_0\varepsilon}\,d\xi\ , \tag{2.43}$$

$$dZ = W\,dt\ . \tag{2.44}$$

Recall that $\sigma_w = \sigma_w(z)$ is an Eulerian velocity statistic, and that MOST gives a formula for its height variation (in a neutrally-stratified surface layer it is in fact constant, $\sigma_w = 1.3u_*$).

It remains to prescribe the $C_0\varepsilon$ product. In homogeneous and stationary turbulence it is possible to relate this to an effective Lagrangian decorrelation timescale

$$T_L = \frac{2\sigma_w^2}{C_0\varepsilon} \; . \tag{2.45}$$

More generally, in a horizontally-homogeneous atmospheric surface layer the profile of ε is

$$\varepsilon = \frac{u_*^3}{k_v z} \; \phi_\varepsilon \left(\frac{z}{L} \right) \tag{2.46}$$

so that it will suffice to choose a fixed value for C_0, the universal dimensionless constant. This amounts to a *calibration* of the LS model.

That (effectively) was done by (Wilson *et al.*, 1981(c)), who optimized the agreement of this LS model with the Project Prairie Grass dispersion trials. Their parameterization for unstable and stable conditions is

$$\frac{2\sigma_w^2}{C_0\varepsilon} = T_L(z) \;\; = \;\; \frac{0.5z}{\sigma_w} \left(1 - 6\frac{z}{L} \right)^{\frac{1}{4}} , \; L < 0 \tag{2.47}$$

$$\frac{2\sigma_w^2}{C_0\varepsilon} = T_L(z) \;\; = \;\; \frac{0.5z}{\sigma_w} \left(1 + 5\frac{z}{L} \right)^{-1} . \; L > 0 \tag{2.48}$$

Eqns. (2.44, 2.44) supplemented by the above formulae for $C_0\varepsilon$ constitute an excellent model for simulation of particle trajectories in the horizontally-homogeneous surface layer, for one may add an alongwind component of motion at the local Eulerian mean velocity $\overline{u} = \overline{u}(Z(t)))$.

Now in the above discussion, the alongwind fluctuation $u^{'}$ had been ignored. Should one include a u' whose correlation with w' is neglected, no complication ensues. However in practice u' *is* correlated with the vertical velocity w', and so one would like, ideally, to accommodate that fact. Doing so leads to a model that, though well-mixed, is not unique. This is an as yet unsolved issue.

However in practise a suitable LS model for multi-dimensional motion in Gaussian inhomogeneous turbulence has been provided, by (Thomson, 1987). We will here cite his two-dimensional model, which includes the Lagrangian alongwind velocity

fluctuation (here symbolized U'):

$$dU' = -\frac{C_0\varepsilon}{2\sigma^2}\left(U'\sigma_w^2 - W\overline{u'w'}\right)dt + \frac{\varphi_u}{g_a}dt + b\,d\xi_u\,, \tag{2.49}$$

$$dW = -\frac{C_0\varepsilon}{2\sigma^2}\left(W\sigma_u^2 - U\overline{u'w'}\right)dt + \frac{\varphi_w}{g_a}dt + b\,d\xi_w\,, \tag{2.50}$$

$$dX = \left[\overline{u}(Z) + U'\right]dt\,, \tag{2.51}$$

$$dZ = W dt\,. \tag{2.52}$$

In these equations $\sigma^2 = \sigma_u^2\sigma_w^2 - u_*^4$, and $g_a(U', W)$ is the height-dependent Eulerian velocity pdf. The new functions φ_u and φ_w are defined

$$\frac{\varphi_u}{g_a} = \frac{1}{2}\frac{\partial\overline{u'w'}}{\partial z} + \frac{1}{2\sigma^2}\left[\frac{\partial\sigma_u^2}{\partial z}\left(\sigma_w^2U'W - \overline{u'w'}W^2\right) + \frac{\partial\overline{u'w'}}{\partial z}\left(\sigma_u^2W^2 - \overline{u'w'}U'W\right)\right] \tag{2.53}$$

$$\frac{\varphi_w}{g_a} = \frac{1}{2}\frac{\partial\sigma_w^2}{\partial z} + \frac{1}{2\sigma^2}\left[\frac{\partial\sigma_w^2}{\partial z}\left(\sigma_u^2W^2 - \overline{u'w'}U'W\right) + \frac{\partial\overline{u'w'}}{\partial z}\left(\sigma_w^2U'W - \overline{u'w'}W^2\right)\right]\,. \tag{2.54}$$

Clearly this model for the evolution of the particle velocity $(\overline{u} + U', W)$ is much more complex than the "one-dimensional" LS model which treates the total particle velocity as being $(\overline{u}, W)$. In most dispersion problems the added complexity buys only a minor gain in accuracy.

It is natural to think in terms of time-forward Lagrangian stochastic models, but in the context of inverse dispersion it is very advantageous to be able to compute paths backwards in time.

2.5.4 Backward Lagrangian Stochastic Model

To compute trajectories backward-in-time a trivial modification to the LS algorithm is needed, but we shall not document that step as it amounts to a tangent. Assuming we can compute backward paths, how does this give us the $C - Q$ relationship that, in the context of inverse dispersion, is the essence of the problem? That relationship was foreshadowed in Section (2.4.2), but we will reiterate here.

Suppose a time-average gas concentration rise $(C - C_{BG})$ relative to background C_{BG} has been measured using a detector in a place distant from a source. The source emits gas at an unknown rate $Q\,[\mathrm{kg\ s^{-1}}]$. The bLS model computes N (many

thousands of) imaginary particle trajectories released independently from the location of the concentration sensor, and for each touchdown on ground records the location and vertical velocity (x_i, y_i, w_i). That data provides

$$\left(\frac{C}{Q}\right)_{\text{simulated}} = \frac{1}{N} \sum_i I\left(x_i, y_i\right) \frac{2}{|w_i|} \tag{2.55}$$

which in combination with the measured concentration enables the inference

$$Q = \frac{C - C_{BG}}{(C/Q)_{\text{simulated}}} \,. \tag{2.56}$$

Used this way the bLS model is flexible and efficient (Flesch, 1996). It provides a means to measure gas emissions from multiple distributed sources (Ro *et al.*, 2011).

2.6 Application of ID technique - WindTrax

The software WindTrax 2.0 is a windows-based computer program developed by Thunder Beach Scientific (B. Crenna). The software allows to simulate short range turbulent transport in the atmospheric boundary layer, using (depending on the problem at hand) a forward- or backward- Lagrangian stochastic model, specifically the Thomson 3-dimensional model for vertically-inhomogeneous Gaussian turbulence. The software provides a user interface upon which one is able to superpose a satellite image of the site, and onto which one may deposit (or draw) sources and detectors of arbitrary geometry. Once linked to a column-organized input file containing concentration data along with necessary meteorological information, WindTraX runs the Lagrangian model to compute (for example) $(C/Q)_{\text{simulated}}$.

Obviously WindTrax requires information about the condition of the surface layer, or more specifically the velocity statistics (and anything else needed to model their variation with height). Specifically, the needed atmospheric inputs are: the friction velocity u_* (Eq. 2.4), the Obukhov length L (Eq. 2.7), the mean wind direction θ and the surface roughness length z_0. Other wind statistics σ_u, σ_v and σ_w can be input, but if they are not, then WindTraX computes them using well-established MOST formulae. Mean air temperature and local pressure are also needed, if concentrations were measured in mixing ratio units (ppm or ppb).

It is frequently the case that more than one source exists, and several concentration sensors are deployed. Suppose there are M_Q sources and one has made M_C

measurements of the concentration rise above a known background concentration C_{BG}. Let Q_j $(j = 1...M_Q)$ label the unknown source strengths and $C_j\,(j = 1...M_C)$ the measured concentrations.

If $M_C < M_Q$ the problem is "underdetermined" and cannot be solved. If $M_C > M_Q$ the problem is "overdetermined" and can be solved to obtain several independent estimates of the Q_j; for example if $M_Q = 1$ but $M_C = 2$ one can obtain two estimates of the Q, depending on which of the two C_j one has dropped (ignored). From the two estimates one could (for example) take an average. Some subjectivity is entailed in choosing the solution to an overdetermined problem. WindTrax provides the "best fit in the least squares sense."

Now suppose $M_Q = M_C$. In this case the inverse dispersion problem, neither over- nor under-determined, can be stated as the matrix problem (Crenna *et al.*, 2008):

$$a_{ij}Q_j + C_{BG} \;\; = \;\; C_i \tag{2.57}$$

where summation over j is implied. The solution is

$$Q_j = a_{ij}^{-1}\;\left(C - C_{BG}\right)_i\;. \tag{2.58}$$

It would appear, then, that one can easily handle multiple sources by including the same number of measurements of a concentration rise. In reality there can be problems in that, depending on the wind direction and the relative sizes, strengths and positions of these sources, the matrix a_{ij} whose inverse is (in effect) needed to procure the solution can be "ill conditioned," meaning there is a large level of uncertainty in the solution (Flesch *et al.*, 2009).

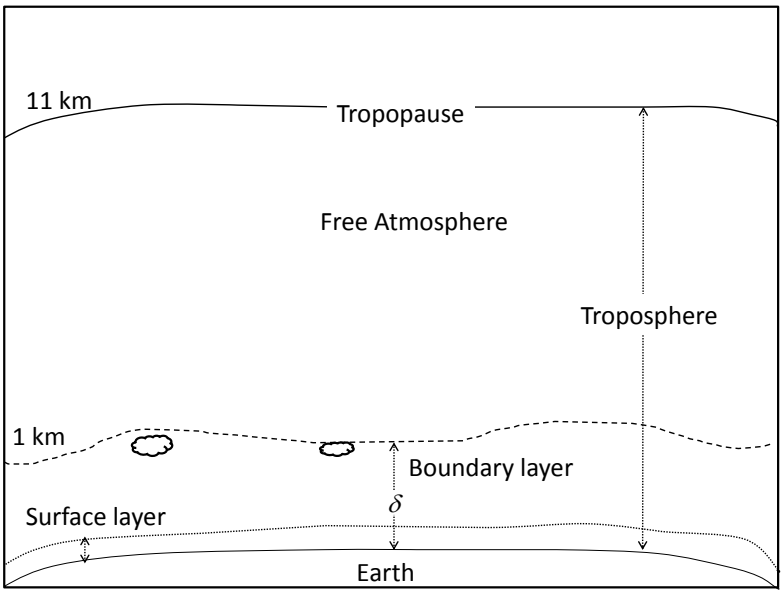

Figure 2.1: Different layers of the troposphere: the surface layer, boundary layer and free atmosphere.

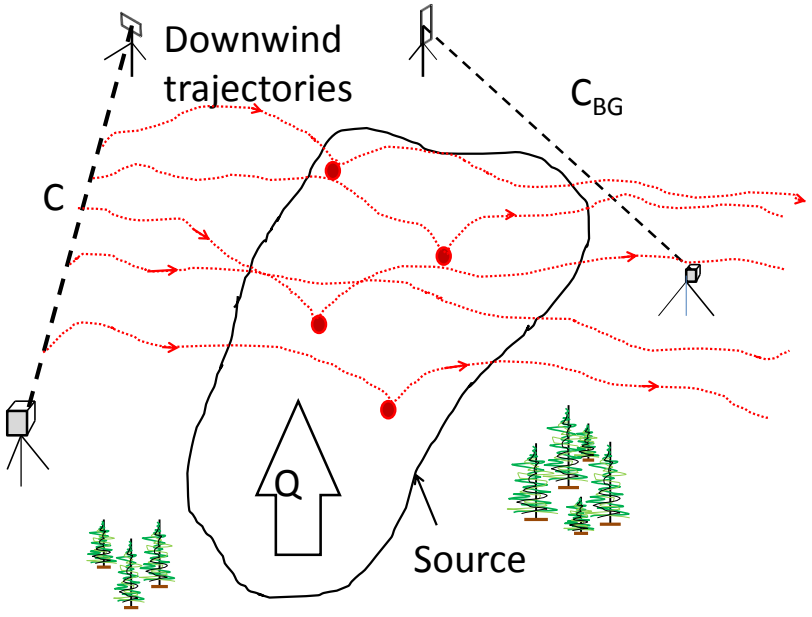

Figure 2.2: Inverse dispersion

Chapter 3

Background methane concentration in and near Edmonton

Chapters (4,5) of this thesis demonstrate the application of inverse dispersion, using specifically the backward Lagrangian stochastic (bLS) method, to infer surface-to-air methane fluxes from local surface area sources. The key measurement $(C - C_{BG})$ underlying bLS is the *increment in concentration* relative to *background concentration* (C_{BG}) that is attributable to the source. Typically in applying bLS one will measure both C and C_{BG}, with each of which is associated some measurement uncertainty ϵ, ϵ_{BG} such that the uncertainty in the mean concentration rise $C - C_{BG}$ is $\pm(\epsilon + \epsilon_{BG})$. In some circumstances, e.g. malfunction of one or more of the concentration detectors, or contamination of the "background" concentration measurement by wafts of methane loaded air born in during an unwanted excursion of the wind direction, it is tempting to substitute (i.e. impose) an *assumed* background concentration, considered representative for the area. Chapter 1 surveyed what is broadly known about ground level methane concentrations over mid- to high-latitude northern hemisphere continents; a figure of about $[CH_4] = 1.8 - 2.0$ppmv is considered normal. Of course the "background" level that actually prevails must reflect many (poorly known, and not necessarily time-invariant) factors, in particular the *true* spatial distribution and strength of diverse sources – including, in the case of Alberta, natural biogenic emissions (from wetlands), agricultural emissions (principally from cattle), fugitive emissions from the oil and gas industry, and other industrial emissions. In addition, the background concentration measured at any particular point must also reflect the prevailing meteorological conditions, viz. mean wind direction and speed, depth of

turbulent mixing, and thermal stratification. It is evident, then, that one *ought not to expect* an unvarying background concentration, and there is ample reason not to be surprised by diurnal and seasonal patterns.

The definition of exactly what is meant by the "background level" of methane is (in the present context) appropriately left a little vague. Loosely, the natural background is that hypothetical level of concentration that would prevail in the *absence* of "nearby" sources. In Chapters (4,5) the background concentration is that prevailing immediately upwind of the waste management centre – or even, in some particular cases, the level immediately upwind of a specific local source, a level that may already reflect the contribution of (other) upwind local sources.

In the context of this study then, and more broadly in the context of ongoing bLS measurements taking place around Central Alberta, it was of interest to confirm pre-existing estimates of normal atmospheric methane concentrations in and around Edmonton. To that end, methane concentrations were monitored continuously, using an open path, infra-red laser gas detector, both in central Edmonton on the University of Alberta campus (for about 6 weeks) and (for a few days, only) at the University of Alberta research farm at St. Albert, a few kilometers outside Edmonton (Figure 3.1).

3.1 Measurements in Edmonton

Measurements were conducted on the roof of the Henry Marshall Tory Building, on the north campus of the University of Alberta. The Tory Building is a fourteen story tower with a height of 58.2 m. The location was chosen not only for its convenience and the high security it offers, but more importantly because measurements some 60 m away from ground should have sampled a well mixed background concentration. The weather data used in analysis of these measurements is drawn from observations at the Tory weather station, i.e. from instruments co-located with the methane detector. Continuous automatic measurements of methane concentration were made by a PKL open path, infra-red laser detector.

The Tory measurements spanned June 28th to July 30th ("summer"), and September 29th to October 14th ("autumn"), 2010. Across this interval the data record is discontinuous, but covers about 31 days of summer and 16 days of autumn. The

source-detector path length of the PKL system was 45 m, and each reading consisted of a line average concentration averaged over a four second interval. The laser and the reflector (Fig. 3.2) were placed in opposite corners of an open (low-walled) rooftop space that measured 46.97 m by 10.99 m. The laser (source) height was $z_{laser} = 1.5\,\mathrm{m}$ while the reflector was much lower.

As indicated above, the point of the measurements was to establish the background methane concentration in Edmonton, and if possible throw light on the question of whether there is a *predictable* daily cycle, hypothetically related to the strength of atmospheric mixing. It was also hoped that there might be a demonstrable correlation between the observed "bulk" (background) atmospheric methane concentration and the principal environmental factors, especially hourly mean wind direction (θ), on the principle that variations in $[CH_4]$ might reflect nearby emissions from (hypothesized) upwind industrial sources, generally the petro-chemicals industries located in north-east Edmonton and in Fort Saskatchewan, i.e. broadly NE of the university campus. In this analysis the data are referred to as "summer" for the interval (28 June – 30 July, 2010) and "autumn" for the interval (29 Sept.– 14 Oct., 2010). In terms of data quality control, the only intervention was that the laser light level (i.e. strength of the reflected beam) should exceed the minimum acceptable level recommended by the manufacturer.

3.2 Daily cycle of methane concentration

Figs. (3.3, 3.4) plot the fifteen-minute mean concentrations for individual days, showing also the mean, maximum and minimum values. These graphs convey that there was strong variation from day to day, particularly during the autumn period.

To look for sign of any coherent daily cycle, Figs. (3.5–3.6) give the time series of 15-min concentration for 3 days of summer and 3 days of autumn, taken as example. (Graphs for all 31 days of summer and 16 days of autumn can be found in an Appendix). For the summer period minimum and maximum values ranged from 1.5ppm to 2.8ppm, while during autumn minimum and maximum values ranged from 1.3ppm to 3.1ppm. Concentration variability in autumn was much stronger than during summer. The oscillatory concentration variations measured 17–27 July are suspicious, as

there is no obvious mechanism for such behaviour; they are provisionally regarded as being false.

Figs. (3.7, 3.8) show the mean daily cycle of methane concentration for the summer and autumn periods. Each plotted point represents the 15 minute average concentration (at a certain time after sunrise) averaged over 31 (or 16) days. Methane concentration attains its minimum value around sunset, after which it increases gradually; and during daytime, while the pattern is not regular, broadly the concentration decreases. In summer the daytime average concentration is 2.109 ppm while in autumn the corresponding value was very similar, viz. 2.121 ppm. The respective nighttime averages were also very similar, viz. 2.140 ppm and 2.144 ppm. Not surprisingly then, the 24-hr average values for summer and autumn were almost indistinguishable, at 2.12 ppm and 2.13 ppm.

3.3 Methane concentration in relation to atmospheric conditions

It is natural to assume that the observed (irregular) daily cycle in methane concentration might be driven by varying strength of methane sources located in and around Edmonton, and/or variability in atmospheric conditions, in particular wind direction and mixing depth of the atmospheric boundary layer (ABL). Therefore a straightforward graphical analysis was performed to look for correlation between the observed atmospheric variables and diurnal cycle of methane concentration.

Figs. (3.9(a), 3.9(b)) show that there was no obvious correlation, in summer or autumn, between hourly mean methane concentration and the corresponding hourly mean wind direction. This would suggest that local sources in and around Edmonton are either of negligible strength, or are distributed rather uniformly. The hourly average methane concentration has been plotted in Figs. (3.10, 3.11) against the corresponding wind speed ($\mathrm{m\,s^{-1}}$), pressure (P), temperature(T) and humidity. Again, no obvious correlation was noted.

3.4 St. Albert field work

Measurements outside the city at the University of Alberta farm in St. Albert spanned only three days, 30 July – 2 Aug. 2010 (Fig. 3.12). The methane detector was operated with a path height of 1.5 m and with various path lengths (88 – 132 m) at two different locations, in each case over a wheat field and surrounded by a mix of wheat and canola crops. There were oil operations in the vicinity, including an oil well (not operational at the time). The observed signals did not show any evidence of local emissions related to the well and/or a nearby pumping station.

Due to instrument failures the record from these measurements is intermittent, and does not warrant an elaborate analysis. Fig. (3.13) shows the discontinuous time series of 15 minute average methane concentration at the farm site. The salient point to be made is that the average concentration was found to be 2.114 ppm, i.e. indistinguishable from average values in the City of Edmonton.

Figure 3.1: Location of the measurement sites in Edmonton and St. Albert

(a) Laser (b) Reflector

Figure 3.2: Laser and reflector setup on roof of Tory building.

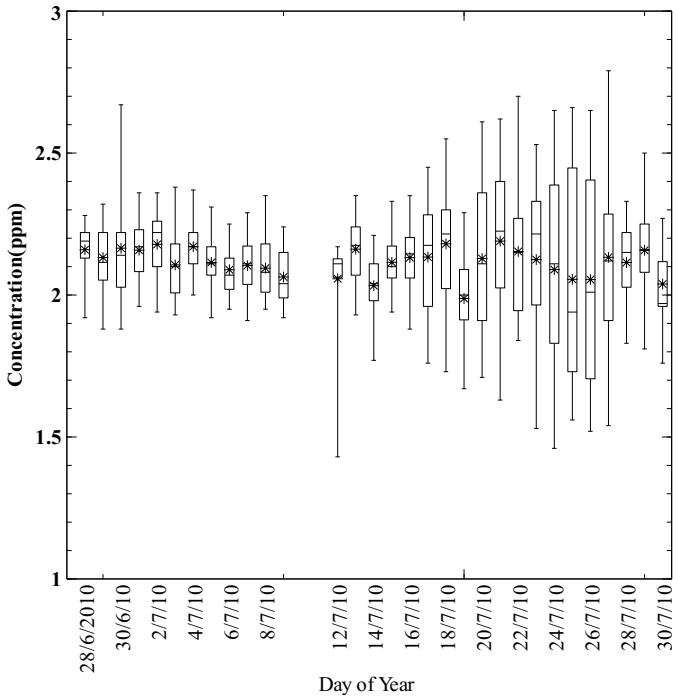

Figure 3.3: Daily average, standard deviation, maximum and minimum concentrations for the 31 individual days of the "summer" period. (The star represents the daily average.)

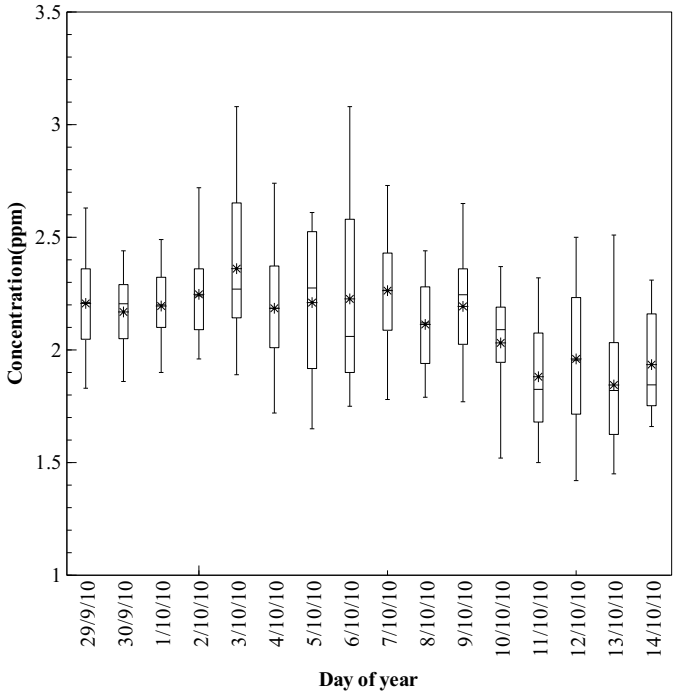

Figure 3.4: Daily average, standard deviation, maximum and minimum concentrations for the 16 individual days of the "autumn" period. (The star represents the daily average.)

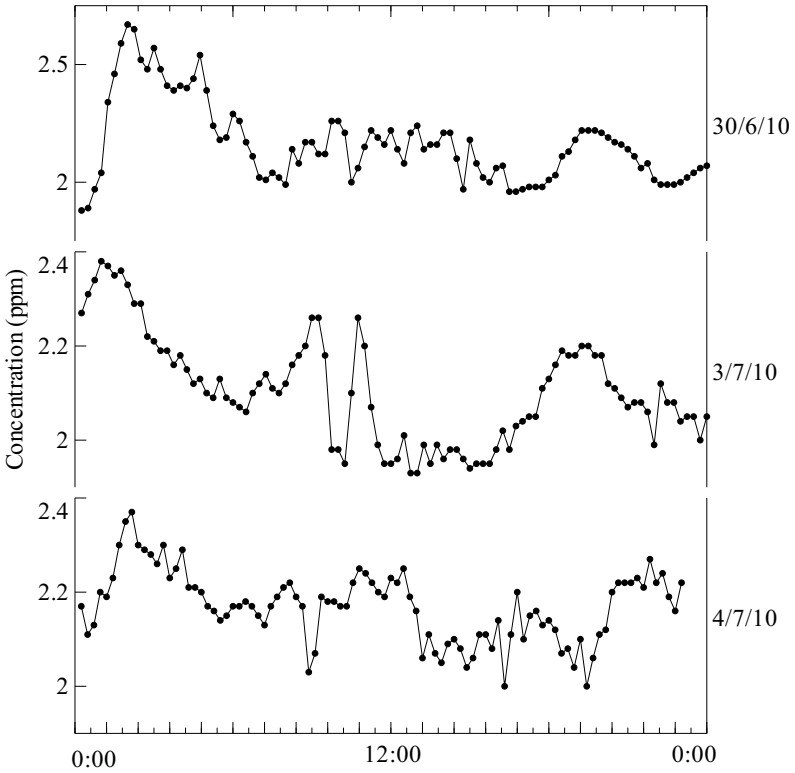

Figure 3.5: The 15 minute average concentration ppm of three individual day has been plotted in a time series graph for 30/6/10, 3/7/10 and 4/7/10 of "summer" period. Date of the corresponding day is indicated in right hand side of the graph. These three days have been selected randomly.

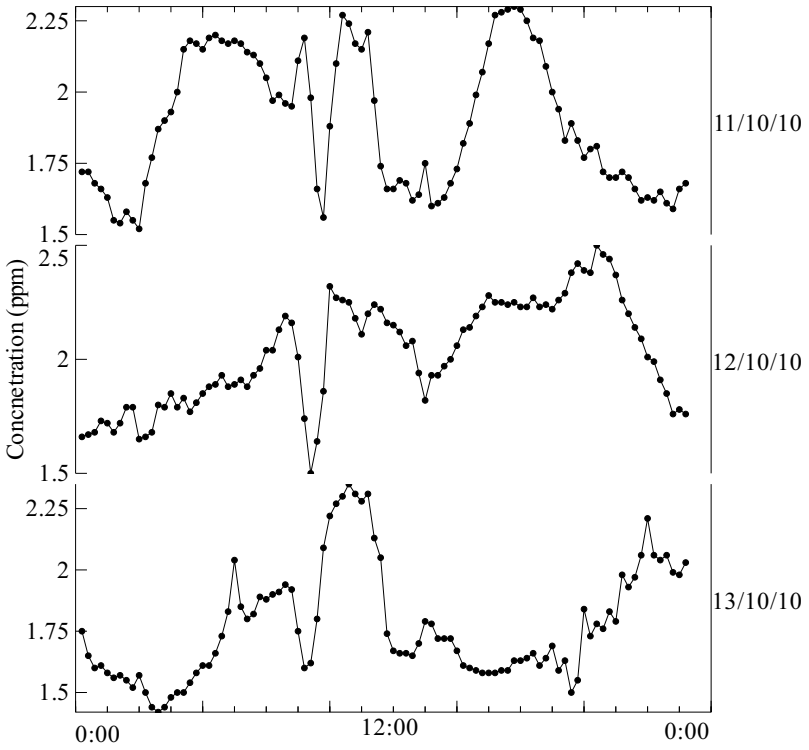

Figure 3.6: The 15 minute average concentration ppm of each individual day has been plotted in a time series graph from 11/7/10 to 13/7/10 of "autumn' period'. Date of the corresponding day is indicated in right hand side of the graph.

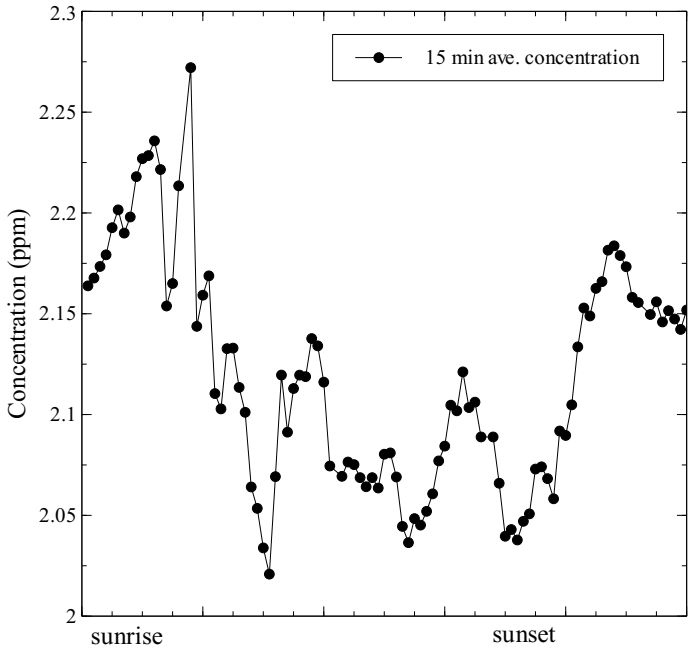

Figure 3.7: Average methane concentration of 15 minute interval for "summer" period from sunrise to sunset

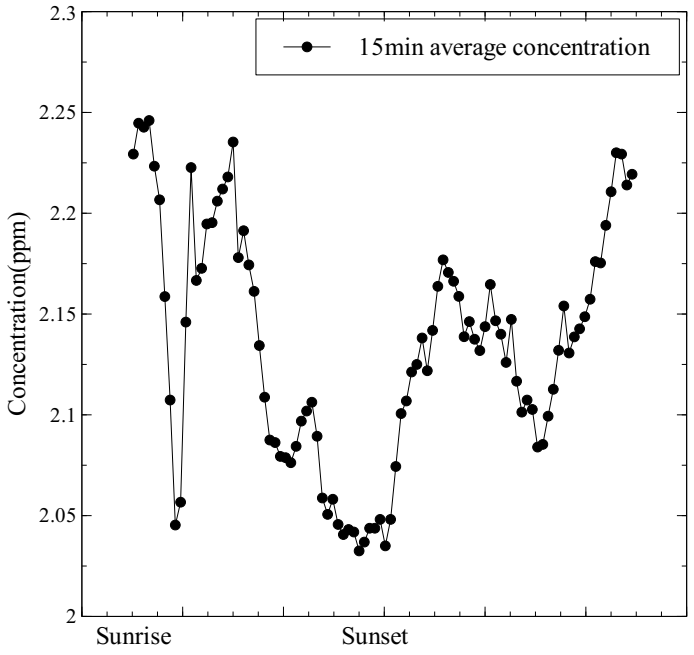

Figure 3.8: Average methane concentration of 15 minute interval for "autumn" period from sunrise to sunset

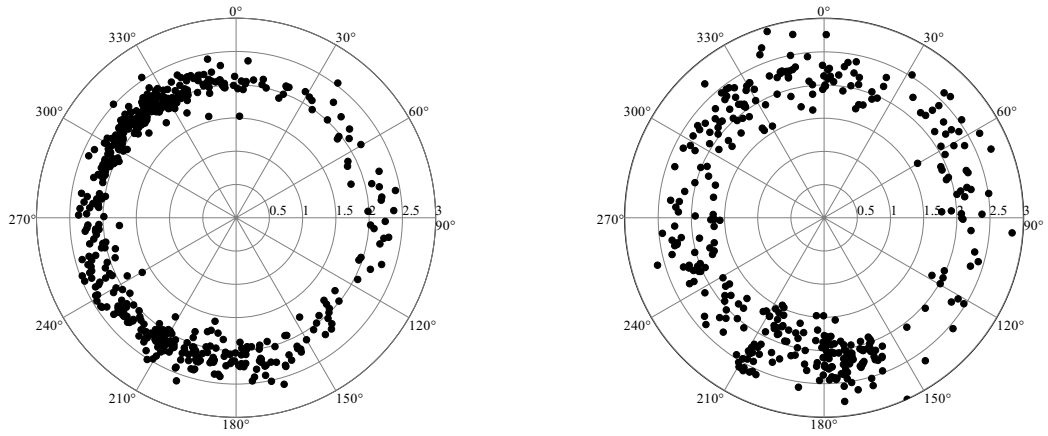

(a) "summer" (b) "autumn"

Figure 3.9: Hourly average concentration with corresponding wind direction for "summer" period and "autumn" period.

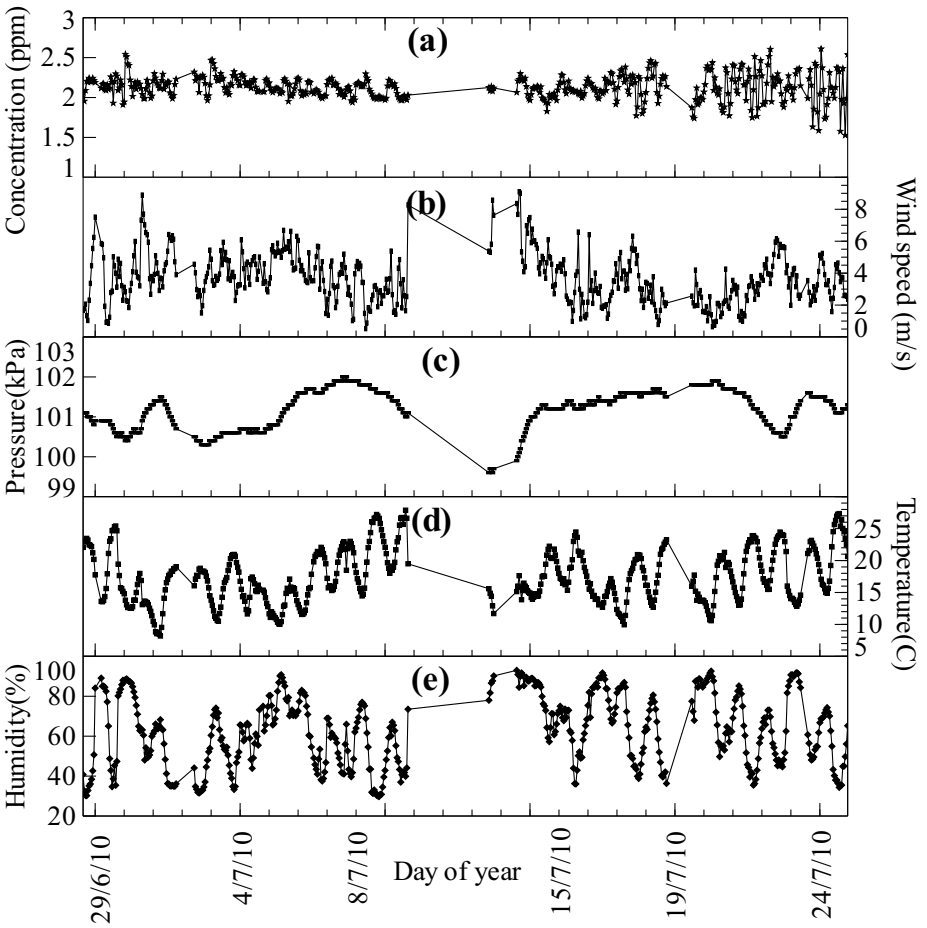

Figure 3.10: Hourly average methane concentration and different atmospheric variables for "summer" period. Hourly average (a) methane concentration in ppm, (b) wind speed in $\mathrm{m\,s^{-1}}$, (c) atmospheric pressure in kPa , (d) temperature in C and (e) humidity in % .

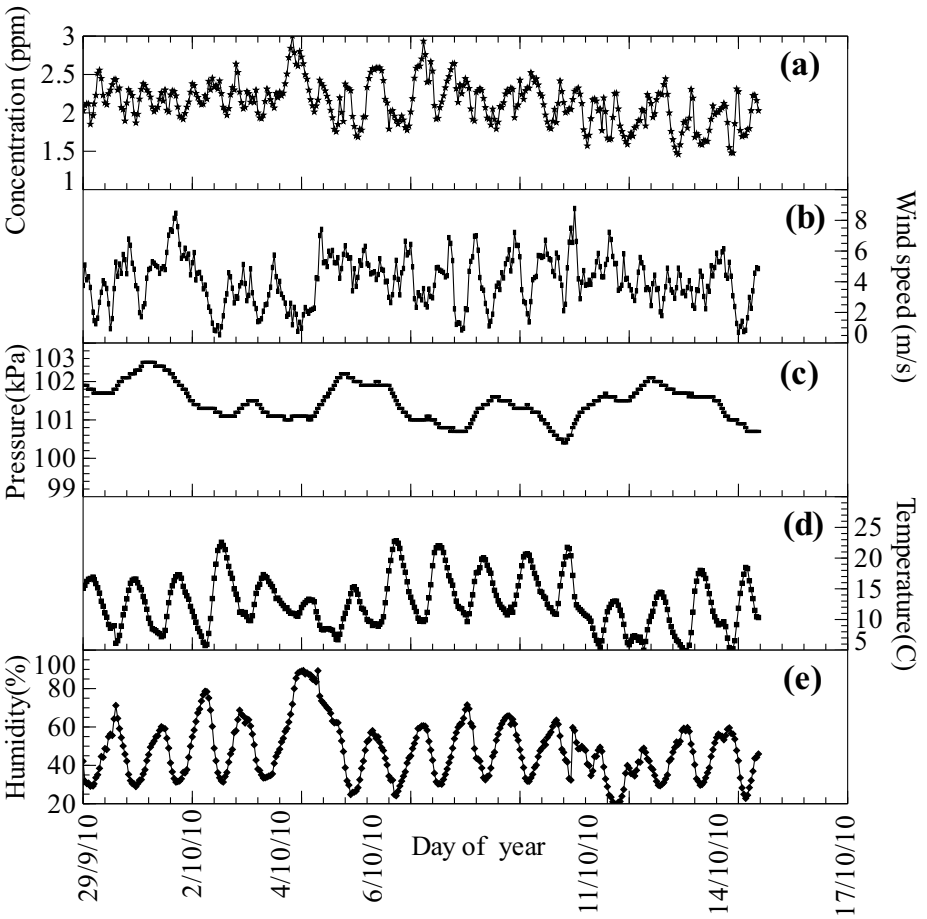

Figure 3.11: Hourly average methane concentration and different atmospheric variables for "autumn" period. In figure time series graph of hourly average (a)- methane concentration in ppm, (b) wind speed in $\mathrm{m\,s^{-1}}$, (c) atmospheric pressure in kPa , (d) temperature in C and (e) humidity in % .

Figure 3.12: Site of methane measurements at University of Alberta Farm, St.Albert.

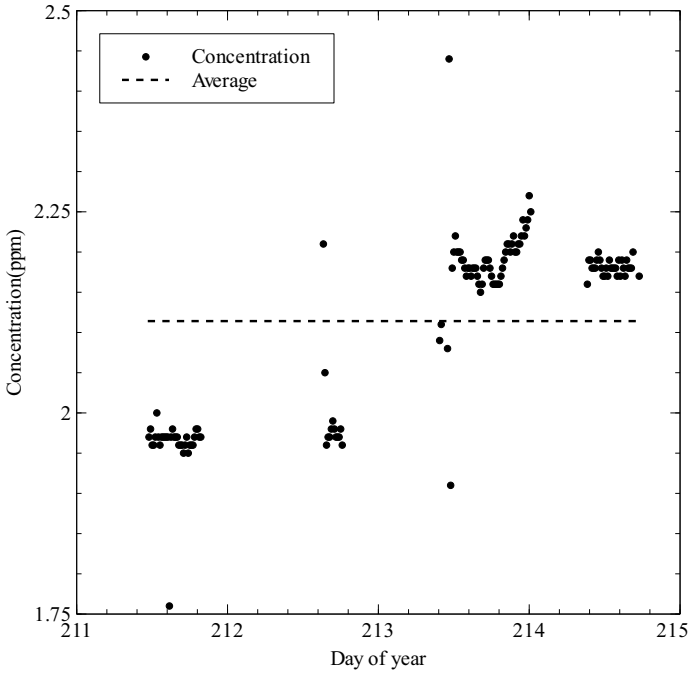

Figure 3.13: 15 minute average methane concentration at St. Albert

Chapter 4

Inverse Dispersion Method Applied to Waste Lagoons

The rate of emission to the atmosphere from a source having a known location can be deduced by measuring the downwind concentration at one or more points, along with relevant information to determine the state of the atmosphere (e.g. mean wind direction, mean wind speed and thermal stratification), and a knowledge (or measurement) of background concentration. Given the possible multiplicity of sources that may affect concentrations at multiple sensors, and the role of wind direction in rendering any one source influential (or otherwise) as regards concentration at any one particular detector, the analyst is called on to make informed decisions as to a satisfactory or optimal configuration for an inverse dispersion analysis.

In this chapter several alternative implementations of the inverse dispersion method are described, in a context that entails multiple area sources. These "alternative implementations" illustrate a range of:

(a) *Different possibilities as to the prescription of background concentration*, e.g. imposed a priori, or equated to the concentration at a sensor known (with certainty) not to have been influenced by the local sources, or treated as unknown and to be deduced from the suite of available concentration data

(b) *Different possibilities as to the number of discrete sources to be quantified*, e.g. focus on a single source by selecting wind directions that eliminate the influence of all others on concentration detectors, or use multiple sensors to (simultaneously) deduce strengths of multiple sources and possibly (also) background con-

centration – with the overall constraint that number of measurement locations for mean concentration must equal or exceed number of unknowns

The inverse dispersion calculations have been made using WindTraX, which performs the necessary dispersion calculations using a well verified Lagrangian stochastic (LS) trajectory simulation model run in backward (bLS) or forward (fLS) mode. WindTraX provides a computational environment for representing the site and instrument layout (mapping), for setting up the wanted "analysis configuration," and for managing the input and output files. Input files contain column-organized time series of (say, 15-min) mean gas concentrations, wind directions and other meteorological data, etc. Output files contain the corresponding time series of quantities that have been calculated by WindTraX, e.g. emission rates.

4.1 Details of Experiments Determining Methane Emissions

The site of the experiments to be described (Figure 4.1) was a municipal waste treatment center having an overall area of 65 hectares ($1\text{hectare} = 10000\,\text{m}^2$). At this centre biosolids from a distant wastewater treatment plant are stored and settled in six sewage lagoons, of which the largest, which will be designated "NE lagoon", is located east of the others at the northeast extremity of a landfill. GPS measurements determined the area of this largest lagoon to be $450 \times 250\,\text{m}^2$, while the collective area of all the other ponds is approximately $450 \times 450\,\text{m}^2$.

Methane concentration was measured with three open path infra-red lasers, using path lengths of order 100 m. Two of the lasers (those designated C_1, C_3) were manufactured by Boreal Laser ("Gas Finder"), while the other (designated C_2) was manufactured by PKL. Broadly, these devices measure the line-averaged concentration of any absorbing gas from the reduction in received spectral intensity over a narrow band attuned to an absorption band of the gas in question. Simultaneous measurements of received intensity in a second waveband *that is not subject to atmospheric absorption* permit to correct (automatically) for variations in the intensity of the source (infra-red laser) and the reflectivity of the retro-reflector. For each sensor the line-average concentration along the path between laser and retro-reflector was

processed to give a 15-min time average. Prior to the methane flux measurements the three lasers were operated side-by-side upwind of the waste treatment centre for an intercomparison of their responses to identical signals (at the background level). Based on that information, corrections were thereafter applied in order to eliminate (or at least reduce) any inter-instrumental bias.

Three lasers were positioned around the large (NE) lagoon, with the objective of determining 1) background concentration, 2) the influence of the other ponds, and 3) the emission rate of the NE lagoon. Boreal laser (C_1) was located on the eastern edge with a 92 m pathlength, PKL laser (C_2) ran along the northern edge with a 104 m path (covering about half of the width of the lagoon), and Boreal laser (C_3) with pathlength 74 m (about 20% of the main lagoon's north-south span) was located on the western edge, standing between the NE lagoon and the suite of five other smaller ponds. This third laser was best placed to detect the influence (impact) of the other sources of methane, i.e. not only the five smaller ponds but conceivably also other sources at the site, including landfill.

The wind direction anticipated for the trials was northwest. Accordingly the sonic anemometer was placed on the eastern edge of the NE lagoon (at a height of 0.96 m and with a fetch, in NW wind, of about 300 m), and experimental runs were rejected (filtered out) if there was an easterly component to the wind, i.e. for all runs analyzed here the mean wind direction $180^{\circ} \leq \theta \leq 360^{\circ}$. The PKL laser ($C_2$) was positioned so that it might determine the background concentration. The height of the laser light paths was about 1 m. Figure (4.1) represents the experimental layout of the measurements.

Figure (4.2) gives the time series of the 15-min mean wind direction and the 15-min mean line-averaged concentrations. As one would expect, during the sustained period of (roughly) WNW winds (mean wind direction $\theta \sim 300^{\circ}$) laser C_2 on the north bank detected a low (plausibly background) methane concentration (of around 2-3 ppm), while laser C_3 on the west bank saw a somewhat higher concentration reflecting the influence of (potentially) the smaller ponds and of the landfill. Of course C_1 on the east (downwind) bank saw elevated concentrations.

Let **U** (with N members) designate the set of all 15-min runs (i.e. periods of measurement). From some (though not necessarily all) of these runs one may *potentially*

extract an estimate of (say) the emission rate of the main (NE) lagoon. The main objective of this chapter is to illustrate the factors that must be considered, and decisions that must be made, in order to arrive at meaningful estimates of gas emission rate from the Inverse Dispersion (ID) method. For any given run, will one impose a *presumed* value of background concentration, will one take the view that one (or more) of the detectors gives that value directly (without need of any bLS analysis) by virtue of its being positioned upwind of all local sources, or will one configure the analysis so as to *infer* background concentration along with one or more emission rates? In any given run, which detectors may have detected methane from more than one of the ponds? In this thesis such prior decisions are said to define the "analysis configuration." The observations during any particular run may be analyzed in several manners, by adopting several alternative analysis configurations, which will provide several alternative estimates $Q_1, Q_2, ...$ of (for example) an emission rate. These different estimates will in general not all be equal, and one will need to decide which analysis configuration provides the highest confidence in the estimate.

It follows from the above that, depending on detector layout and the analysis configuration adopted for ID analysis, it will usually be appropriate to analyze only a subset $\mathbf{V} \in \mathbf{U}$ (with n members) of all available measurement periods, leading (say) to n estimates of source strength. For example, if (in the chosen configuration) a given laser is assumed to measure background concentration, one will need to ensure the set $\mathbf{V}$ of runs to be analyzed does not include those whose wind direction had possibly (or certainly) caused this laser's light path to occasionally (or constantly) intersect the methane plume off a local source. "Input-filtering" refers to the elimination from WinTraX *input* files of all those runs that are *incompatible* with the chosen analysis configuration.

Irrespective of the analysis configration, in every case the experimental data $\mathbf{U}$ has been filtered to require that the mean wind direction satisfies $180^o \leq \theta \leq 360^o$, in order to eliminate cases where the sonic anemometer, positioned on the east bank to determine winds with a westerly component, was in reverse flow. Figure (4.2), shows time series of mean wind direction and methane concentration measured by the three lasers. The time series of calculated temperature, friction velocity (u_*), roughness length (z_0), and Obukhov length (L) has been shown in Figure (4.3).

Some of the n estimates (of one or more source strengths, and possibly background concentration) stemming from implementation of WindTraX in a given configuration may be eliminated by imposing of additional criteria, e.g. satisfactory distribution of trajectories linking a source to a detector. This step will be referred to as "Output-filtering," for it refers to rejection of *outputs* from WindTraX. For every analysis configuration WindTrax output data has been filtered by requiring the satisfaction of the following two conditions:

Condition 1: *Well-defined micrometeorological state* – acceptable runs must have friction velocity $u_* \geq 0.1\,\mathrm{m\,s^{-1}}$, roughness length $z_0 \leq 0.1$ m, and Obukhov length $|L| \geq 5$ m

Condition 2: *Source of interest must be linked to detector(s) by a large ensemble of wind paths* – in addition to satisfying Condition 1, the fractional area of the source covered by touchdowns must exceed 10%

In some cases a further **Condition 3** has been invoked, restricting the acceptable range of wind directions more stringently than had been done at the input file.

4.2 Results across a range of ID configurations

4.2.1 Configuration A: upwind laser gives background; single downwind laser

In this configuration (Figure 4.4) downwind laser (C_1)'s concentration determines the emission rate for the lagoon, with the signal from the upwind laser (C_2) interpreted as being the background concentration (C_{BG}). Only one quantity (Q_1) (emission rate of the lagoon) is considered to be unknown. The other ponds are treated as inactive methane sources (i.e. their source strength is treated as being zero) and the signal from laser (C_3) on the west bank of the lagoon is not used. A compact symbolic representation of this configuration is:

$$C_{BG} = C_2\,, \tag{4.1}$$

$$aQ_{1A} + C_{BG} = C_1\,. \tag{4.2}$$

Of course depending on the wind direction, this configuration risks to falsely ignore the influence of the five smaller ponds. Obviously too, since it is assumed that C_2

is exposed to background concentration, it is essential to exclude periods when the wind has a southerly component advecting methane off the large lagoon to C_2; hence it was required that $270^o < \theta < 360^o$ (condition 3). Figure (4.5) is a screen shot of WindTrax while analyzing data for configuration A.

Results for configuration A

When the emission rates given by WindTraX are filtered according to Conditions 1, 2 & 3 the average emission rate of the large lagoon was found to be $78\,\mathrm{kg\,hr^{-1}}$ (see Table 4.1). The maximum value found was $137\,\mathrm{kg\,hr^{-1}}$, occuring during an interval with wind direction $\theta = 287^o$, while the minimum value of $16.7\,\mathrm{kg\,hr^{-1}}$ occurred during a period when $\theta = 352^o$. No negative estimates for source strength arose with the analysis configured in this way.

Associated with the largest analyzed emission rate (i.e. $137\,\mathrm{kg\,hr^{-1}}$ with mean wind direction $\theta = 287^o$) was a value for the confidence ratio[1] $\sigma_Q/\langle Q\rangle$ of 5%. The wind speed during that run was also high (see Figure 4.7). Nothing relating to the analysis suggests any problem, and one may only conclude that other ponds had (in effect) provided a background concentration differing from that detected on the north bank by laser C_2, so that a more stringent restriction on wind direction needed to be imposed. The lowest analyzed emission rate was also associated with a confidence ratio $\sigma_Q/\langle Q\rangle = 5\%$, but the mean wind speed in this case was small ($1.10\,\mathrm{m\,s^{-1}}$). It is reasonable to suggest inverse dispersion analysis is less reliable in light winds, because a light wind field is liable to be less well described by the Monin-Obukhov similarity theory.

As laser C_2 had provided a concentration that was directly adopted as background in the WindTrax calculation, here the background concentration value has not been filtered with any condition. The average value of the background concentration ($\langle C_{BG}\rangle$) was 2.40 ppm. The maximum and minimum values were 17.7 ppm (with mean wind direction $\theta = 324^o$) and 1.8 ppm (with $\theta = 342^o$). The minimum value occurred during a period when the concentration was steady, with an average

[1]The confidence ratio is provided by WindTraX, which actually gives 10 estimates of all inferred quantities by breaking the ensemble of trajectories into ten sub-ensembles. The standard deviation of any inferred property across the 10 outcomes is divided by the overall mean to provide the confidence ratio.

value of of 1.90 ppm for 2 hours. In contrast the maximum value was a short-lived fluctuation from a previously measured C_2 concentration of 4.5 ppm (Figure 4.6), associated with a wind speed that had dropped suddenly from an average $3.8\mathrm{m\,s^{-1}}$ (over the previous 8 hours) to only $0.33\mathrm{m\,s^{-1}}$.

In summary, Table: 4.1 shows the inferred value of the methane emission rate of the NE lagoon (Q_{1A}) as analyzed using configuration A, and the (nominal) background concentration (C_{BG}) as measured by the upwind laser (C_2). The time series of apparent emission rate is given by Figure (4.7).

Name of the variable	No. of input data	No. of (-)tv value	Ave.	Max. value	Min. value	Std. Dev.
Q_{1A}	167	-	78 $\mathrm{kg\,hr^{-1}}$	137.34 $\mathrm{kg\,hr^{-1}}$	16.70 $\mathrm{kg\,hr^{-1}}$	19
C_{BG}	167	-	2.40 ppm	17.73 ppm	1.83 ppm	1.4

Table 4.1: WindTrax output data for methane emission rate of lagoon (analysis configuration A).

4.2.2 Configuration B: constant background imposed, single downwind laser

Configuration B (Figure 4.8) is even simpler than A, for it imposes a constant, assumed value of background concentration and (like A) for each run employs only a single measured concentration in order to determine the emission rate from a single source. This configuration demands the minimum of instrumentation, but its obvious drawback is that it considers the background concentration as being constant even though it is known that the atmospheric concentration of methane undergoes an irregular diurnal cycle. Furthermore this analysis configuration can only be adopted for locations where previous studies have determined a plausible value of background.

The calculation of emission rate (Q_{1B}) using a single detected concentration is straightforward, and may be represented symbolically as

$$C_{BG} = 1.9\,\text{ppm}\,, \tag{4.3}$$

$$aQ_{1B} + C_{BG} = C_1\,, \tag{4.4}$$

where it has been assumed that background concentration for Edmonton is 1.9 ppm. The WindTraX input file includes all runs with mean wind direction $180^o \leq \theta \leq 360^o$.

Results for configuration B

Output filtering Conditions 1,2 were applied to WindTrax analyzed emission rates. The average, maximum and minimum values of the emission rate were respectively $86.6, 167.2$ and $34.1\text{kg}\,\text{hr}^{-1}$. The maximum and minimum values corresponded to runs with mean wind directions 287^o (at 123.13) and 343^o (at 124.83), and the wind speeds asociated with these maximum and minimum values were $6.5\,\text{m}\,\text{s}^{-1}$ and $1.7\,\text{m}\,\text{s}^{-1}$. Figure (4.9) gives the time series of inferred emission rate, and broadly resembles that produced by configuration A.

Name of the variable	No. of input data	No. of (-)tv value	Ave.	Max. value	Min. value	Std. Dev.
Q_{1B}	192	-	86.6 $\text{kg}\,\text{hr}^{-1}$	167.17 $\text{kg}\,\text{hr}^{-1}$	34.14 $\text{kg}\,\text{hr}^{-1}$	22
C_{BG}	192	-	1.9 ppm	-	-	-

Table 4.2: WindTrax analyzed output data for methane emission rate of lagoon in configuration B.

4.2.3 Configuration C: two concentration signals (C_1, C_2) assimilated, background concentration inferred

Analysis configuration C (Figure:4.10) utilizes two measured concentrations, the downwind laser C_1 and the "upwind" laser C_2, to determine two unknown parameters, viz. the emission rate Q_1 of the NW lagoon and the background concentration C_{BG}. Other methane sources are treated as inactive (i.e. their source strength is assigned the value zero) and information from the third laser (C_3) is not included in the calculation. A symbolic depiction of this configuration is

$$a_{11}Q_{1C} + C_{BG} = C_1, \quad (4.5)$$

$$a_{21}Q_{1C} + C_{BG} = C_2, \quad (4.6)$$

(i.e. two equations in two unknowns). Runs with with mean wind directions in the range $180^o \leq \theta \leq 360^o$ were included in the WindTraX input file.

Results for configuration C

Using configuration C the average emission rate of the NE lagoon was found to be $84.22\,\mathrm{kg\,hr^{-1}}$. The highest apparent emission rate ($195.86\,\mathrm{kg\,hr^{-1}}$) occurred at 123.05 with a wind direction of 229^o, and the lowest (20.34 ppm) at 125.18 with a wind direction of 352^o. The wind speeds corresponding with the maximum and minimum values were $2.02\,\mathrm{m\,s^{-1}}$ and $1.10\,\mathrm{m\,s^{-1}}$. Figure (4.11) shows that the most extreme values are found when the wind speed is less than $2.5\,\mathrm{m\,s^{-1}}$, although there are also some large values at solid wind speeds of order $4 - 6\,\mathrm{m\,s^{-1}}$.

Using this configuration six of the WindTrax analyses produced *negative values* for the background concentration, the average, maximum and minimum values being respectively 1.93 ppm, 9.44 ppm and -11.34 ppm. Figure (4.12) shows the association between the inferred background concentration and the wind direction. The extreme values and all the negative values are found over the wind direction range $180^o - 300^o$. The maximum "background" concentration value of 9.44 ppm has been found for a wind direction of 283^o and the minimum value (-11.34 ppm) has been found for 192^o. The undoubted existence of other methane sources situated westward of the NE lagoon explains the extreme values. The wind direction necessary to provide a true background concentration at C_2 (i.e. carry fresh air to laser C_2) would presumably span about $300^o - 360^o$.

4.2.4 Configuration D: two concentration signals (C_1, C_3) assimilated, background concentration inferred

This configuration is similar to configuration C, except that the laser pairing is different (Figure 4.13). The downwind laser (C_1) is active , along with laser (C_3) on the western bank (see Figure 4.13). However laser C_2 has been treated as inactive

Name of the variable	No. of input data	No. of (-)tv value	Ave.	Max. value	Min. value	Std. Dev.
Q_{1C}	192	0	84.22 ($\mathrm{kg\,hr^{-1}}$)	195.86 ($\mathrm{kg\,hr^{-1}}$)	20.34 ($\mathrm{kg\,hr^{-1}}$)	27
C_{BG}	192	6	1.93	9.44	-11.34	1.7

Table 4.3: WindTrax analyzed output data for lagoon emission rate in configuration C. Here the background concentration was deduced by WindTrax.

(i.e. signal not used) in the analysis. Ponds upwind of C_3 are considered as inactive sources, and WindTrax calculates the background concentration and the rate of emission from the NE pond:

$$C_{BG} = \text{Unknown}, \tag{4.7}$$

$$a_{11}Q_{1_D} + C_{BG} = C_1, \tag{4.8}$$

$$a_{31}Q_{1_D} + C_{BG} = C_3, \tag{4.9}$$

As noted above, configuration D is analogous to configuration C, the only difference being the position of the lasers to measure the concentration. Although the western ponds are considered in the analysis to be *inactive* sources of methane, the signal measured by laser (C_3) might in fact be influenced by emission from them. The goal of including this analysis configuration was to judge the influence of other ponds on inferred emission rate from the main lagoon, by finding the difference between configuration C and configuration D.

Results for configuration D

The average, maximum and minimum values of the emission rate from the lagoon were respectively 66 $\mathrm{kg\,hr^{-1}}$, 108 $\mathrm{kg\,hr^{-1}}$ and 2.14 $\mathrm{kg\,hr^{-1}}$. The inferred background concentration (C_{BG}) was found to average 3.16 ppm, which is high w.r.t to the generally accepted local atmospheric methane concentration of about 1.9 ppm. Maximum and minimum "background" concentrations were 8.4 ppm and 2.14 ppm.

Name of the variable	No. of input data	No. of (-)tv value	Ave.	Max. value	Min. value	Std. Dev.
Q_{1D}	192	-	66 $\mathrm{kg\,hr^{-1}}$	108 $\mathrm{kg\,hr^{-1}}$	2 $\mathrm{kg\,hr^{-1}}$	13
C_{BG}	192	-	3.16 ppm	8.4 ppm	2.14 ppm	1

Table 4.4: WindTrax analyzed output data for lagoon emission rate in configuration D. Here the background concentration was deduced by WindTrax using upwind and downwind lasers.

4.2.5 Configuration E : three laser concentrations, one assumed to represent background concentration, two unknown emission rates.

In this analysis configuration (Figure 4.14) the background concentration (C_{BG}) is treated as measured by laser C_2. The remaining two lasers permit to deduce *two* emission rates, viz. that of the NE lagoon (unknown emission rate Q_1) and that of the other ponds, which are considered collectively as having a uniform unknown emission rate (Q_2), i.e. their locations and areas differ but they share a common (à priori, unknown) aggregated per-unit-area rate of emission ($\mathrm{kg\,m^{-2}\,s^{-1}}$). Symbolically, the analysis can be described:

$$C_{BG} = C_2 \tag{4.10}$$

$$a_{11}Q_{1E} + a_{12}Q_{2E} + C_{BG} = C_1, \tag{4.11}$$

$$a_{31}Q_{1E} + a_{32}Q_{2E} + C_{BG} = C_3. \tag{4.12}$$

Results for configuration E

Table 4.5 summarizes the analysis based on configuration E. The average source strength of the main (NE) lagoon is found to be 79 $\mathrm{kg\,hr^{-1}}$, with maximum and minimum values of 124 and 41 $\mathrm{kg\,hr^{-1}}$ corresponding to wind directions of 311° and 348° respectively.

For the other (western) ponds in aggregate the average, maximum and minimum inferred methane emission rates are respectively 34 $\mathrm{kg\,hr^{-1}}$, 58 $\mathrm{kg\,hr^{-1}}$ and -71 $\mathrm{kg\,hr^{-1}}$. This configuration gives rise to only one *negative* emission rate, the associated wind direction and wind speed being 282.6° and 3.2 $\mathrm{m\,s^{-1}}$ (i.e. unproblematic). The wind

direction corresponding with the maximum value was 303°. As the wind direction, wind speed and the touchdown coverage were all satisfactory, that specific time period is anomalous.

The average value inferred for the background concentration (C_{BG}) was 2.27 ppm, with maximum and minumum values being 10.13 ppm and 1.84 ppm. The maximum undoubtedly reflects contaminated air blown into the path of laser C_2 from ponds to the west, for the associated mean wind direction was 282.6° (west wind). The minimum was associated with wind direction 341°, indicating the incursion of fresh air to laser C_2 from the north.

Name of the variable	No. of input data	No. of (-)tv value	Ave.	Max. value	Min. value	Std. Dev.
Q_{1F}	166	-	79 $\mathrm{kg\,hr^{-1}}$	124 $\mathrm{kg\,hr^{-1}}$	41 $\mathrm{kg\,hr^{-1}}$	13
Q_{2F}	166	1	34 $\mathrm{kg\,hr^{-1}}$	58 $\mathrm{kg\,hr^{-1}}$	-71 $\mathrm{kg\,hr^{-1}}$	17
C_{BG}	166	-	2.27 ppm	10.13ppm	1.84 ppm	0.94

Table 4.5: WindTrax analyzed output data for lagoon emission rate in configuration E.

4.2.6 Configuration F: three laser concentrations, imposed C_{BG}, two unknown emission rates.

In this configuration the background concentration (C_{BG}) is treated as known, with an imposed value of 1.9 ppm. All three lasers contribute their concentration measurements (Figure 4.15), yielding three items of information. The western ponds are considered in aggregate to be an active source of methane, with an unknown per-area emission rate (Q_2), while (as usual) the NE lagoon is also methane source with unknown emission rate (Q_1). Configuration F, then, seeks to evaluate two unknowns (Q_1, Q_2)on the basis of three items of data. This is an over-determined problem, and

may be represented

$$C_{BG} = 1.9\text{ppm}, \tag{4.13}$$

$$a_{11}Q_{1F} + a_{12}Q_{2F} + C_{BG} = C_1, \tag{4.14}$$

$$a_{21}Q_{1F} + a_{22}Q_{2F} + C_{BG} = C_2, \tag{4.15}$$

$$a_{31}Q_{1F} + a_{32}Q_{2F} + C_{BG} = C_3. \tag{4.16}$$

As the background concentration is imposed and all lasers are active for measurement, this configuration permits using runs with all the wind directions satisfying $180^o \leq \theta \leq 360^o$.

Results for configuration F

Table (4.6) gives the analyzed methane emission rates (filtering conditions 1,2 were applied). The average emission rate of the NE lagoon is found to be $90\,\text{kg}\,\text{hr}^{-1}$, with the maximum and minimum values being $161\,\text{kg}\,\text{hr}^{-1}$ (associated wind direction 287^o) and $41\,\text{kg}\,\text{hr}^{-1}$ (344^o). For the other ponds the average, maximum and minimum emission rates are respectively $23\,\text{kg}\,\text{hr}^{-1}$, $68\,\text{kg}\,\text{hr}^{-1}$ and $1.3\,\text{kg}\,\text{hr}^{-1}$. No negative emission rates resulted in this analysis.

Name of the variable	No. of input data	No. of (-)tv value	Ave.	Max. value	Min. value	Std. Dev.
Q_{1F}	194	-	90 $\text{kg}\,\text{hr}^{-1}$	161 $\text{kg}\,\text{hr}^{-1}$	41 $\text{kg}\,\text{hr}^{-1}$	16
Q_{2F}	194	-	23 $\text{kg}\,\text{hr}^{-1}$	68 $\text{kg}\,\text{hr}^{-1}$	1.3 $\text{kg}\,\text{hr}^{-1}$	12
C_{BG}	194	-	1.9 ppm	-	-	-

Table 4.6: WindTrax analyzed output data for lagoon emission rate in configuration F.

4.2.7 Configuration G: three laser concentrations; unknown background concentration; two source strengths quantified.

Configuration G (see Figure 4.16) uses all available information in a manner that entails the least imposition of prior information, because from three measured con-

centrations the analysis extracts background concentration, and the emission rates of both the NE lagoon (Q_1) and the western ponds inaggregate (Q_2).

Laser C_1 at the east edge of the NE lagoon is far from the other (western) ponds and so responds mainly to the concentration pume off the NE lagoon immediately upwind. Laser C_3 at the western edge of the NE lagoon is positioned so as to be strongly influenced by the western ponds during westerly winds. Laser C_2 should often be exposed to background methane concentrations. WindTrax of course "handles" the matter quantitatively. The logic of the analysis can be encapsulated as:

$$C_{BG} = \text{Unknown}, \tag{4.17}$$

$$a_{11}Q_{1G} + a_{12}Q_{2G} + C_{BG} = C_1, \tag{4.18}$$

$$a_{21}Q_{1G} + a_{22}Q_{2G} + C_{BG} = C_2, \tag{4.19}$$

$$a_{31}Q_{1G} + a_{32}Q_{2G} + C_{BG} = C_3, \tag{4.20}$$

Results for configuration G

Table (4.7) summarizes the results of the analysis using configuration G. After filtering with conditions 1,2 there occured three negative values for the emission rate of the NE lagoon, for which the average rate is $75\,\mathrm{kg\,hr^{-1}}$. The maximum and minimum rates are 391 and -364 $\mathrm{kg\,hr^{-1}}$ associated with wind directions 260° and 229°.

For the aggregate strength of the western ponds the analysis yields a mean value of $15\,\mathrm{kg\,hr^{-1}}$, with a maximum of $38\,\mathrm{kg\,hr^{-1}}$ (wind direction 192°) and minimum of $-64\,\mathrm{kg\,h^{-1}}$ (wind direction 229°). There are four negative values found for the strength of the western ponds (even after filtering with conditions 1, 2).

With the output filtered by condition 1 (alone) eight negative values are reurned for the background concentration, whose average value is indicated as 3.30 ppm. The maximum and minimum values were 103 ppm and -33.10 ppm with corresponding wind directions respectively 229^o and 256^o.

Name of the variable	No. of input data	No. of (-)tv value	Ave.	Max. value	Min. value	Std. Dev.
Q_{1G}	192	3	74.5 $\mathrm{kg\,hr^{-1}}$	390.66 $\mathrm{kg\,hr^{-1}}$	-363.92 $\mathrm{kg\,hr^{-1}}$	73.35
Q_{2G}	192	4	15.1 $\mathrm{kg\,hr^{-1}}$	38.41 $\mathrm{kg\,hr^{-1}}$	-63.73 $\mathrm{kg\,hr^{-1}}$	11
C_{BG}	192	8	3.30 ppm	102 ppm	-22 ppm	11

Table 4.7: WindTrax analyzed output data for config.G. The first and second row contain of methane emission rate for lagoon and other ponds and third row contains deduced value of $\mathrm{C_{BG}}$.

4.3 Summary of investigation of alternative analysis configurations for lagoon emissions

Table (4.8) recapitulates the results of the different configurations. Those configurations that entail using a *measured* background concentration (C_{BG}) (configurations A,E) proved more accurate than those which adopted the imposed value $C_{BG} = 1.9\,\mathrm{ppm}$ (configurations B,F). When C_{BG} was treated as one of the unknowns to be deduced from the available information some puzzling anomalies occurred for no (evidently) logical reason, suggesting such a configuration is untrustworthy.

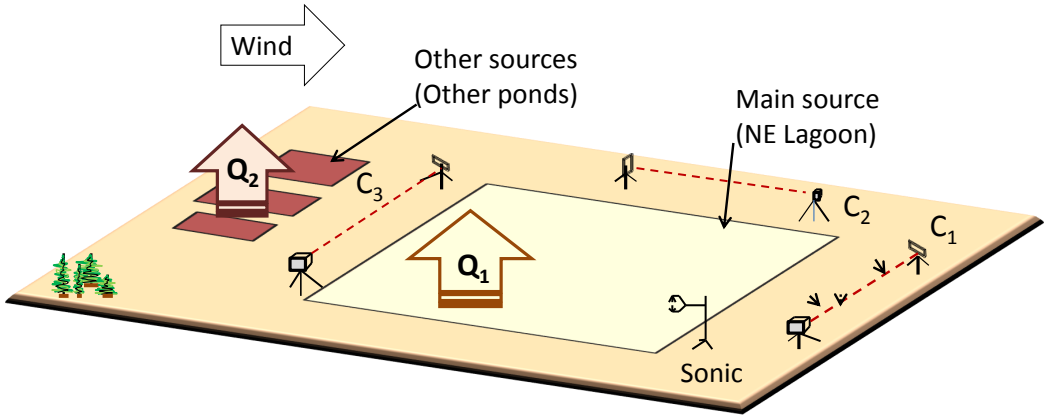

Figure 4.1: Experimental setup during the lagoon experiment. Dashed lines show laser light paths. The right edge of the diagram is oriented north-south. The east-west dimension of the NE lagoon is 250 m, the north-south dimension 450 m.

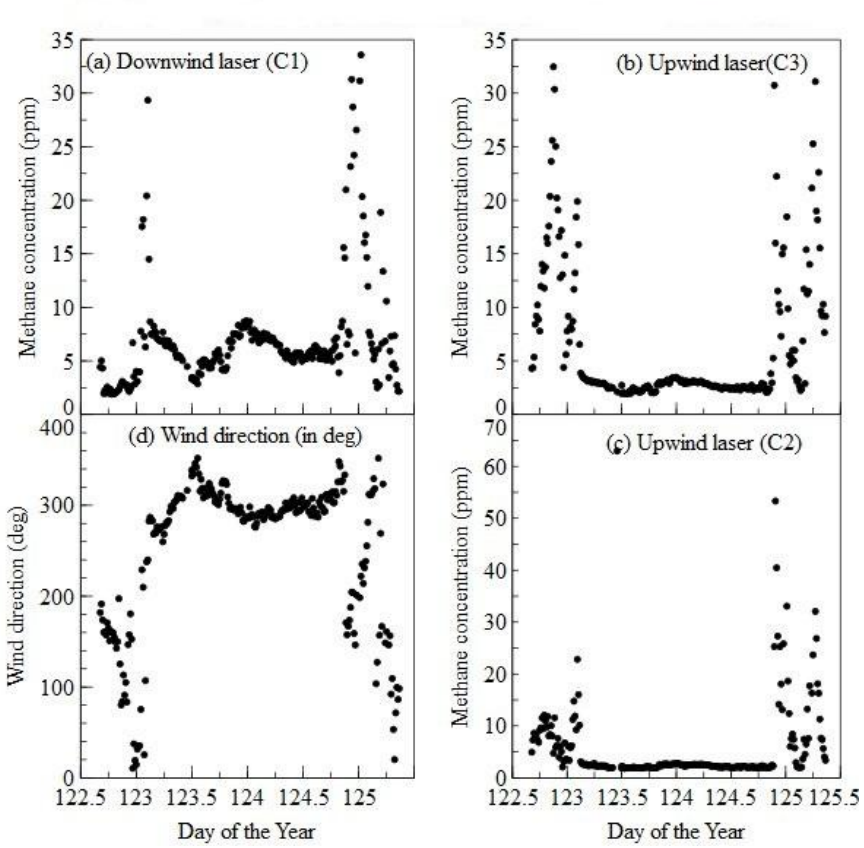

Figure 4.2: Time series of methane concentration and mean wind direction during the lagoon experiment.

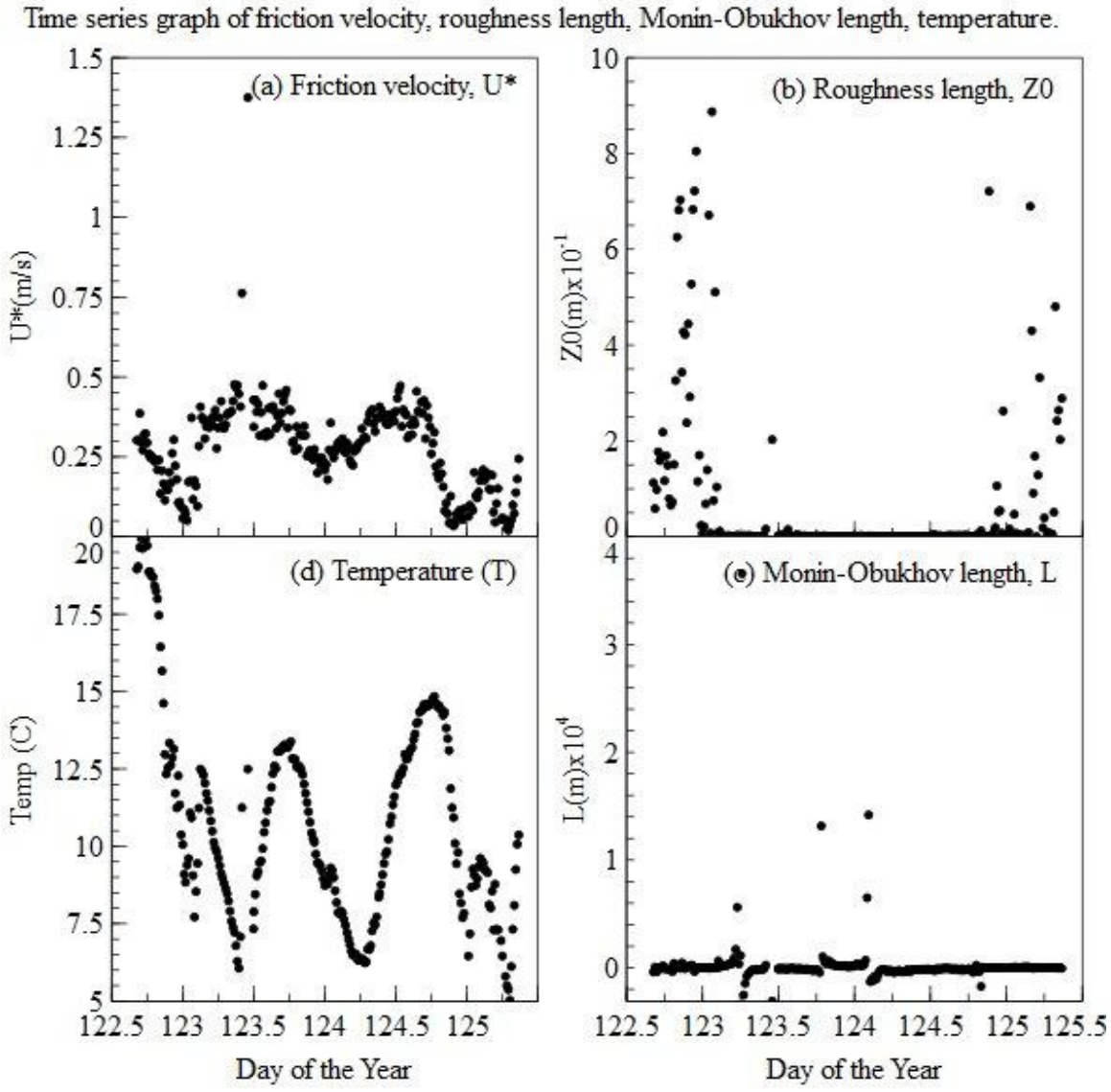

Figure 4.3: Measured temperature and the calculated value of friction velocity, roughness length and Obukhov length during the lagoon experiment.

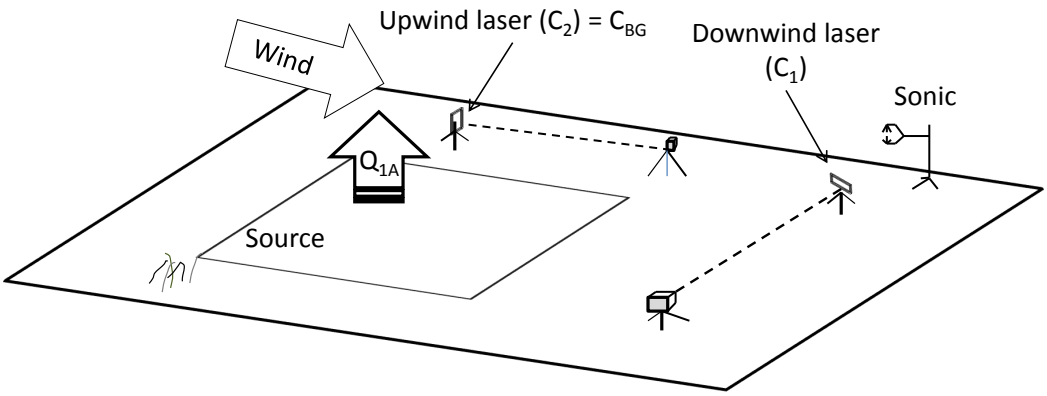

Figure 4.4: Configuration A. Upwind laser determines background concentration, concentration rise at single downwind laser establishes flux off a single source.

Figure 4.5: Example of WindTrax analysis using configuration A. A single plume of touchdown points is visible, emanating from the downwind laser, and plotted in red when touching down on the source or in grey over land (or over the inactive sources, i.e. other ponds). Background concentration is equated to the concentration signal from the upwind laser, not visible here because obscured by touchdowns.

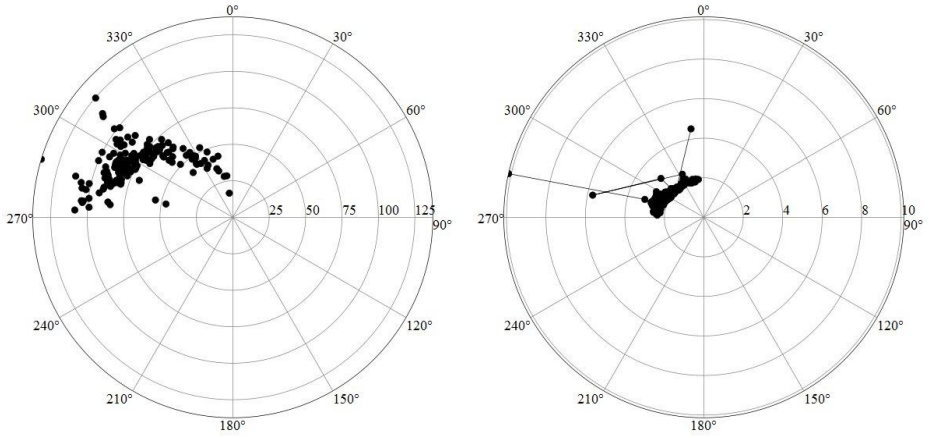

Figure 4.6: (left) Emission rate ($\mathrm{kg\,hr^{-1}}$) and (right) background concentration (ppm), as deduced with configuration A, plotted with corresponding wind direction.

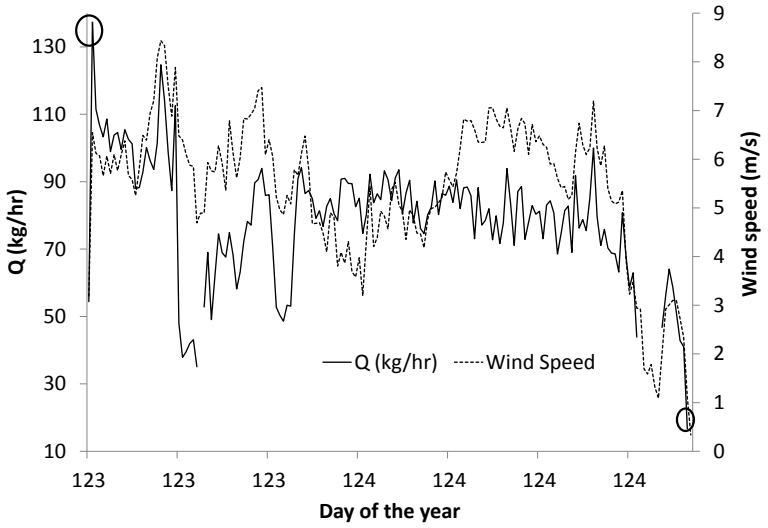

Figure 4.7: The analyzed emission rate from configuration A with corresponding wind speed.

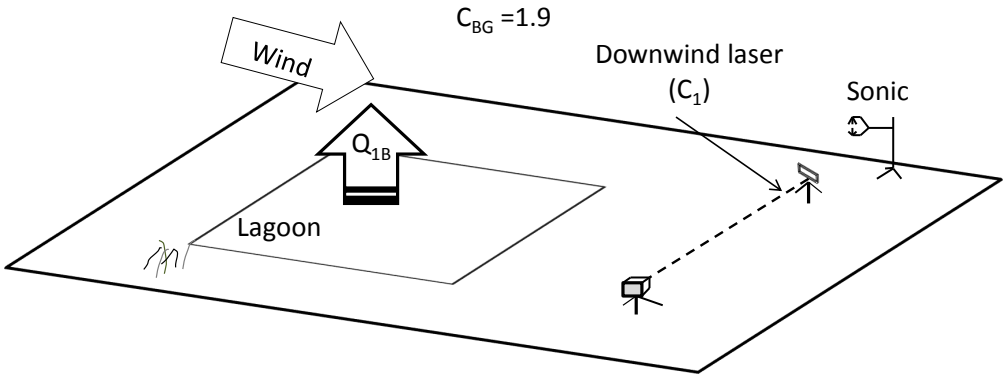

Figure 4.8: Configuration B. Here the background is assumed to be 1.9 ppm and a downwind laser measures the concentration due to lagoon emissions.

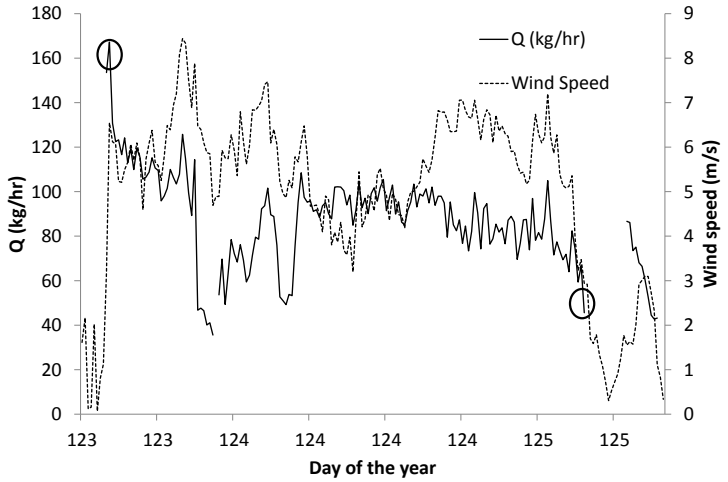

Figure 4.9: The analyzed emission rate of lagoon with corresponding wind speed from configuration B.

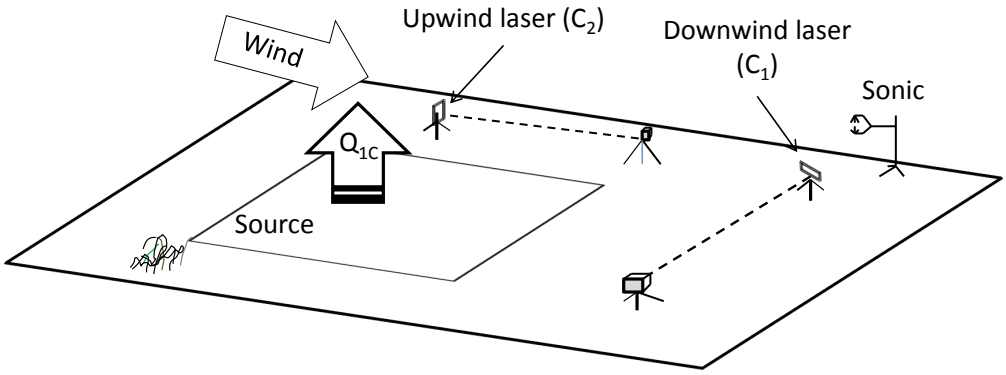

Figure 4.10: Experimental layout of Config. C. Two laser concentration signals permit WinTrax to infer emission rate and background concentration.

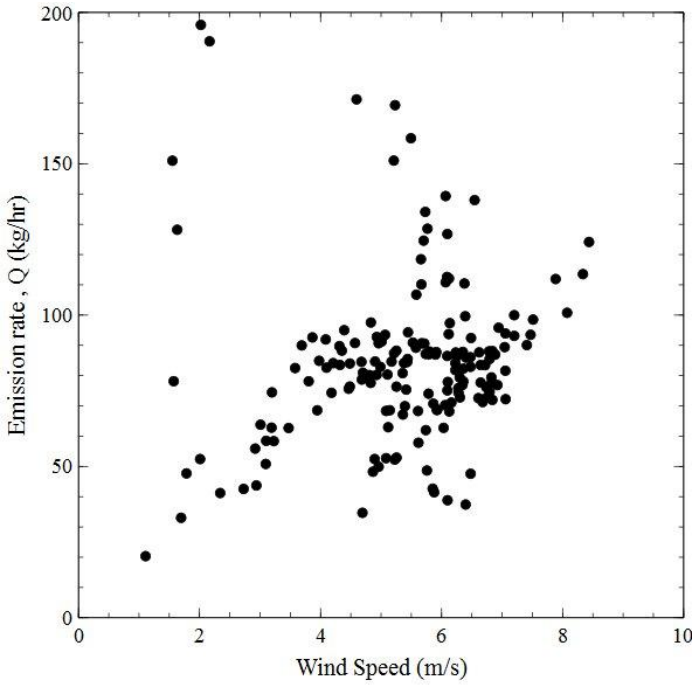

Figure 4.11: Emission rate (Q) versus wind speed- Config. C

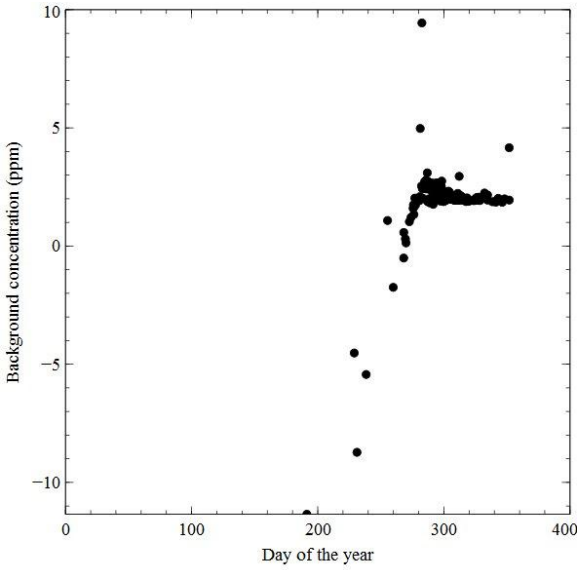

Figure 4.12: Background concentration deduced using configuration C.

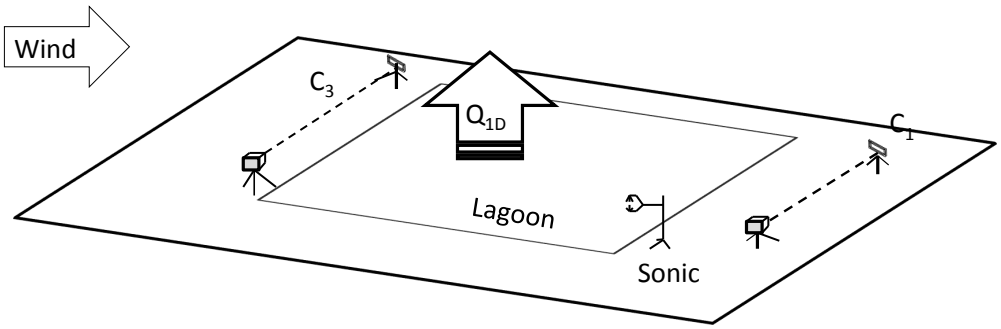

Figure 4.13: Configuration D. Two laser concentration measurements. Emission rate of the main lagoon and background concentration are deduced by WindTrax. The other ponds are present in the layout to show their possible influence, but the WindTrax calculation treats them as inactive.

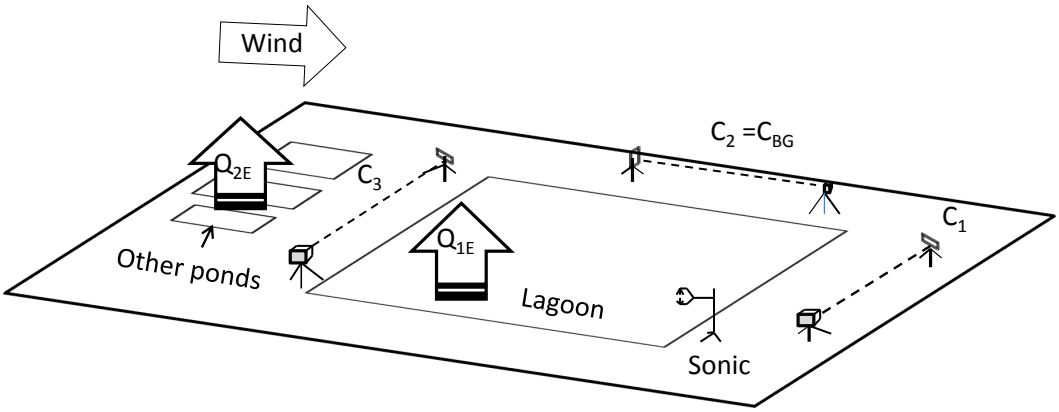

Figure 4.14: Basic WindTrax configuration of configuration E

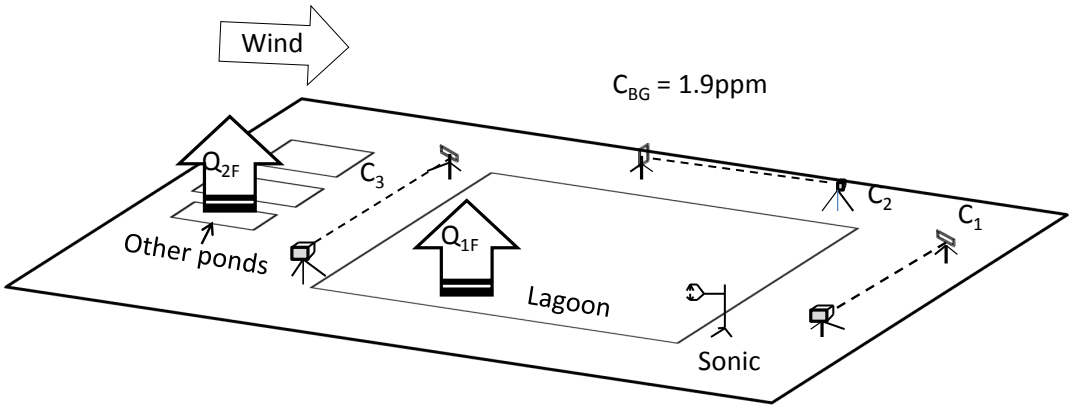

Figure 4.15: Basic experimental layout of Config. F

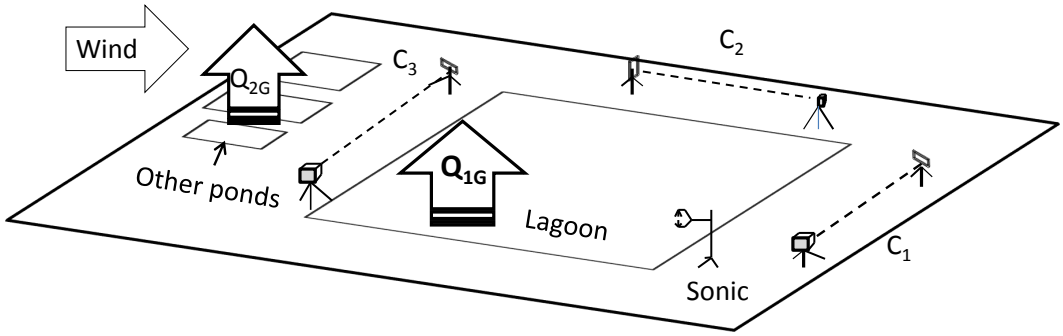

Figure 4.16: Basic experimental layout of Config. G

Name of config.	No. of the Obs	Emision rate of the Lagoon					Emision rate of the other ponds					Background Concentration				
		No. (-) values	Q($\mathrm{kg\,hr^{-1}}$)			Std. Dev.	No. (-) values	Q($\mathrm{kg\,hr^{-1}}$)			Std. Dev.	No. (-) values	C_{BG} (ppm)			Std. Dev.
			Ave	Max	Min			Ave	Max	Min			Ave	Max	Min	
A	166	-	82	137	41	15						-	2.29	10	1.8	1
B	192	-	90	167	37	19						-	1.9	-	-	-
C	192	-	88	196	41	25						3	1.94	9.4	-11	2
D	192	-	66	108	2	13						-	3.16	8.4	2.14	1
E	166	-	79	124	41	13	1	34	58	-71	17	-	2.27	10	1.8	1
F	194	-	90	161	41	16	-	23	68	1.3	12	-	1.9	-	-	-
G	192	3	79	391	-637	80	4	15.1	38.4	-63	14	8	3.04	102	-22	11

Table 4.8: WindTrax output data for all analysis configurations. Each row details WindTrax output for NE lagoon source strength, and (where available) for the emission rate of other sources in aggregate and/or for background concentration C_{BG}.

Chapter 5

Inverse Dispersion to quantify fugitive methane emission from landfill

When waste is buried in a landfill, chemical and biological processes generate landfill gas (LFG). The primary components of LFG are methane ($40\% - 60\%$) , carbon dioxide ($60\% - 40\%$) and other trace gases (Reinhart & Townsend, 1998). Properly collected, LFG is a valuable energy resource, with a fuel energy value of $18-22\,\mathrm{MJ\,m^{-3}}$ (Spokas *et al.*, 2006). However fugitive emissions of LFG pose a threat to the global environment (and in rare cases, a local safety hazard). Therefore it is useful to quantify the volume of fugitive methane being emitted from landfills for the rational development of economic and regulatory incentives, including carbon-offset trading, renewable energy credits, and renewable energy production tax credits.

Additionally, landfill is a complex, composite source, with a spatially variable source strength for "landfill gas" (LFG). For this reason it is difficult to estimate the total amount of LFG that is being produced. Most estimates of the production rate of landfill gas are based on calculations of the degradation rate of decomposing wastes. It is estimated that landfills contribute about 2% of the total global GHG emissions (AEA, 2008). Depending on its fate, LFG represents a source of energy or a fugitive emission of greeenhouse gas: $700\mathrm{m^3\,hr^{-1}}$ of 50% CH_4 can generate 1 MW, and the fact of *not* emitting that $700\mathrm{m^3\,hr^{-1}}$ is equivalent (in terms of impact on GHG

budgeting and climate change) to a reduction of $10^4 \mathrm{kg\,hr}^{-1}$ of CO_2 (Budisulistiorini, 2007). Obviously the economic, environmental and social impacts of fugitive methane are high, so that quantifying fugitive emissions of methane from a waste management centre to the atmosphere is valuable.

Several methods exist for the direct measurement of fugitive methane emissions from a landfill (Spokas *et al.*, 2006), but there is no unique method that can work for all sites. Methods include the tracer gas technique, laser radial plume mapping, differential absorption light detection and ranging (DIAL lider), and helicopter-borne spectroscopy (Babilotte *et al.*, 2010). Here, the inverse dispersion (ID) method has been implemented to deduce the emission rate of fugitive methane sources in a waste management centre, and the thesis will document application to sources that differ greatly in their size, shape and strength. This "bLS" method for inverse dispersion had been developed by Flesch et al.(Flesch, 1995) and subsequent contributors (not least B. Crenna, who has developed the software "WindTraX" for bLS calculations). Application of the bLS technique has already been demonstrated for several types of complex sources, e.g. agricultural crops (Gimson & Uliasz, 2003), dairy farms (Flesch *et al.*, 2005; Flesch *et al.*, 2007) and multi-source problems (Flesch *et al.*, 2009).

Given the complex topography and the spatial inhomogeneity of the methane emission rate at a typical landfill, *exact* measurements of source strength will always be difficult or impossible to obtain. It is important, therefore, not to hold the present methodology to an unattainable and unrealistic standard of perfection. It will become obvious to the reader that a large measure of uncertainty is associated with the emissions estimates provided here, an uncertainty that may exceed a factor of two and which is most clearly seen by looking at the dependency of the estimated emission rate on which *prior assumptions* are made as regards (for example) background concentration and (more crucially) the true locations and boundaries of the sub-sources making up the overall source distribution. Notwithstanding the undeni-

able uncertainty of the present estimates, they are useful in the following sense. By establishing the order of magnitude of the fugitive emissions rate, the present estimates provide a basis for deciding whether the expense and effort of making more definitive measurements might be worthwhile.

The landfill under consideration here covers an area of 65 hectares, and extends 7m below and 60m above the natural grade. Measurements permitting the application of the Inverse Dispersion method were conducted from May 5 to May 10, 2011. Instruments were temporarily placed over the landfill in four different locations (Figure 5.1) in sequence. The locations are named as source location A (L_A), source location B (L_B), source location F (L_F) and source location G (L_G), however there were other sources located nearby (see Figure 5.1), locations indicated as source C, source D and source E.

At each of these sites the local rate of emission of fugitive methane was assessed by Inverse Dispersion on the basis of concentration measurements from three open path laser methane sensors, supplemented by needed local meteorological data measured using a 3-D sonic anemometer. The ground surface over the landfill was variable and irregular in terms of its topography and vegetation cover, an aspect that is problematic for the Inverse Dispersion technique (which assumes the wind flow is in equilibrium with the local terrain). Areas of dead vegetation and/or sterile soil were visible. Instrument locations were chosen on the assumption such visually striking features would correlate with strong sources of fugitive methane.

Applying Inverse Dispersion to estimate landfill emissions is complicated not only by the irregularity of the terrain (and therefore, wind), but by the fact that a landfill represents a complex, composite source. The emission rate is spatially variable, whereas the bLS method demands that one be able to attribute the observed concentrations to one or more discrete sources with known boundaries. And even where there *was* reason to believe one had identified a discrete source with a definite bound-

ary, skillful application of ID required attention to the possibility of contributions to the measured concentrations from other, neighbouring sources.

The fugitive methane sources in a landfill can be considered to be of several types. Some are large in their areal extent (e.g. area of order $100\,\mathrm{m}^2$) while others resemble isolated "vents" with diameters merely of centimeters, perhaps occurring in clusters, and having such large volume emission rates as to be audibly hissing. In short it was obvious by inspection that the ground-air flows (emissions) are highly "patchy." In this situation two possible approaches can be taken. The first approach (below labelled "Individual Source") is to isolate and quantify a manageable number of dominant individual sources (such as the vents) while treating the residual area (or areas) as a larger, weaker but spatially uniform source. The second approach ("Aggregated Sources") is to set up the concentration detectors so as to quantify an effective *aggregate* source, within whose boundary the local emission rate would in reality be highly variable.

Accordingly the experimental setup was arranged along these two alternative conceptual approaches. "Individual Source" trials entailed ringing the laser detectors, using relatively short pathlengths, around a small area hypothesized to represent a well defined source with a definite boundary (the latter correlating with the edge of an area of sterile ground – dead or non-existent vegetation). The "Aggregated Sources" trials entailed long laser light paths set up to detect the aggregate impact of all sources.

For the purpose of this thesis, which is to illustrate the methodology and emphasize the prevailing uncertainties, only a subset of the measurements over the landfill will be described. Regardless of the experimental configuration, inverse dispersion is predicted on there being a well-defined dispersion regime. Therefore for all configurations the selection criteria for acceptable measurements were that the friction velocity $u_* \geq 0.1\,\mathrm{m\,s^{-1}}$, the roughness length $z_0 \leq 0.1$ m, and the Obukhov length $|L| \geq 5$ m.

These properties had been measured at a single point by the sonic anemometer (z_0 being extracted as that figure which would reconcile the measured mean wind speed with the momentum and sensible heat fluxes, in the framework of Monin-Obukhov [MO] similarity theory), and the selection principle corresponds to what – in the context of flow over an ideal, flat and uniform surface – may be termed a "well-defined micrometeorological state." It is however worthwhile to remind the reader that at the landfill, the ground surface was irregular in its slope, elevation and ground cover. Thus the wind flow "connecting" the source(s) to the laser detectors (i.e. controlling the turbulent wind paths from the source on ground into the laser beams) was *not* horizontally homogeneous. The flow statistics provided by the sonic anemometer represent an imperfect characterization of the prevailing flow.

5.1 Implementation of bLS Method on Individual Sources

Here the experimental setup entailed placing lasers on two or more "sides" of a single, well delineated source. The source strength Q was computed by (in effect) solving with Eq. 5.1, background concentration C_{BG} either imposed Eq. 5.2, or treated as an unknown Eq. 5.3,

$$a_i Q + C_{BG} = C_i \,, \tag{5.1}$$

$$C_{BG} = 1.9\,\text{ppm} \tag{5.2}$$

$$C_{BG} = \text{unknown} \,. \tag{5.3}$$

The problem is overdetermined if the number of laser signals exceeds the number of unknowns, and in such instances WindTraX provides that solution which is optimal.

5.1.1 Fugitive methane source A

Landfill methane source A, with total area $93\,\text{m}^2$ and approximate dimensions $12\,\text{m} \times 8\,\text{m}$, was a small area source located on distinctly sloping terrain of about 20^o (see

Figure 5.1).

Instruments were operated for 135 min from 9:15 am to 11:30 am on May 6, 2011, during which interval the winds were generally from the west. In view of the small areal scale of the experiment, the concentration measurements and the meteorological data were organized into 5-min blocks for analysis by WindTraX. Eighteen 5-min data periods were obtained with an acceptable mean wind direction ($225^{o} \leq \theta \leq 315^{o}$). Two lasers were operated, one standing distinctly upwind and the other downwind from the source , Figure (5.2).

The calculated source strengths (see Table 5.1) for source A were $8.03\,\mathrm{kg\,h^{-1}}$ (C_{BG} imposed) and $7.99\,\mathrm{kg\,h^{-1}}$ (C_{BG} inferred). These values are nicely consistent (see Figure 5.3). Figure (5.4) plots the inferred background concentration C_{BG}, varying from $(1.9-2.09)\,\mathrm{ppm}$, against corresponding wind direction. The average value of C_{BG} for L_A is $1.99\,\mathrm{ppm}$, which is very realistic w.r.t the daytime background atmospheric methane concentration expected in Alberta.

Name of the variable	No. of input data	No. of (-)tv value	Ave. emission rate $\mathrm{kg\,hr^{-1}}$	Max. value $\mathrm{kg\,hr^{-1}}$	Min. value $\mathrm{kg\,hr^{-1}}$	Std. Dev.
C_{BG} imposed	18	-	8.03	9.15	6.92	0.63
C_{BG} deduced	18	-	7.99	9.10	6.89	0.62

Table 5.1: WindTrax output data for the methane emission rate of source A (Q_A).

5.1.2 Fugitive methane source B

Source B was located on a gently sloping western flank of the landfill, but the source itself and the area over which the instruments operated was rather homogeneous (Figures 5.1, 5.5). The total area of the source was $115\,\mathrm{m^2}$, approximately 14 m × 8 m. Instruments were operated for 21 hrs ($11:40\,\mathrm{am}$ on May 5 to $8:15\,\mathrm{am}$ on May 6, 2011). The experimental setup included three lasers and the sonic anemometer.

Measurements were again averaged into 5-min intervals, and filtered to accept only

intervals with mean wind direction $200^o \leq \theta \leq 340^o$. With the latter restriction the two additional sources (shown on Figure 5.6 along with source B) could be treated in the WindTrax calculation as being *inactive*, for they could not have contributed to the laser concentration signals. In Table 5.2, the analyzed methane source strength Q_B for location B has been shown. When C_{BG} is assigned the value 1.9 ppm the average source strength is $6.39\,\mathrm{kg\,h^{-1}}$, while with C_{BG} treated as unknown the average computed emission rate is $4.46\,\mathrm{kg\,h^{-1}}$. These figures differ by 30% and plotted in Figure 5.7.

Name of the variable	No. of input data	No. of (-)tv value	Ave. emission rate $\mathrm{kg\,hr^{-1}}$	Max. value $\mathrm{kg\,hr^{-1}}$	Min. value $\mathrm{kg\,hr^{-1}}$	Std. Dev.
C_{BG} imposed	112	-	6.39	13.78	3.33	2.2
C_{BG} deduced	112	-	4.46	11.85	1.2	1.9

Table 5.2: WindTrax output data for methane emission rate of source B, (Q_B).

Figure (5.8) gives the inferred values of background concentration (recall, for all analyzed intervals the restriction $200^o \leq \theta \leq 340^o$ had been applied). The average, maximum and minimum values of C_{BG} for L_B are $15, 59$ and 11 ppm respectively. It is natural to suspect that where it has been inferred by the bLS analysis, the estimated C_{BG} reflects an influence of neglected nearby sources. Figure (5.9) displays an (apparent) inverse relationship between the inferred values of source strength Q and the inferred background concentration C_{BG}, which makes no physical sense and is an artifice of the analysis: if a given measured (fixed) concentration is to be "explained" as representing the sum $C_{BG} + f(Q)$ of background plus a contribution from a source (where $f(Q)$ increases with increasing Q), then inevitably an increased C_{BG} must be accompanied by a decreased Q.

This section indicates that, applied to well defined sources and provided other nearby sources can be neglected (by virtue of the imposition of suitable criteria on wind direction in relation to locations of the sources and the lasers), the ID technique

is probably returning estimates of emission rate that are "good" to better than a factor of 2.

5.2 Implementation of bLS Method on Aggregated Sources

Two experimental confiurations will be discussed in this section, quantifying the emission rates of sources "F" and "G" (the terminology reflects that used in the field logbooks). The effective (i.e. aggregate) source "F" encompasses a large area within which there were certainly many small sources, some well localized (e.g. the "vents") and some for which it was impossible to attribute a well-defined boundary. Within source area F we identified a smaller (but still large) source area "G."

For WindTraX (i.e. bLS inverse dispersion) analyses of this section the measurements were organized into 15-min averaging intervals. In all analyzed cases it has been assumed that $C_{BG} = 1.9\,\text{ppm}$. No restriction was imposed on the mean wind direction.

5.2.1 Fugitive methane source F

In the configuration for assessment of the effective source strength of location F (see Figure (5.1) measurements with three lasers and the sonic anemometer took place for a duration of 66 hours (2:45 pm on May 6th to 9:45 am on May 9, 2011). Figure (5.10) shows the experimental setup.

Laser light path C_1 ran up a ridge at the western end of the source area of interest. Laser path C_3 was situated at east of the source, and generally measured concentrations close to the assumed background level (Figure 5.11). The other laser path C_2 spanned a flat but partially vegetation-covered surface close to the most intense local sources (the "vents"). This layout was not centered around any one particular source, instead being chosen in the attempt to acquire an effective emis-

sion rate for the entire northern flank of the landfill, where (as noted earlier) many different shapes and sizes of sources are located. To the extent that the inferred value of Q_F can be trusted, it represents potentially the most useful figure deduced from the experimental campaign.

As earlier noted, an inverse dispersion analysis as implemented in bLS (WindTraX) mandates the delineation of the effective source area or areas. Obviously this could not be otherwise than an *arbitrary* specification on the part of the analyst (and writer). Four different analysis configurations (see Figure 5.12), differing only as regards the shapes and numbers of sources, have been processed using WindTraX to deduce the apparent methane emission rate Q_F (Table 5.4).

The mean values for the emission rate are very similar across the four analysis configurations (standard devation of the four estimates $1.5\,\mathrm{kg\,hr^{-1}}$). Figure (5.13) plots the individual run-by-run estimates of source strength Q_F as function of time, for each of the assumed source distributions. Given the modest range in temperature over the period of measurements and noting that temperature variation within the landfill would be highly damped, the apparent variability of the emission rate with time is probably not real. It may correlate with the changing meterology and reflect the imperfection of the technique as here applied — with its neglect of the spatial inhomogeneity of the wind field, and its very subjective attribution of the effective source area. In any case Figure (5.13) indicates that the four (assumed) source configurations result in more or less the same pattern in the apparent emission rate.

5.2.2 Fugitive methane source G

Measurements focused on source G spanned 24 hours (1:00 pm on May 9th to 1:30 pm on May 10th, 2011). Source G (see Figures 5.1, 5.14) lay within the boundary of the larger source area F, and consisted of many small sources, some well localized and very strong, others (hypothetically) weaker and with indefinite boundaries. There

Name of the assump.	No. of input data	Area (m^2)	Ave. emission rate ($kg\,hr^{-1}$)	Max. value ($kg\,hr^{-1}$)	Min. value ($kg\,hr^{-1}$)	Std. Dev.
L_{F1}	100	5140	30.26	49.95	10.60	8.3
L_{F2}	100	6422	32.93	62.67	14.63	8.3
L_{F3}	100	13563	30.39	68.81	11.83	8.9
L_{F4}	100	22308	32.82	83.94	9.93	11

Table 5.3: WindTrax output data for methane emission rate of location F, (Q_F).

were areas of standing water, and while in some places LFG was visibly bubbling to the surface, presumably gas was also escaping elsewhere, but at a rate insufficient to strike the eye. In short it was very difficult to identify the sources and estimate the source strength. For the WindTrax inverse dispersion analyses exact and unvarying locations have been prescribed for some of the component sources, while several assumptions were made as regards the outline of other source areas. These options are defined on Figure (5.14). Configuration L_{G1} attempts very precise localization of some dominating sources (multiple small, intense sources) while configurations L_{G2} and L_{G3} distribute the (assumed) emissions (i.e. the emissions causing the observed laser methane signals) as an effective uniform rate over an extended area. The (postulated) sources were surrounded by two of the open path laser methane detectors, while the third was placed upwind with respect to the prevailing wind direction (Figure 5.15).

For each analysis configuration the inferred source strength Q_G has been shown in the Table (5.4), along with extreme values and the standard deviation. The standard deviation (across the configurations) of the mean emission rate was $1.8 kg\,hr^{-1}$. The configuration L_{G1} (small size – multiple sources) yields the more extreme estimates, with a high average standard deviation (see Figure 5.16).

The surprising aspect of Table (5.4) is that taken at face value source F, whose strength was analyzed in the previous section and found to be $Q_F \sim 30 kg\,hr^{-1}$,

Name of the assump.	No. of input data	Area m^2	Ave. emission rate $kg\,hr^{-1}$	Max. value $kg\,hr^{-1}$	Min. value $kg\,hr^{-1}$	Std. Dev.
L_{G1}	21	310	65.90	116.11	10.33	29
L_{G2}	21	2727	64.83	89.69	43.92	14
L_{G3}	21	3106	62.36	88.77	26.81	16

Table 5.4: WindTrax output for methane emission rate of source G (Q_G).

contains within it source G whose apparent emission rate $Q_G \sim 65 kg\,hr^{-1}$ is larger by a factor of two. This of course is a contradiction. But rather than invalidating the inverse dispersion analysis, this result is constructive. For it can suggest at least the order of magnitude of the uncertainty that stems from the necessity to arbitrarily designate the effective source area(s). If one's best reasonable choices contradict each other to no worse extent than a factor of two, then it would appear reasonable to conservatively take the larger rate (as a measure of the potentially useful LFG being harmfully released to the environment) and recommend it as being uncertain by a factor of two — but not by a factor of ten. Relative to one's prior 100% ignorance of the rate of fugitive emission, this represents progress.

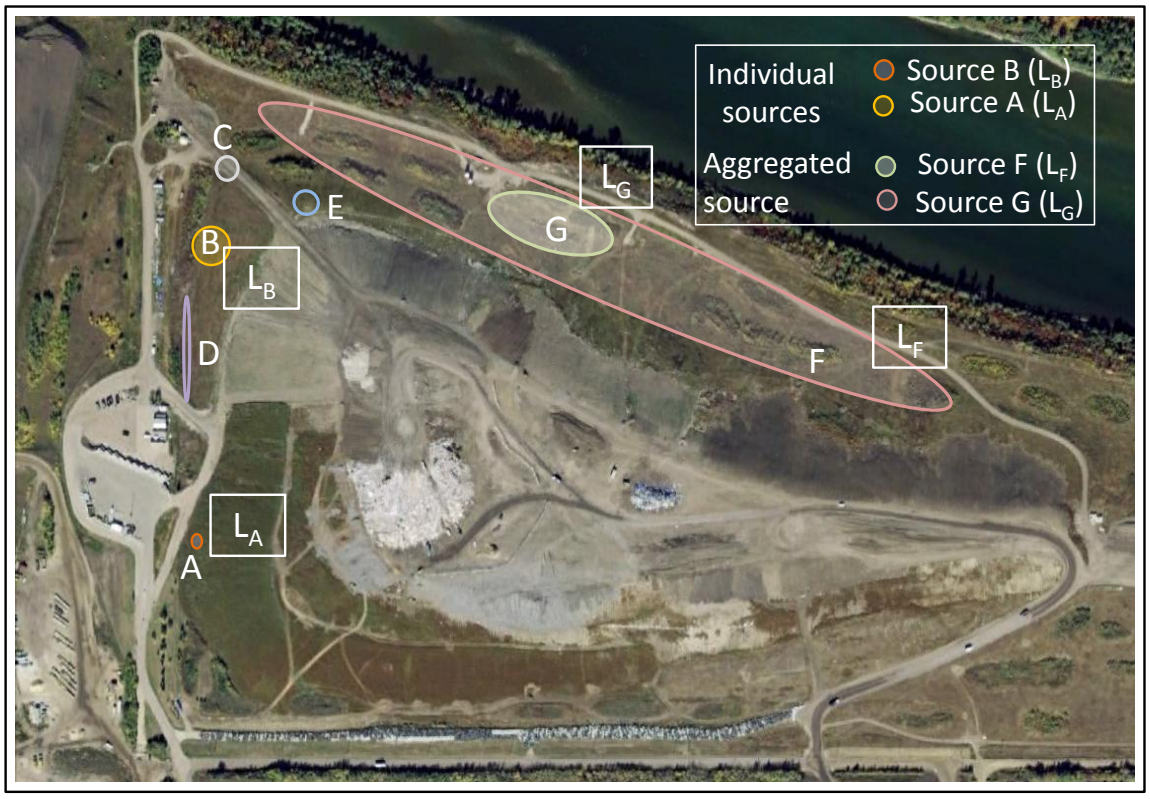

Figure 5.1: Experimental setup positions and individual sources location. Here project 1, indicates the source B and source A as small area source for analysis and project 2 refers big and undefined area sources (location F and location G).

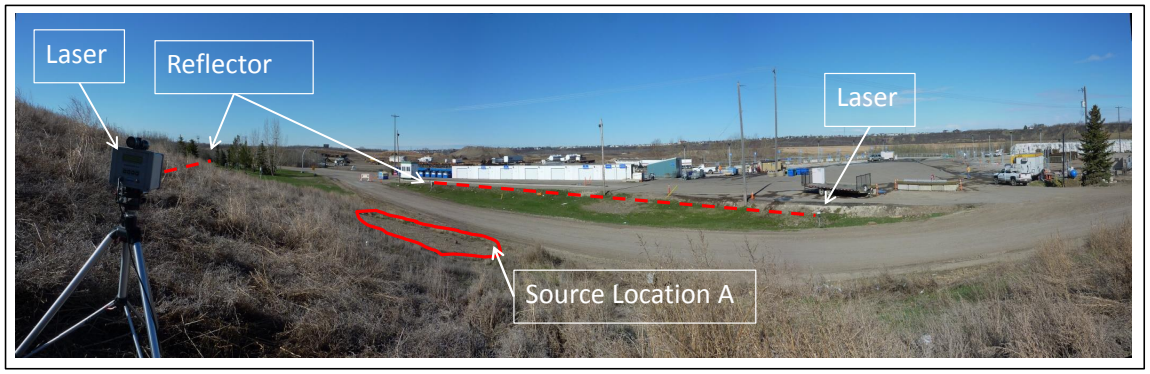

Figure 5.2: Experimental setup for source location A (source L_A).

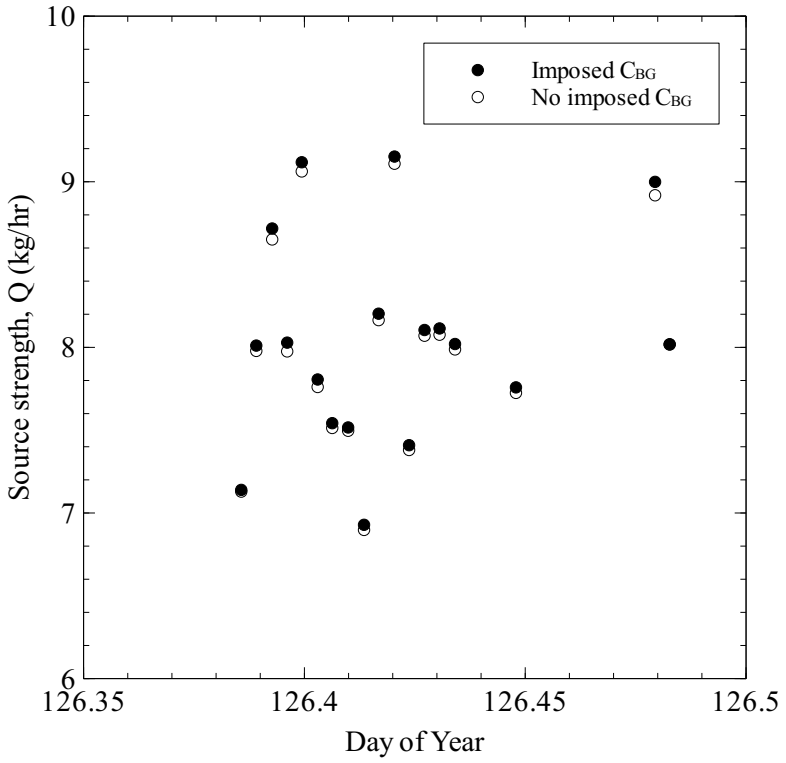

Figure 5.3: For "imposed" and "no imposed" assumption of C_{BG} , source strength Q_{LA} has been plotted.

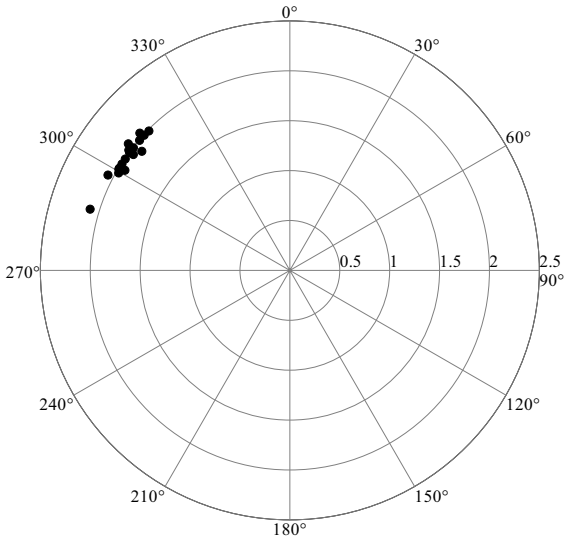

Figure 5.4: Deduced C_{BG} with corresponding wind direction (θ) for (L_A). The calculated background concentration is very steady.

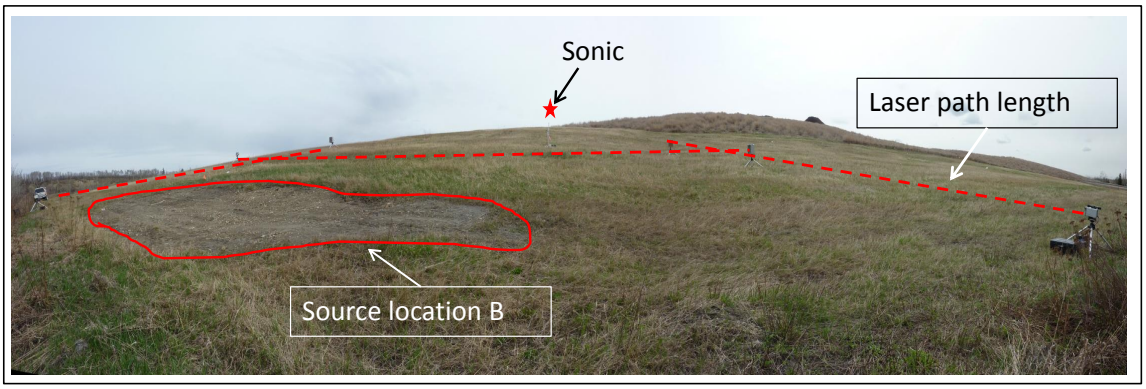

Figure 5.5: Experimental setup for location B (source L_B).

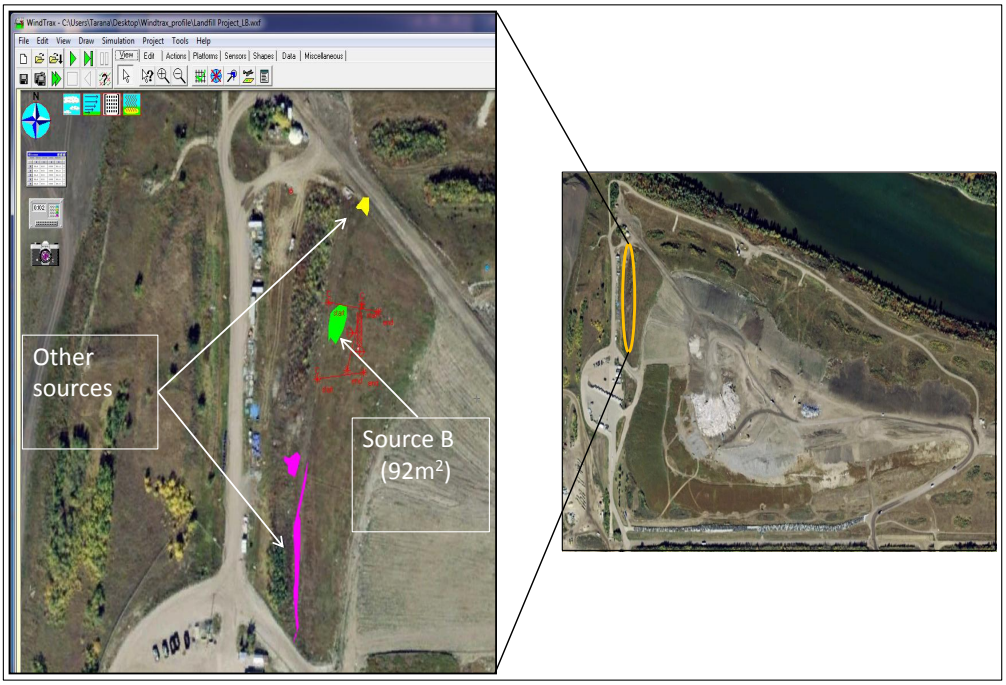

Figure 5.6: WindTrax snapshot for location B. In this figure, other sources (source C and source D) are present with source B. The dimension of source B is 14 $\times$ 8 m^2.

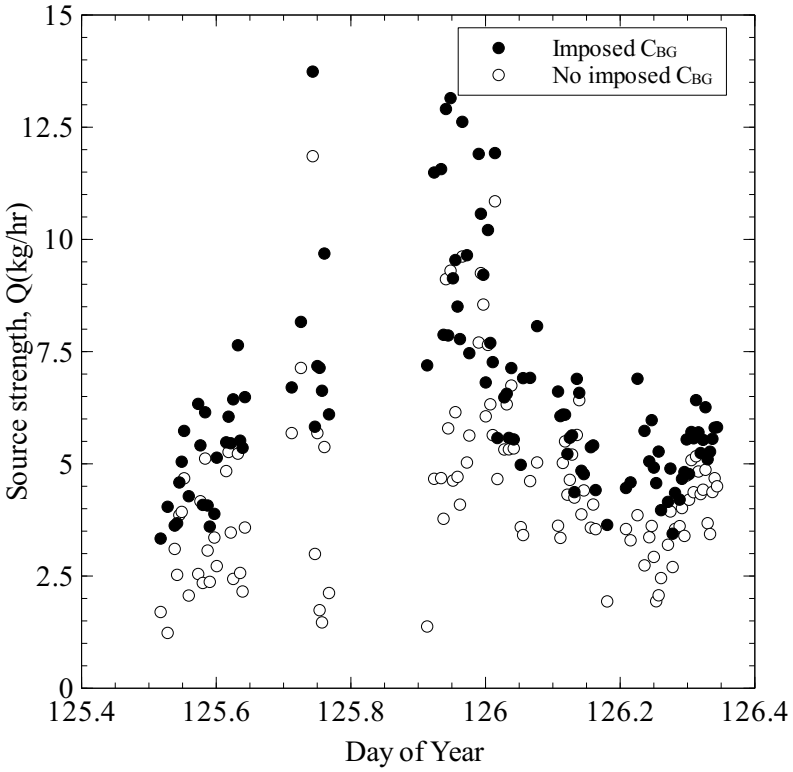

Figure 5.7: Source strength $Q(\mathrm{kg\,h^{-1}}$
) of source location B. Open circles: background concentration imposed "1.9ppm. Average values for the inferred source strength were 6.33 $\mathrm{kg\,h^{-1}}$ (background imposed) and 4.41 $\mathrm{kg\,h^{-1}}$

.

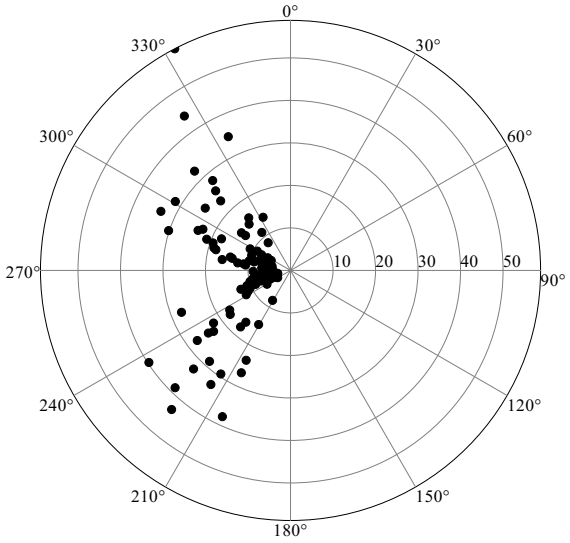

Figure 5.8: Inferred background concentration, C_{BG} (ppm) versus mean wind direction, for measurements at location B (L_B).

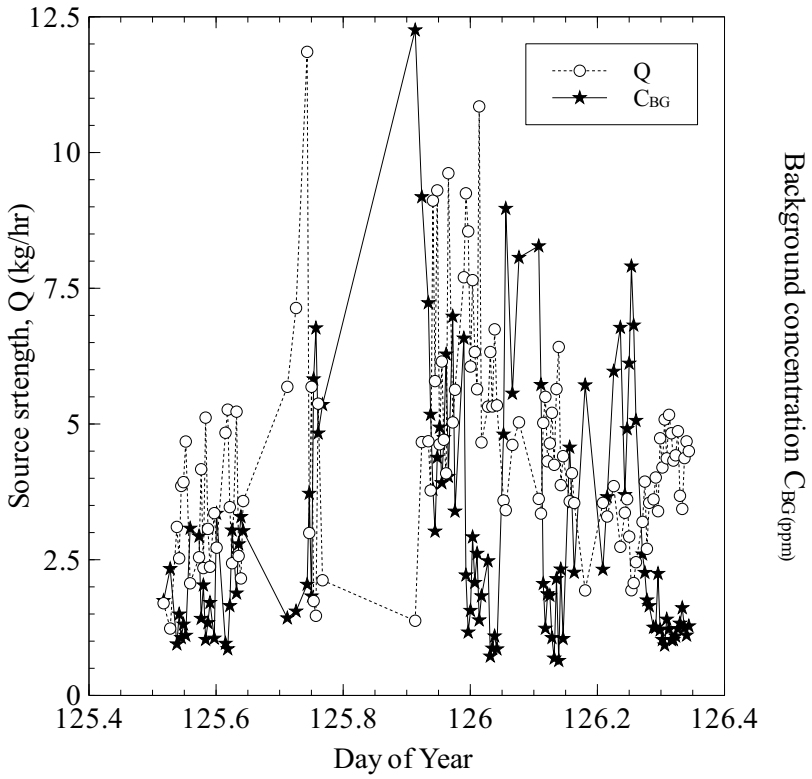

Figure 5.9: Inferred background concentration, C_{BG} (ppm) and source strength (Q), when C_{BG} was not "imposed"for location B (L_B). Q and C_{BG} exhibit an inverse relation.

.

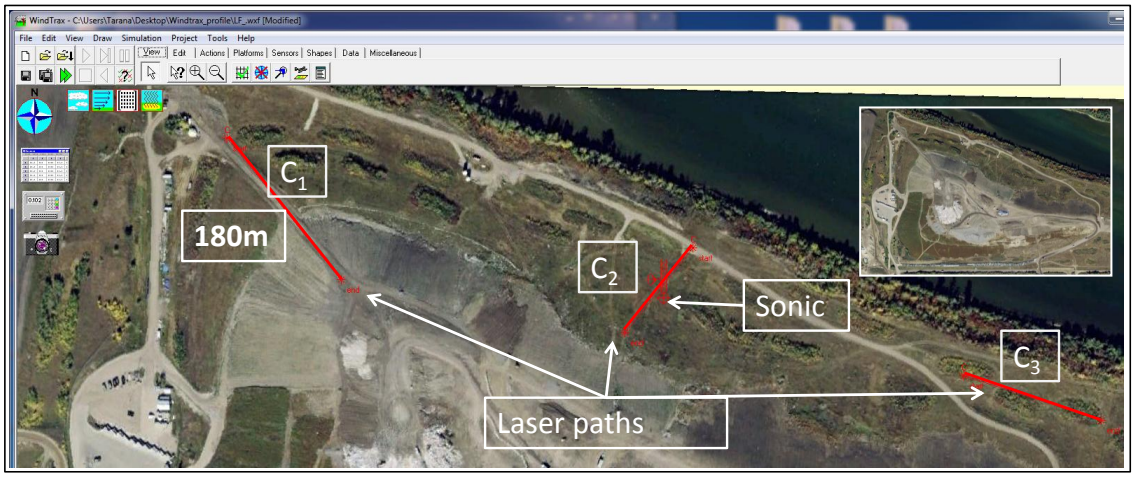

Figure 5.10: Sensor locations in experimental setup for source L_F.

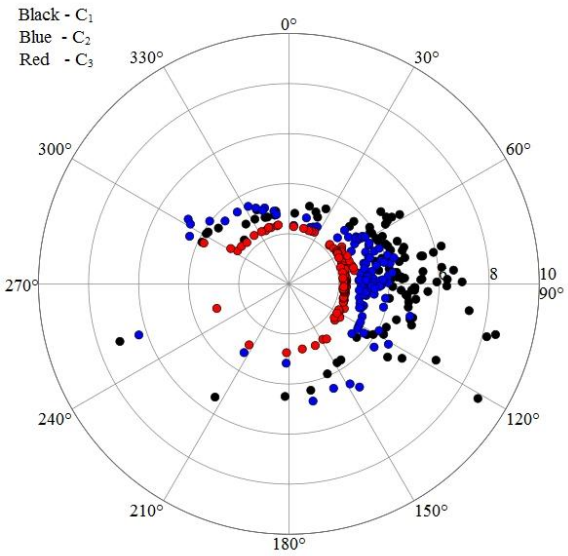

Figure 5.11: Measured concentration value of different sensors w.r.t the wind direction for source L_F.

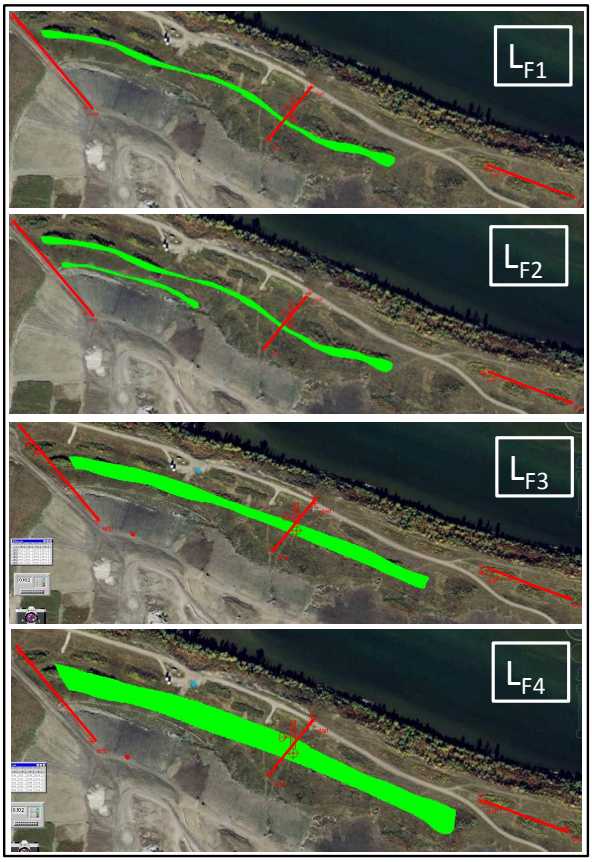

Figure 5.12: Different assumptions based on shape and size of source area of L_F.

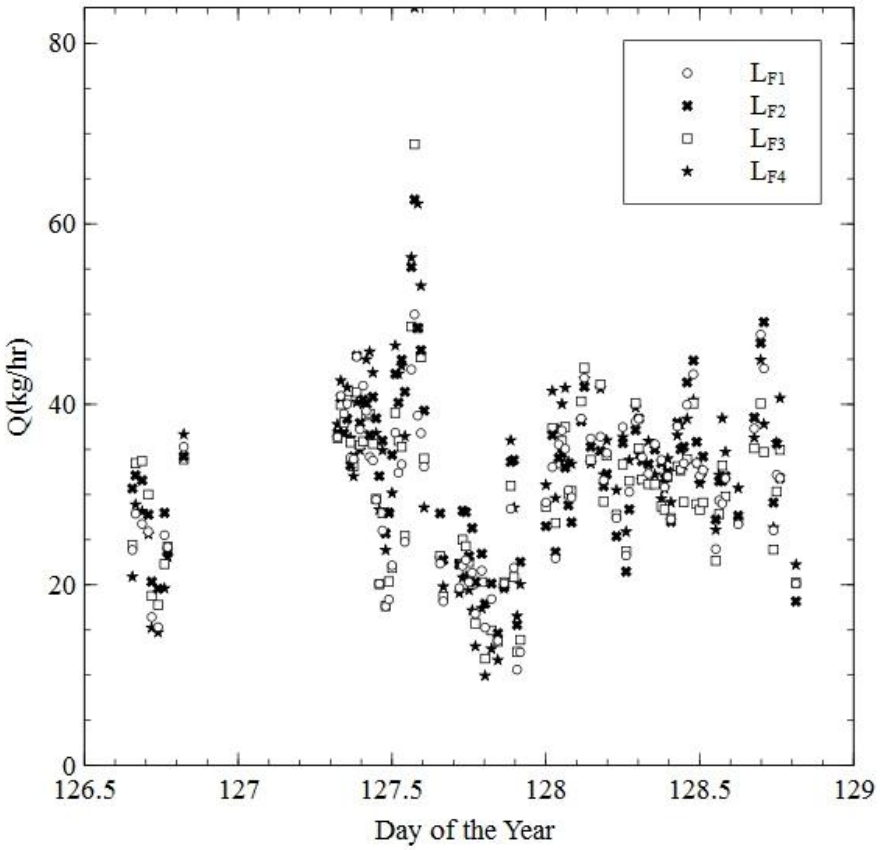

Figure 5.13: The source strength, Q_F of source location F L_F for different assumptions based on shape and size of source area.

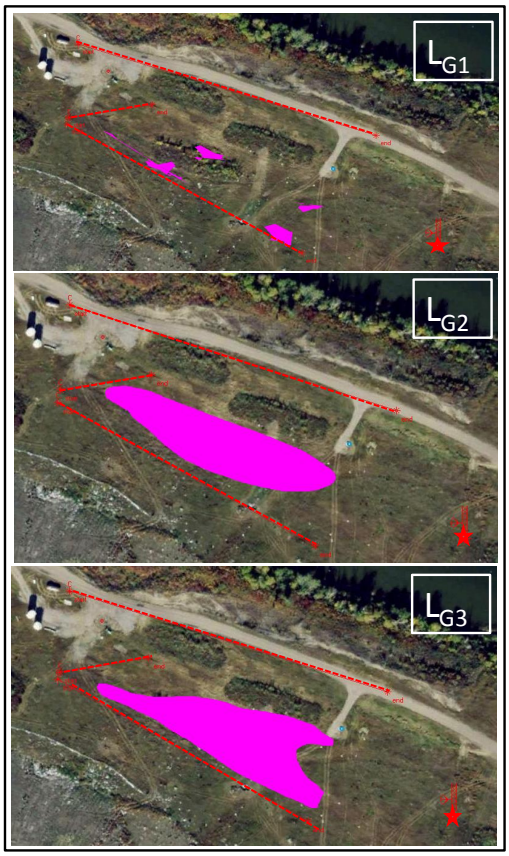

Figure 5.14: Different assumptions based on source area for source location G. The area of L_{G1}, shows the individual, exact locations of some sources, source area of L_{G2} covers the whole area of all sources and L_{G3} is a modify of the extended source area.

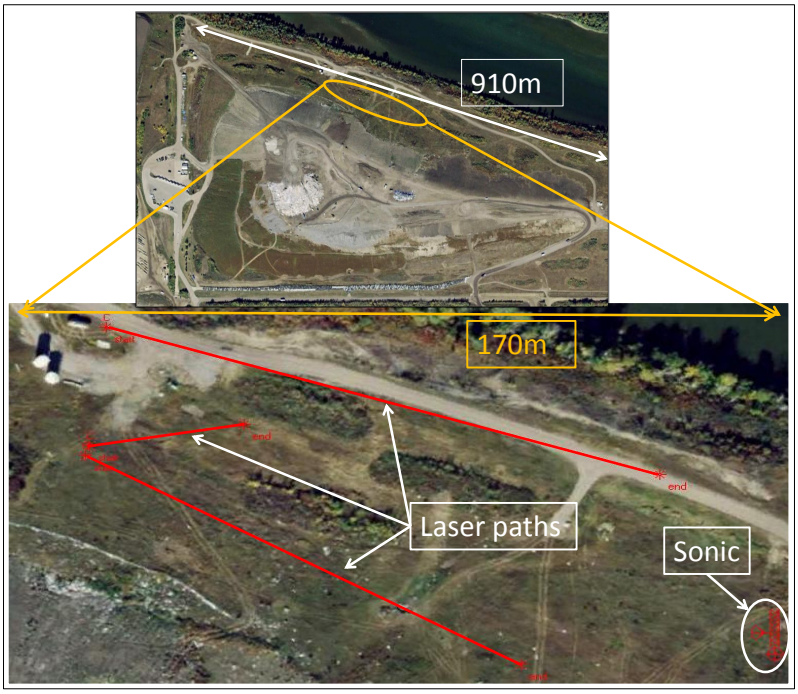

Figure 5.15: Sensor locations in experimental setup of of L_G.

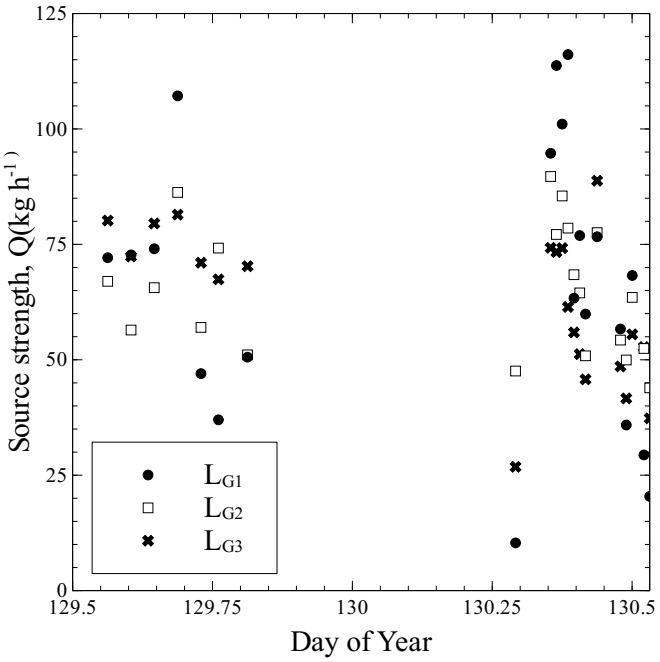

Figure 5.16: Source strength of different assumptions based on source area for source location G.

Chapter 6

Results and Discussion

A short campaign of monitoring the atmospheric concentration of methane in Edmonton, covering a summer period and an autumn period, failed to show any explainable pattern other than the daytime concentrations being a little smaller than the nighttime values. Variation in methane concentration was not found to correlate with the basic meteorological variables tested (i.e. wind direction, speed, etc). Mean values for the summer and the autumn were almost identical (2.12 ppm and 2.13 ppm, respectively). Those values do not seem to be in any way unusual or surprising, either in an Alberta context or the global context.

A campaign to deduce the methane emission rates from waste lagoons and landfill vents or leaks yielded release rates that appear to be very plausible (however independent estimates from the site are not available, and neither are we aware of comparably specific data from other, similar sites). The methodology adopted was "inverse dispersion," based on a backward Lagrangian Stochastic Model for atmospheric transport. Inverse dispersion is one of a number of techniques that can be applied to estimate emissions from these sorts of sources, the best known of the alternatives being the chamber method — which disturbs the system, and unless replicated in number, provides only a spot estimate — and eddy covariance, whose accuracy is predicated on the flow being undisturbed and the flux footprint lying over the source. Naturally the inverse dispersion method is only as good as the wind transport model that underlies

it, and in that context it can be stated that the Lagrangian stochastic model used here is more or less the "gold standard." It satisfies the "well-mixed condition," the most rigorous selection criterion known for dispersion models of any class, and has been proven by numerous investigators (working independently) to be in very good agreement with artificial tracer dispersion trials on ideal terrain. To the extent that the turbulent flow linking the source(s) to the detectors deviates at real world sites from the ideal (Monin-Obukhov) flow assumed by the Lagrangian model, a loss of accuracy is incurred. It is impossible to provide general guidelines as to the severity of that type of error, which will however have been more severe for the landfill measurements than for the lagoons — because the latter provide hundreds of metres of level surface over which the surface layer must at least approach being in the ideal state alluded to.

The case that the methane source is one or more lagoons is the easier one, for here (1) one has well-defined source boundaries, (2) the source strength is *probably* fairly uniform (though this is a conjecture), and (3) as noted above the flatness of the emitting surface prompts the development of a layer of wind flow that is probably well characterized by the Monin-Obukhov similarity theory. The co-existence of several sources does however complicate the problem. In the case that two sources are to be quantified it was found that best results (by the criterion of there being no negative predictions for source strength, and smallest variation from run to run and day to day in emission rate) are obtained by (a) imposing a constant background concentration C_{BG} of about 1.9 ppm wherever the wind direction and source distribution is such as to make that a priori assignment plausible; or (b) accepting only those runs for which one detector provides an unambiguous background concentration, while two other detectors $C_j,\ (j = 1, 2)$ permit to deduce $Q_j,\ (j = 1, 2)$.

Inverse dispersion applied to small, well-defined and isolated sources on the landfill returned consistent and very plausible rates of methane emission. The situation is

not as tidy when the detector configuration is responding to a large area embracing strong point sources and poorly delineated area sources. However even in that case the results given in Chapter 5 suggest the technique gives a very useful first indication of the emission rate, albeit with a level of uncertainty that is at least 100%.

It is hoped that this thesis adequately conveys the methodology applied here to extract information on a topic of immediate social relevance, viz. how to quantify anthropogenic greenhouse gas fluxes. Inverse dispersion is an exceedingly convenient method for determining surface-to-atmosphere fluxes. However (just as does any alternative technique one might contemplate adopting) it entails some subjectivity, requiring that judgements be made as to best instrument layout, as to the acceptability of wind conditions during this run or that, and so forth. Although the thesis does not offer a formal "protocol" to eliminate or reduce ambiguity of the "bLS method" (as the technique is widely named), the need for such a protocol is perhaps the most important implication for future research of this type.

References

2008. *End user GHG inventories for England, Scotland, Wales and Northern Ireland: 1990, 2003 to 2007.*

Babilotte, Antoine, Lagier, Thomas, Fiani, Emmanuel, & Taramini4, Vincent. 2010. Fugitive Methane Emissions from Landfills: Field Comparison of Five Methods on a French Landfill. **136**.

Boughton, B. A., Delaurentis, J. M., & Dunn, W. E. 1987. A stochastic model of particle dispersion in the atmosphere. *Boundary-Layer Meteorology*, **40**, 147–163. 10.1007/BF00140073.

Budisulistiorini, Sri Hapsari. 2007. Electricity generation from Landfill gas. **3**, 9–15.

Crenna, B. P., K.Flesch, Thomas, & Wilson, J. D. 2008. Influence of source-sensor geometry on multi-source emission rate estimates. *Atmospheric Environment*, **42**, 7373–7383.

Dyer, A.J., Bradley E.F. 1982. An alternative analysis of flux-gradient relationships at the 1976 ITCE. *Boundary-Layer Meteorology*, **22**(1), 3–19. cited By (since 1996) 59.

Ehhalt, D. H., & Schmidt, U. 1978. Sources and sinks of atmospheric methane. *Pure and Applied Geophysics*, **116**, 452–464. 10.1007/BF01636899.

Flesch, T. K., Wilson, J. D., Harper, L. A., Todd, R. W., & Cole, N. A. 2007. Determinig Ammonia emissions from a cattle feedlot with an inverse-dispersion technique. *Agricultural and Forest Meteorology*, **144**, 139–155.

Flesch, Thomas K. 1996. The footprint for flux measurements, from backward Lagrangian stochastic models. *Boundary-Layer Meteorology*, **78**, 399–404. 10.1007/BF00120943.

Flesch, Thomas K., Wilson, John D., & Yee, Eugene. 1995. Backward-Time Lagrangian Stochastic Dispersion Models and Their Application to Estimate Gaseous Emissions. *J. Appl. Meteor.*, **34**(6), 1320–1332.

Flesch, Thomas K., Wilson, J. D., Harper, Loowry A., & Crenna, Brian P. 2005. Estimating gas emissions from a farm with an inverse-dispersion technique. *Atmospheric Environment*, **39**, 4863–4874.

Flesch, Thomas K., Harper, Loowry A., Desjardins, Raymond L., Gao, Zhiling, & Crenna, Brian P. 2009. Multi-source emission determination using an inverse-dispersion technique. *Boundary-layer Meteorology*, **132**, 11–30.

Flesch, T.K., Wilson J.D. Yee E. 1995. Backward-time Lagrangian stochastic dispersion models and their application to estimate gaseous emissions. *Journal of Applied Meteorology*, **34**(6), 1320–1332. cited By (since 1996) 116.

Friborg, Thomas, Soegaard, Henrik, Christensen, Torben R., Lloyd, Colin R., & Panikov, Nicolai S. 2003. Siberian wetlands: Where a sink is a source. *Geophys. Res. Lett.*, **30**(21), 2129–.

Gimson, Neil R., & Uliasz, Marek. 2003. The determination of agricultural methane emisions in New Zealand using inverse modeling technique. *Atmospheric Environment*, **37**, 3903–3912.

Haarlem, R P Van, Desjardins, R L, Gao, Z, Flesch, T K, & Li, X. 2008. Methane and ammonia emissions from a beef feedlot in western Canada for a twelve-day period in the fall. *Canadian Journal of Animal Science*, **88**(4), 641–649.

Heikkinen, Juha E P, Maljanen, Marja, Aurela, Mika, Hargreaves, Ken J, & Martikainen, Pertti J. 2002. Carbon dioxide and methane dynamics in a sub-Arctic peatland in northern Finland. *Polar Research*, **21**(1), 49–62.

Ito, A, Takahashi, I, Nagata, Y, Chiba, K, & Haraguchi, H. 2000. The long-term evolutions and the regional characteristics of atmospheric methane concentrations in Nagoya, 19831997. *Science of The Total Environment*, **263**(1-3), 37 – 45.

Khalil, M. A. K., & Rasmussen, R. A. 1983. Sources, Sinks, and Seasonal Cycles of Atmospheric Methane. *J. Geophys. Res.*, **88**(C9), 5131–5144.

Lemons, D.S., & Langevin, P. 2002. *An introduction to stochastic processes in physics: containing "On the theory of Brownian motion" by Paul Langevin, translated by Anthony Gythiel.* Johns Hopkins Paperback. Johns Hopkins University Press.

Munn, R. E. 1966. *Descriptive Micrometeorology.*

Obukhov, A.M. 1971. Turbulence in an Atmosphere with a Non-Uniform Temperature. *Boundary-Layer Meteorol*, **2**, 7–29.

Paulson, C. A. 1970. The Mathematical Representation of Wind Speed and Temperature Profiles in the Unstable Atmospheric Surface Layer. *J. Appl. Meteor.*, **9**(6), 857–861.

Reinhart, D.R., & Townsend, T.G. 1998. *Landfill bioreactor design and operation.* Lewis Publishers.

Ro, Kyoung S., Johnson, Melvin H., Hunt, Patrick G., & Flesch, Thomas K. 2011. Measuring Trace Gas Emission from Multi-Distributed Sources Using Vertical Radial Plume Mapping (VRPM) and Backward Lagrangian Stochastic (bLS) Techniques. *Atmosphere*, **2**(3), 553–566.

Spokas, K., Bogner, J., Chanton, J. P., Morcet, M., Aran, C., Graff, C., Golvan, Y. M., & Hebe, I. 2006. Methane mass balance at three landfill sites: What is the efficiency of capture by gas collection systems? *Waste Management*, **26**(5), 516–525.

Stull, Roland B. 1950. *An Introduction to Boundary Layer Meteorology.* Kluwer Academic Publishers.

Thomson, D.J. 1987. Criteria for the selection of stochastic models of particle trajectories in turbulent flows. *Journal of Fluid Mechanics*, **180**, 529–556. cited By (since 1996) 560.

Wilson, J. D., Thurtell, G. W., & Kidd, G. E. 1981(c). Numerical simulation of particle trajectories in inhomogeneous turbulence, III: Comparison of predictions with experimental data for the atmospheric surface layer. *Boundary-Layer Meteorology*, **21**, 443–463. 10.1007/BF02033593.

Wilson, J.D., Thurtell, G.W., Kidd, G.E., & Beauchamp, E.G. 1982. Estimation of the rate of gaseous mass transfer from a surface source plot to the atmosphere. *Atmospheric Environment (1967)*, **16**(8), 1861 – 1867.

Wuebbles, Donald J, & Hayhoe, Katharine. 2002. Atmospheric methane and global change. *Earth-Science Reviews*, **57**(3-4), 177 – 210.

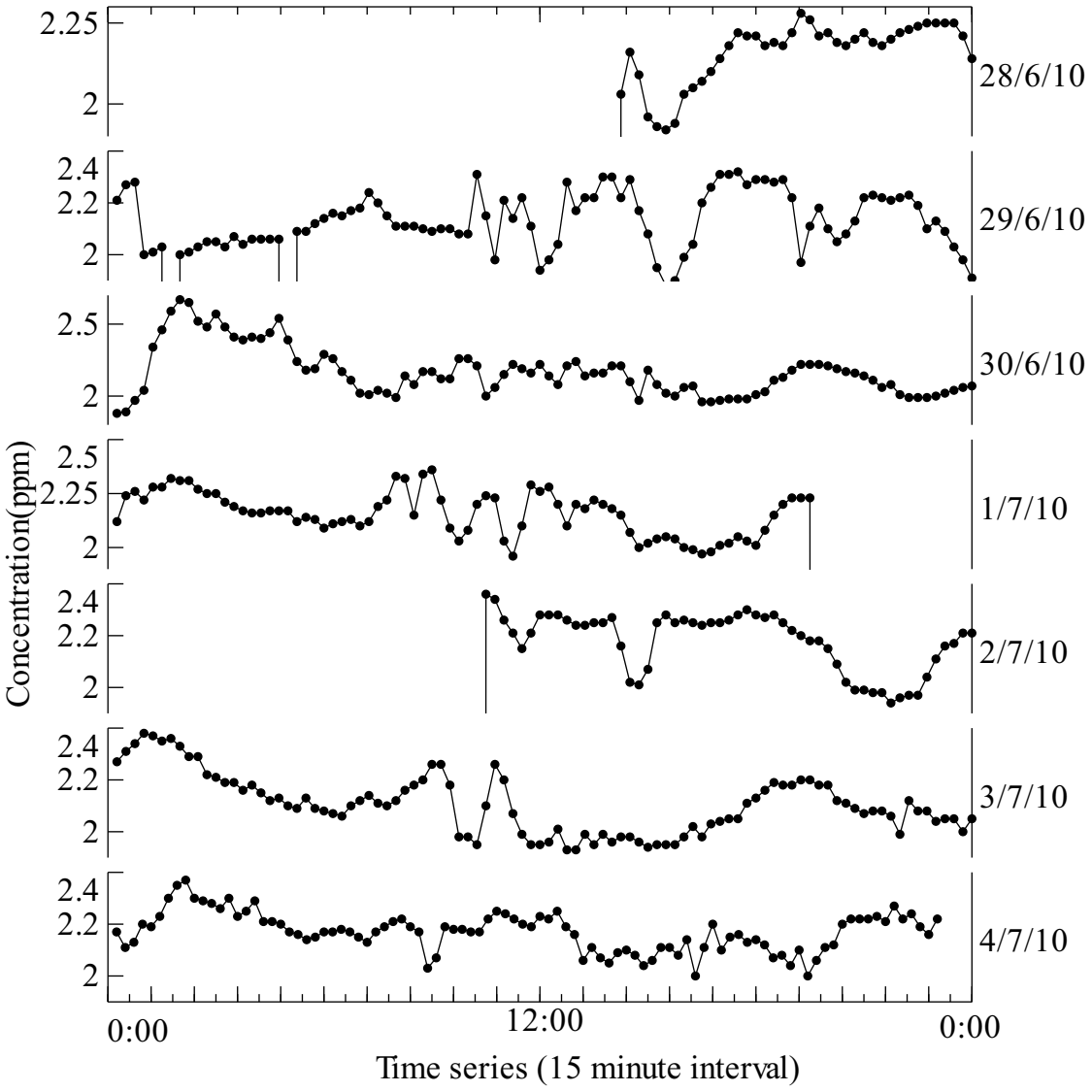

Figure 1: The 15 minute average concentration ppm of each individual day has been plotted in a time series graph from 28/6/10 to 4/7/10. Date of the corresponding day is indicated in right hand side of the graph.

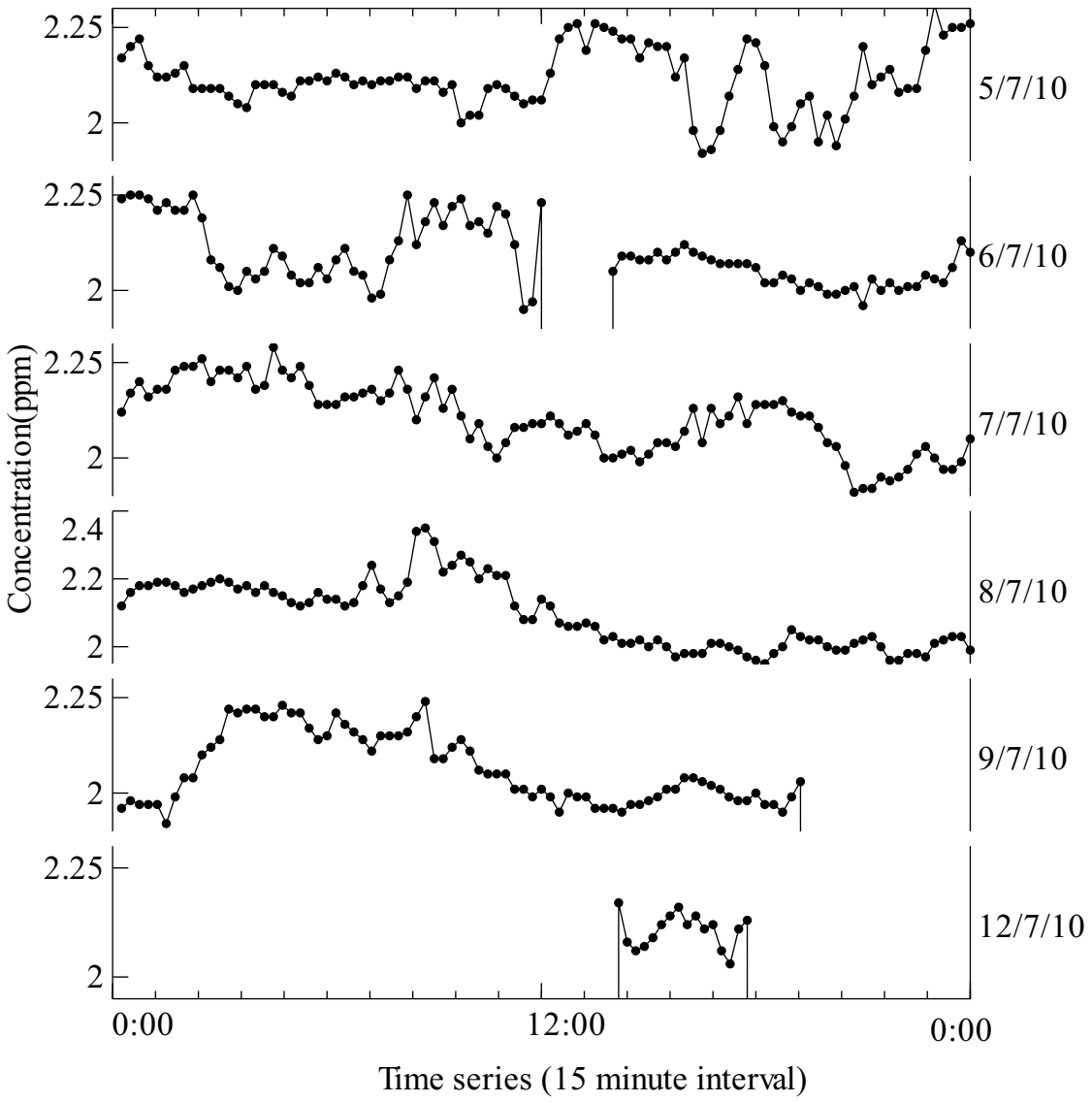

Figure 2: The 15 minute average concentration ppm of each individual day has been plotted in a time series graph from 5/7/10 to 12/7/10. Date of the corresponding day is indicated in right hand side of the graph.

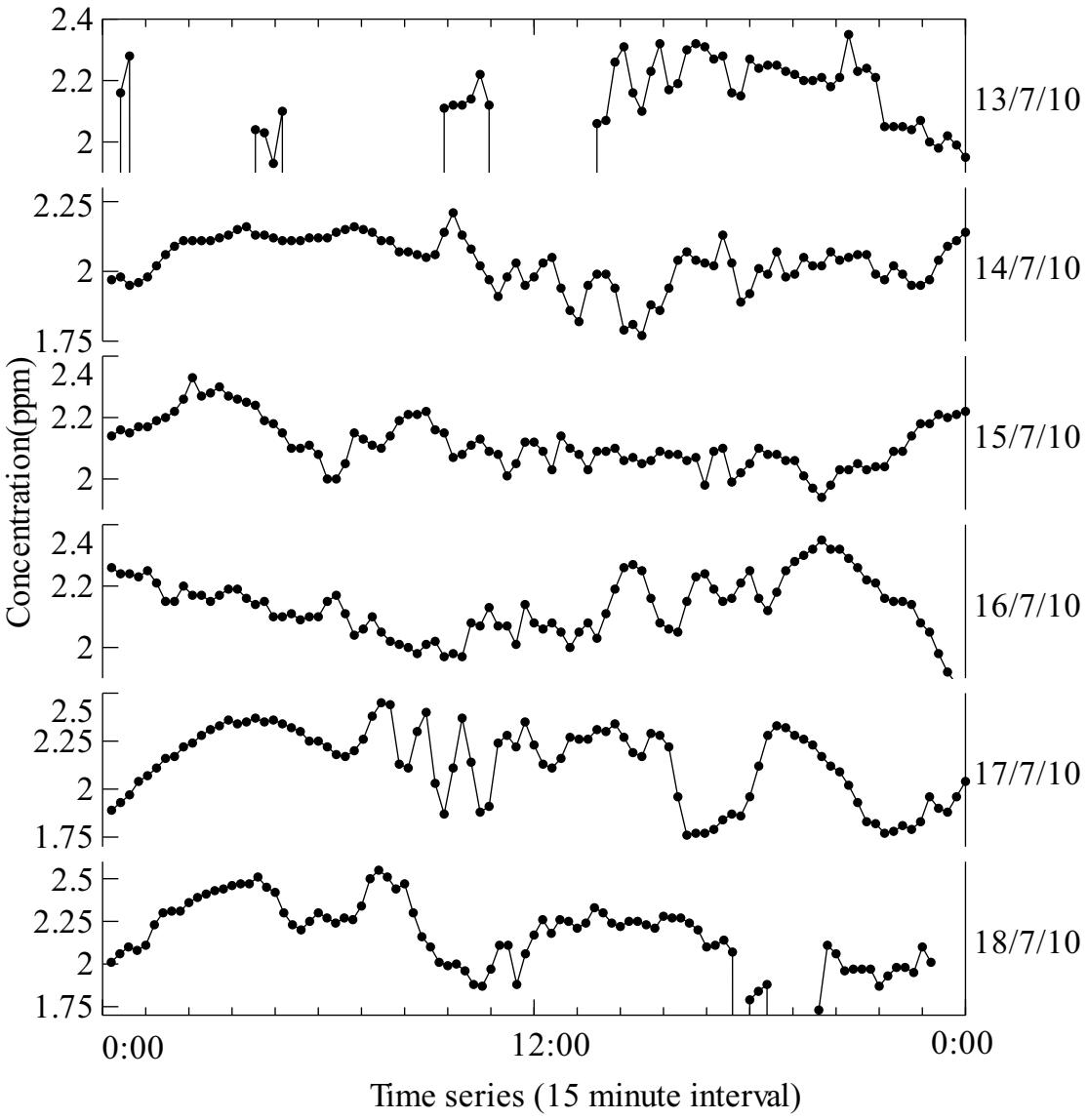

Figure 3: The 15 minute average concentration ppm of each individual day has been plotted in a time series graph from 13/7/10 to 18/7/10. Date of the corresponding day is indicated in right hand side of the graph.

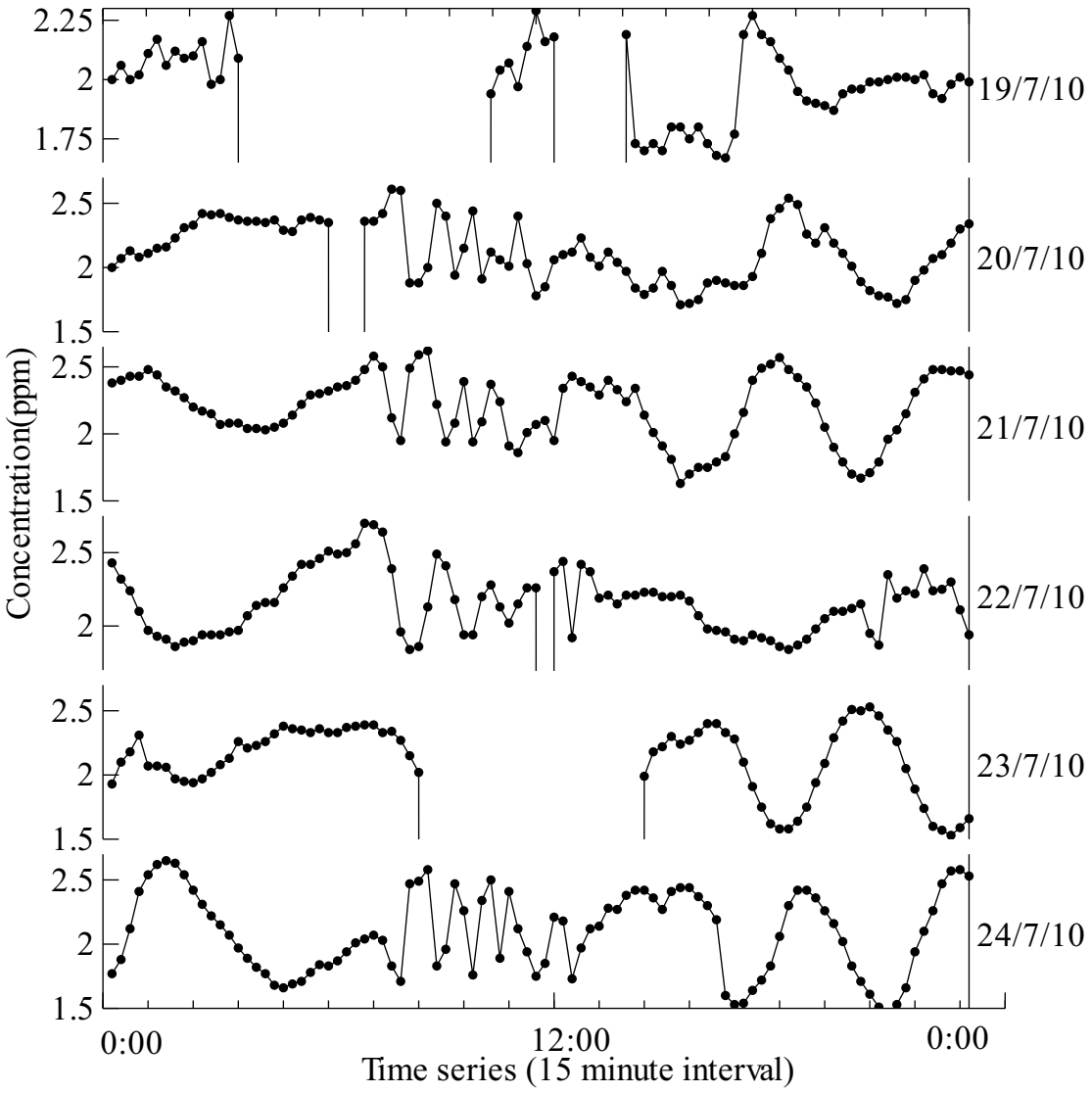

Figure 4: The 15 minute average concentration ppm of each individual day has been plotted in a time series graph from 19/7/10 to 24/7/10. Date of the corresponding day is indicated in right hand side of the graph.

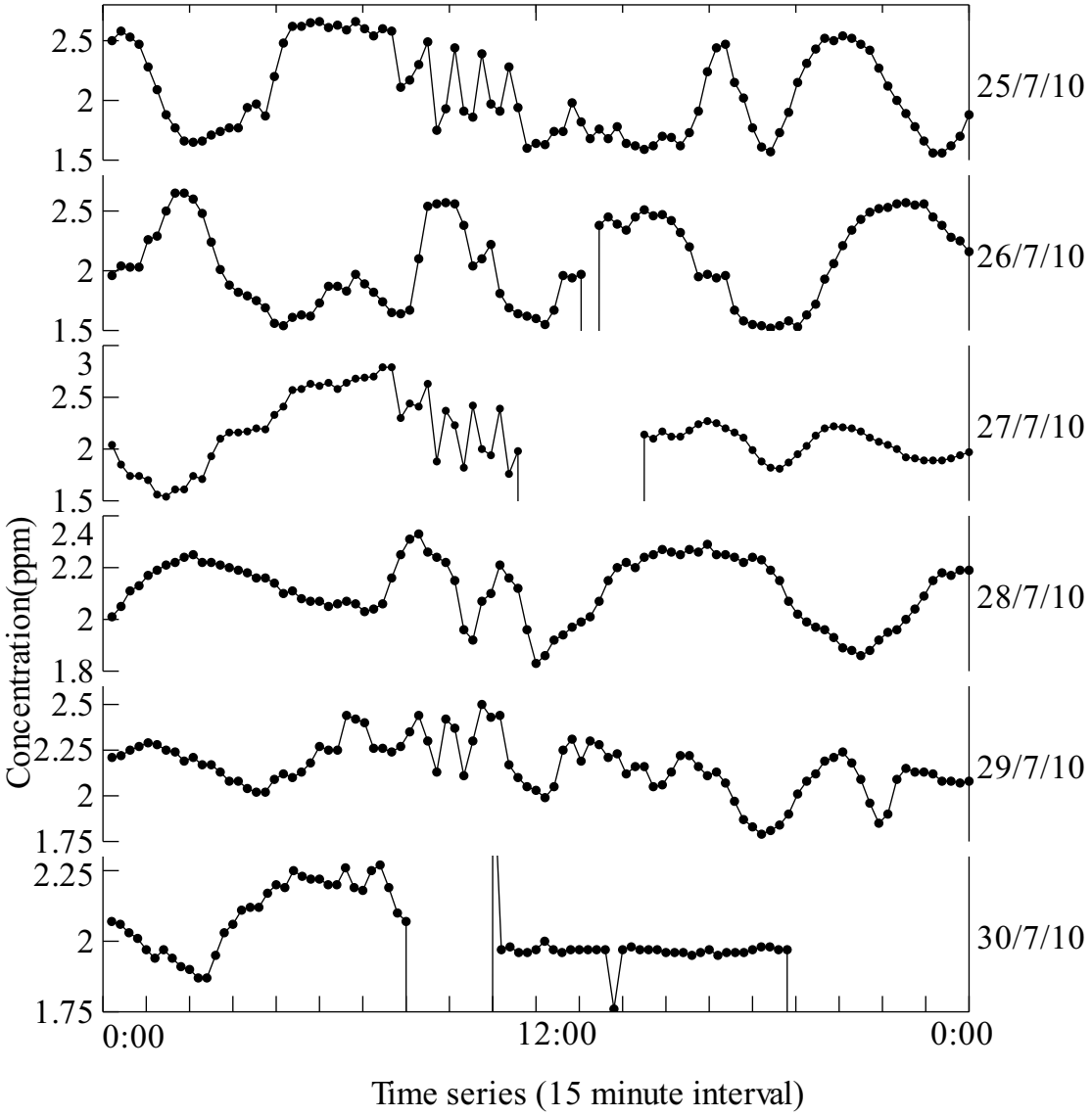

Figure 5: The 15 minute average concentration ppm of each individual day has been plotted in a time series graph from 25/7/10 to 30/7/10. Date of the corresponding day is indicated in right hand side of the graph.

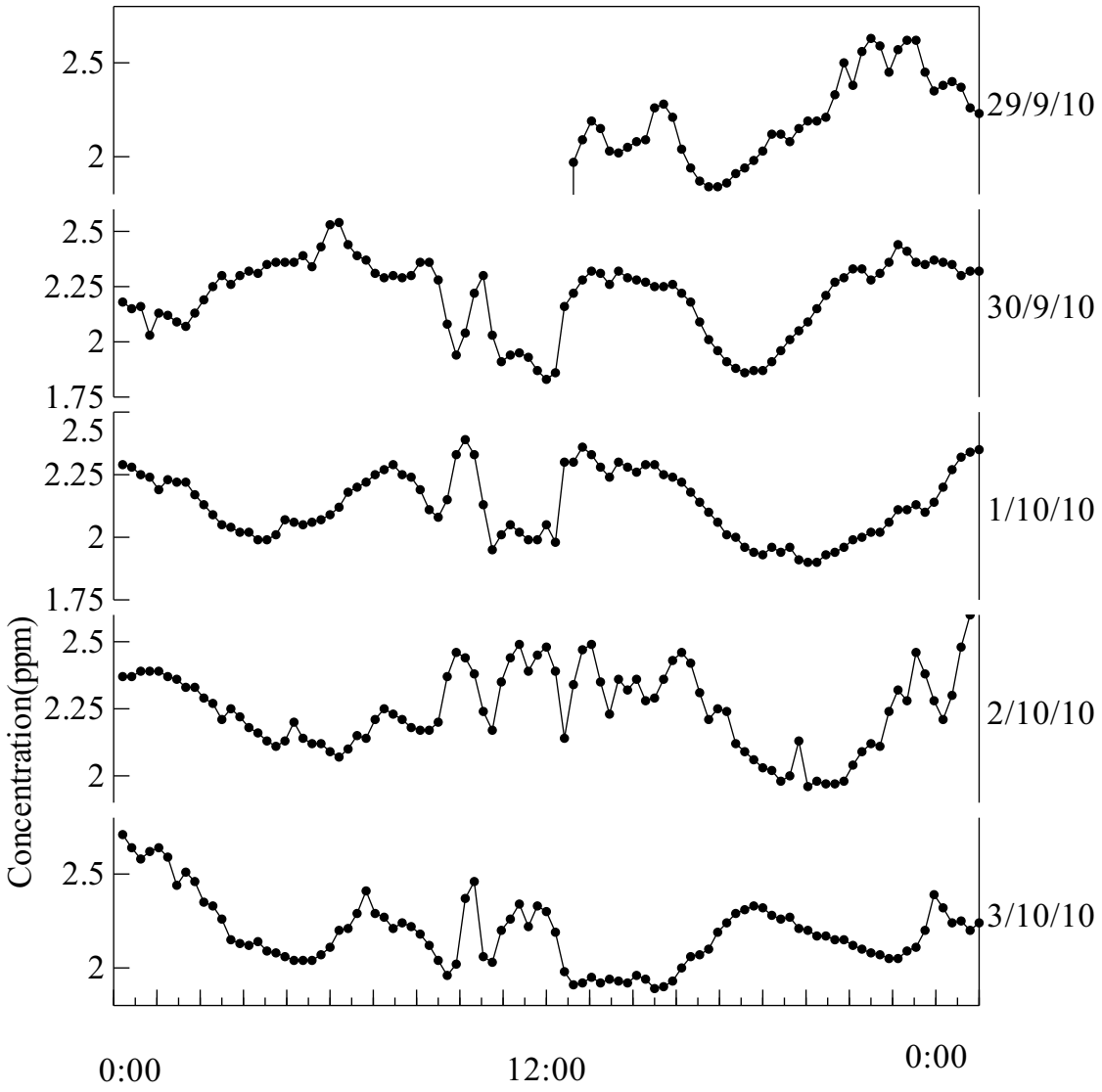

Figure 6: The 15 minute average concentration ppm of each individual day has been plotted in a time series graph from 29/9/10 to 3/10/10. Date of the corresponding day is indicated in right hand side of the graph.

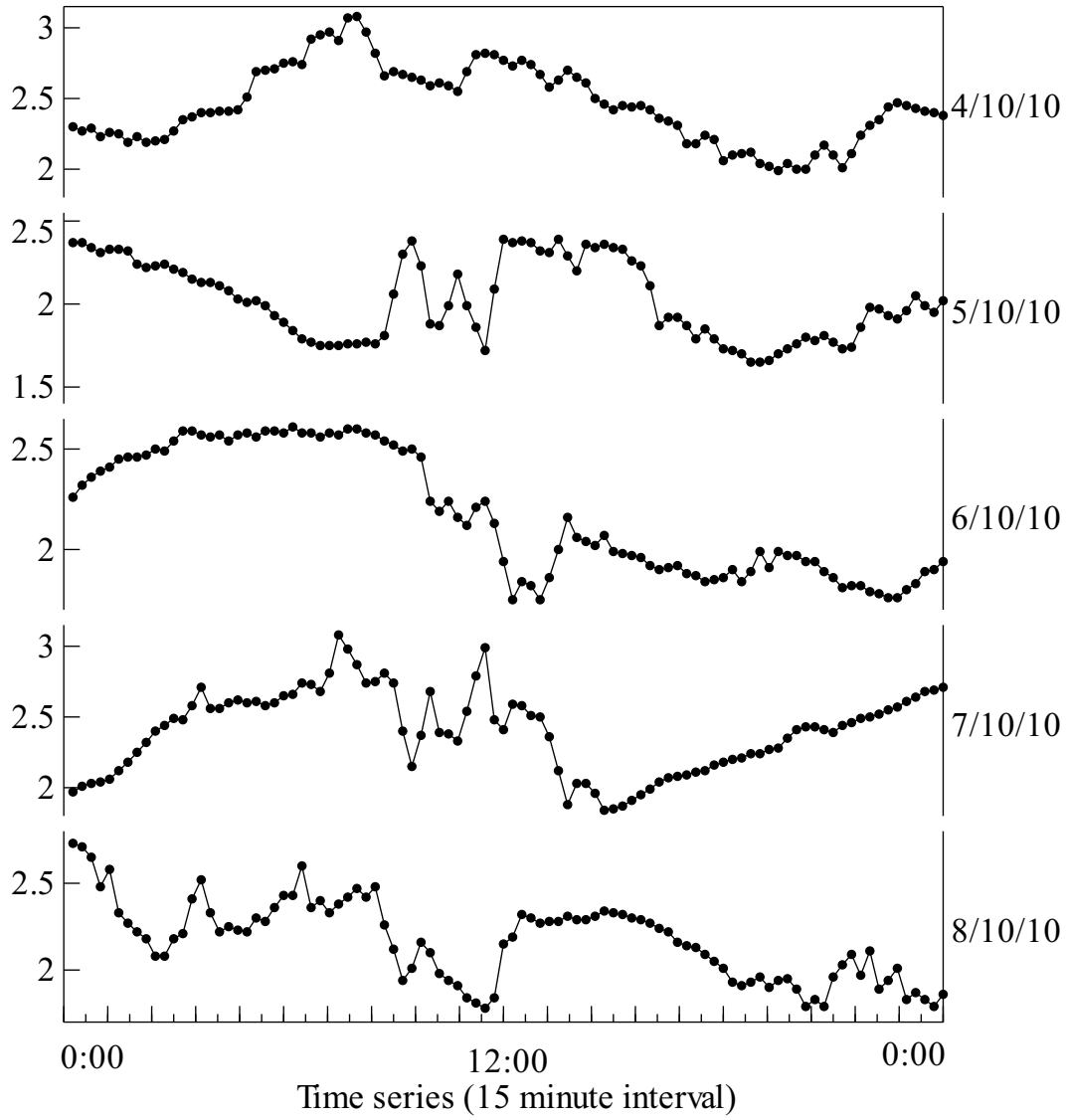

Figure 7: The 15 minute average concentration ppm of each individual day has been plotted in a time series graph from 4/10/10 to 8/10/10. Date of the corresponding day is indicated in right hand side of the graph.

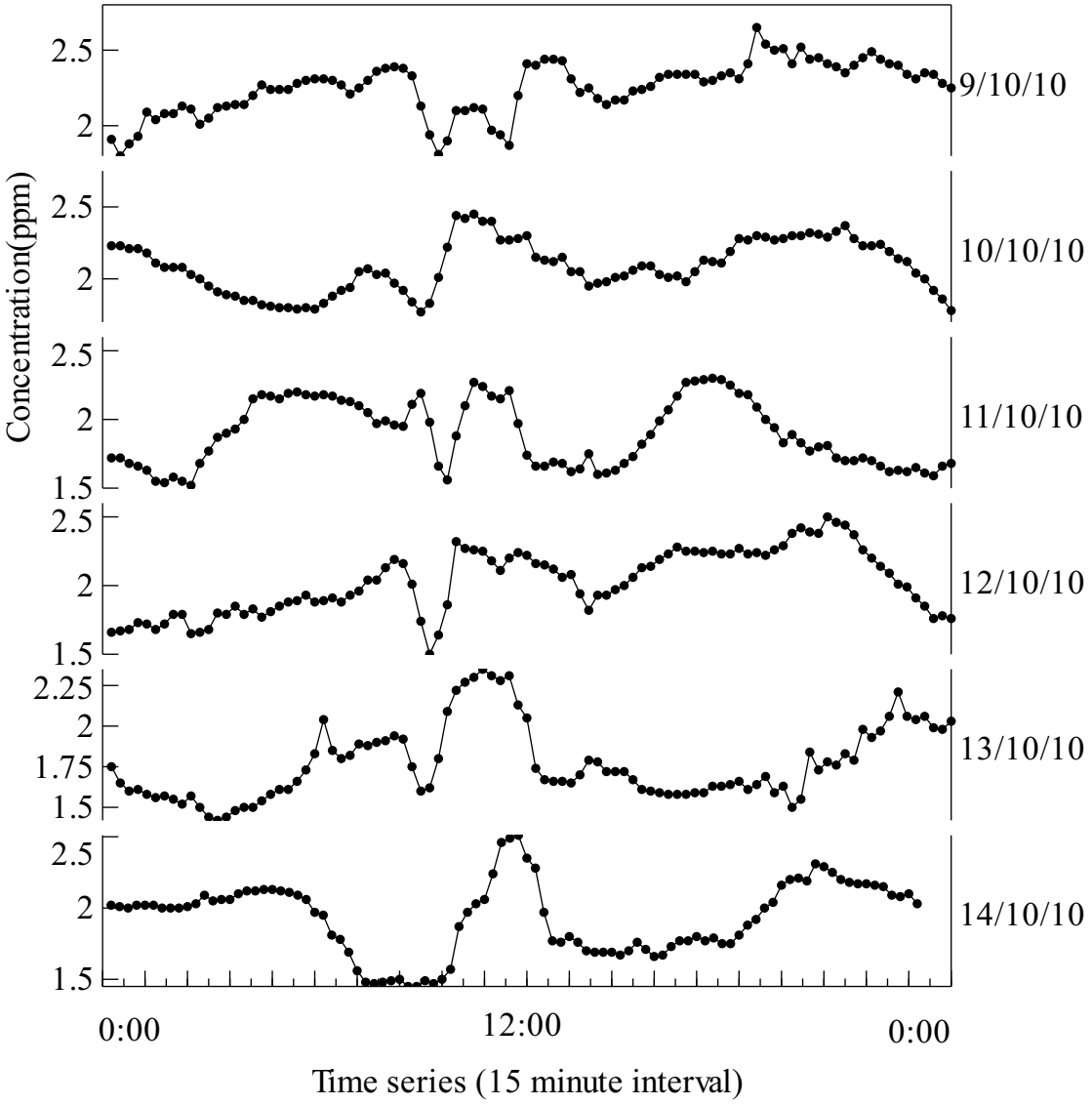

Figure 8: The 15 minute average concentration ppm of each individual day has been plotted in a time series graph from 9/10/10 to 14/10/10. Date of the corresponding day is indicated in right hand side of the graph.